NOVEL APPLICATIONS OF FLUOROPOLYMERS IN SOLUTION-PROCESSED ELECTRONICS

A Dissertation

Presented to the Faculty of the Graduate School

of Cornell University

in Partial Fulfillment of the Requirements for the Degree of

Doctor of Philosophy

by

Carol Newby

January 2014

NOVEL APPLICATIONS OF FLUOROPOLYMERS IN SOLUTION-PROCESSED ELECTRONICS

Carol Newby, Ph.D.

Cornell University 2014

After deposition, solution-processed organic materials are susceptible to redissolution by similar solvents. This solvent problem puts undesirable restrictions on the subsequent processing of electronic devices that contain organic materials. In particular, formation of multiple stacked layers is prohibited, as is the patterning of, or on, organic materials. *Orthogonal processing* utilizes chemically orthogonal fluorinated material systems to resolve these issues and open up previously unattainable processing routes.

Four such processes are developed in this work, with one related to stacked devices and three related to patterning organic materials. More specifically, on one hand, a technique is developed to fabricate monolayers of conjugated polymer in stacked OLED devices. On the other hand, fluoropolymers are used to enable patterning of organic materials with otherwise incompatible commercial (organic) photoresists, via roll-to-roll compatible inkjet printing and, finally, for high resolution studies with electron beam lithography.

BIOGRAPHICAL SKETCH

Born in Devon, England, Carol enjoyed an idyllic childhood with much time spent in the garden with her sister, many days (rain or shine) spent by the sea and on the cliffs, and many weekends spent exploring the south-west with her family.

She attended Woolsery C. P. School and then Bideford College where the teachers provided a superb education. She loved every aspect of school and it was in these places she first uncovered her tendency to drift toward the technical disciplines.

Carol started her studies in Natural Sciences at Cambridge University in 2003. She leapt at the opportunity to spend a year on exchange at the Massachusetts Institute of Technology in Boston, USA, an experience which deeply reinforced her enthusiasm for science and engineering. She returned to Cambridge and graduated in 2007 having specialized in Materials Science and Metallurgy.

Next, an interest in organic spintronics led her to Bologna, Italy where she conducted research in the group of Dr. A. V. Dediu and enjoyed a very wholesome lifestyle with many warm friendships, and much good food and wine.

Finally, a desire to pursue a PhD in electronic materials brought her to Cornell University where she has enjoyed many nights in the superb Cornell Nanofabrication Facility, endless days thinking about things in the wonderful libraries on campus, and many happy times, particularly as an RA on west campus, gallivanting and interacting with so many interesting people.

For A, B and L.

Couldn't have got here without you.

ACKNOWLEDGEMENTS

It is humbling to consider how many people have helped me along the way to producing this work and I am deeply grateful for my interactions with each and everyone of you.

Thanks must go first and foremost to my advisor and friend, Prof. C. K. Ober. I have benefited greatly from his wisdom, guidance (and endless patience) and will remain forever grateful. The group he has built at Cornell has been a tremendous environment in which to spend the past years. I'm also particularly grateful to Prof. J. K. Lee for inspiring me in my first few years to strive toward being a creative and persistent scientist, and also for providing the initial sparks of creativity that started several of these projects. Thanks are also due to Prof. F. Rana, Prof. E. Giannelis and Prof. M. O. Thompson for serving on my special committee and providing extremely valuable and insightful feedback. I'm also grateful to Prof. G. G. Malliaras for initial guidance and Prof. R. H. Friend for being a gracious collaborator.

This work was also greatly enhanced by help from the CNF staff, particularly Alan Blier and Vince Genova, and the CCMR staff, particularly Jon Shu and Tony Condo. I'm also very grateful to my predecessor Priscilla G. Taylor who was a kind and generous mentor, and my collaborator at Cambridge University, Thomas Piachaud. Thanks go to a number of other group members too, including Alwin Wan, Yefei Zhang, Yosuke Hoshi, Claudio dos Santos and my undergraduate helpers Dan Kim, Alisha Vimawala and Melissa Kunkel.

On a more personal note I'd like to thank Anna, Phil, Alwin (again) and Shahyaan for keeping me grounded, providing support and remaining good friends when I maybe deserved less. I'm also grateful to many others, you know who you are: DQH, AR, AVD, IMC, AJP, MEK, FMR, EI, KJW, AKM, DM...

TABLE OF CONTENTS

LIST OF TABLES

LIST OF FIGURES

CHAPTER 1

AN INTRODUCTION TO FLUORINATED POLYMERS AND THEIR POTENTIAL IN PROCESSING AND PATTERNING APPLICATIONS

The work described in this dissertation spans topics from the fundamentals of conjugated polymer adhesion through organic device fabrication to volume manufacturing considerations. The uniting theme throughout is the use of fluorinated materials to develop and investigate otherwise unattainable processing capabilities.

This chapter first examines the motivations for incorporating organic materials in electronic devices, with the key advantage being the opportunity to use solution-processing. This, however, brings with it significant material compatibility challenges. The resolution of these issues is the motivation for developing and working with *orthogonal processing*. Other approaches to solving this problem are surveyed in the literature review. A section on the fundamentals of bonding in fluorinated materials is included to detail how this leads to their orthogonal properties, followed by some background on the current uses of fluoropolymers and fluorous solvents in today's world. Finally an overview of the following chapters is given.

Portions of this chapter are adapted from Ref. [7] with permission from The Royal Society of Chemistry.

1.1 Organic Materials in Electronics

Conventional electronic devices customarily contain only inorganic materials as they are significantly more robust and generally have better electronic properties than organic materials. However, motivations are now emerging to incorporate organic materials into electronic devices too. The processing advantages that derive from fabricating electronics from organic materials may, for some future applications, be substantial enough to compensate for poor electrical properties. Organic materials can also offer new functionalities, or, in very rare cases, superior performance compared to inorganic materials.

The most notable example of organic materials being used in electronics today is that of electroluminescent small molecules in organic light emitting diode (OLED) flat screen displays [8, 9]. These achieve vivid colors and better contrast thanks to each pixel being its own light source and not requiring a back light. Such displays are also substantially thinner and lighter than other flat screen technologies. In combination with polymeric substrates, organic-based electronics is also being developed for applications such as organic photovoltaics (OPV) [10] and wearable sensors [11] that would benefit from being large-area, light-weight or even flexible.

The manufacture of conventional inorganic electronics is energy intensive, requires batch vacuum chamber processes and is therefore costly. Fabricating electronics from organic materials that can be deposited from solution is a key advantage that allows continuous, low-temperature and therefore low-cost manufacture via roll-to-roll processing. The inherently poor electronic

properties of organic materials mean that while solution-processed electronics cannot compete with conventional applications, lower production costs could instead enable new applications by making conventionally passive products 'smart' such as smart packaging [12] and disposable radio frequency identification (RFID) tags [13]. Note that this approach might also utilize inorganic materials altered to be solution-processible by, for example, attaching ligands to nanoparticles [14] (although this often comes at the cost of reduced performance compared to bulk or thin film properties).

Bioelectronics is another area that looks set to incorporate more organic materials into conventional electronic devices [15]. Due to their chemical similarity, organic materials are better suited to applications such as neural probes that interface directly with physiological tissue [16]. Use of very specific organic molecules may also be necessary in applications such as biosensors [17].

1.1.1 Processing Advantages and Challenges

The ability to solution-process organic electronic materials offers some potentially significant benefits. However, the solubility of organic materials turns out to be both a blessing and a curse in the fabrication of electronics. Once a soluble organic material has been deposited it generally *remains* soluble. Contact with any other organic solvent will damage it at best and most likely remove it completely which puts significant restrictions on subsequent processing steps. Further solution-processed organic layers cannot be deposited on top of the first, causing two problems:

1. Devices with more than one stacked organic layer are prohibited, as may be desired for example in polymeric organic light emitting diodes (OLEDs), and,
2. Patterning that requires any type of organic resist on top of the organic layer is also prohibited as organic solvents are required for deposition, development and stripping of the resist material. This includes patterning the organic itself or patterning inorganic materials on top of it, e.g. by lift-off.

These issues, referred to throughout as "the solvent problem", directly motivated the development of orthogonal processing (described below) and the work described in subsequent chapters. Reaching a convincing solution would have significant benefit to both the manufacture and understanding of organic electronic devices. To date, much of the investigative work on organic electronic materials has been done with simple, single-layer device architectures. However, the body of work on more complex architectures is growing as researchers find ever inventive approaches, reviewed in the next section, to circumventing the solvent problem.

1.2 A Review of Organic Patterning Methods

This section reviews methods for patterning organic materials, with an emphasis on how the use of organic solvents is managed or avoided. Similar topics have previously been reviewed [18, 19] as have techniques to fabricate multi-

layer OLEDs [20], and synthesis of semiconducting polymers with improved processibility [21, 22]. For reference Table 1.1 summarizes all of the approaches featured in the following sections.

1.2.1 Orthogonal Processing

Fluoropolymers are generally only soluble in similarly fluorinated solvents and the resulting fluorinated solutions are immiscible with organic and aqueous solutions. The changes in the nature of the intermolecular bonding (discussed in Section 1.3) give fluorinated materials a tendency to be excluded when intimately mixed with non-fluorinated materials which have stronger intermolecular bonding (which is dispersive in nature for organic compounds and polar in nature for compounds with permanent dipoles), as shown in Figure 1.1. These properties, referred to as chemical orthogonality, allow solution processing steps in which a liquid comes into contact with an organic material to be reversible and non-damaging. This use of fluoropolymers and fluorosolvents for processing organic materials has been termed *orthogonal processing* and is the common theme that unites the chapters of this dissertation.

Figure 1.2 demonstrates the use of orthogonal processing (specifically fluorinated methacrylate polymers dissolved in hydrofluoroethers) to form bilayers with organic materials that do not suffer from interfacial intermixing. The Ober group has previously demonstrated the use of hydrofluoroether (HFE) solvents to process a fluorinated small-molecule resist on top of organics [23] and went on to expand this work in several directions. A polymeric fluorinated photore-

Table 1.1: Comparison of organic processing techniques.

Technique	Bilayers?	Pattern org?	Pattern on org?	Resolution	Device(s)	Ref(s)
Hydrofluoroethers		•	•	80 nm	OTFT	[23, 24, 25, 26]
Fluorinated LE polymers	○	•	•	100 μm	OTFT	[25, 27, 28]
Water-soluble organics	•			-	OLED	[29]
Supercritical CO_2		•		1.3 μm	OTFT	[30]
Interlayer lithography		•		2 μm	OTFT	[31, 32]
Non-chlorinated solvents		•		-	OTFT	[1]
Parylene barrier layer		•	•	1 μm	OTFT	[33]
Cytop barrier layer		•	○	2 μm	Junction	[34, 35]
Al2O3 barrier layer		•	•	?	OLED	[36]
PVA/PMMA barrier layer		○	•	?	OTFT	[37]
Thermal crosslinking	○	○	○	-	OLED	[2]
Cross-linkable side chains	○	•	○	55 μm	OLED	[3, 4]
Cross-linking additive	•	○	○	-	OPV	[38]
Self-patternable conductor		•	•	?	OTFT	[39]
Self-patternable LE polymers		•		?	OLED	[5, 40]
Self-patternable LE polymers		•		?		[6]
Additive metal contact printing			•	500 nm	OTFT	[41]
Additive org. contact printing		•		?	OTFT	[42]
Add./Sub. org. contact printing		•		10 μm	OLED	[43]
Multi. add. org. contact printing	•	•		?	OTFT	[44]
High res. shadow mask			•	75 nm	Biosensor	[45, 46]
Resist bridge			•	100 nm	OTFT	[47, 48]
Strippable mask		○		40 μm		[49]

• = *demonstrated,* ○ = *possible but not demonstrated. Resolutions and devices fabricated are listed where reported but are often not optimized so it is expect that some methods can achieve more than reported.*

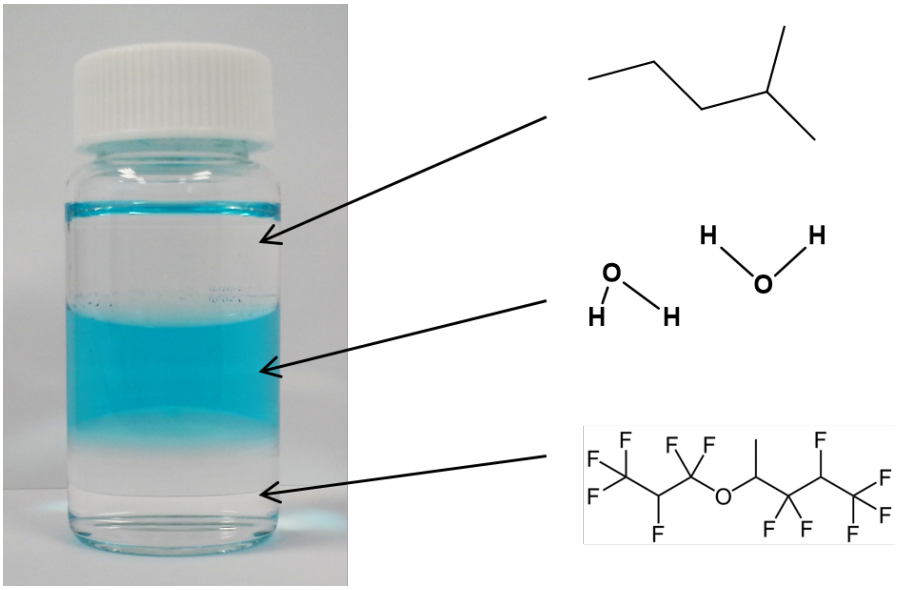

Figure 1.1: A vial containing organic, aqueous and fluorous solvents. It can be seen that hey separate into three layers. Top layer: hexanes (organic), middle layer: water (with blue dye), lower layer: HFE 7600 (fluorous).

sist was developed [24] which is also non-chemically amplified so that acidic materials like PEDOT do not interfere with resist function [25]. The fluorinated small molecule resist, a resorcinarene, is used in multilevel patterning of more than one organic layer, and, in combination with e-beam patterning, can demonstrate negative-tone 80 nm features [26]. Additionally, active materials with a high degree of fluorination are developed such that they can be deposited from HFEs and are not damaged by conventional photoresists [27, 50]. The materials developed comprised a set of light-emitting fluorinated polyfluorenes copolymerized with various moieties to achieve emission in the red, green and blue. With this diverse set of orthogonal solvents, materials and resists a wide range of otherwise unattainable devices can be fabricated, including top-contact P3HT transistors with 200 nm channel lengths and 12-stage ring oscillators based on

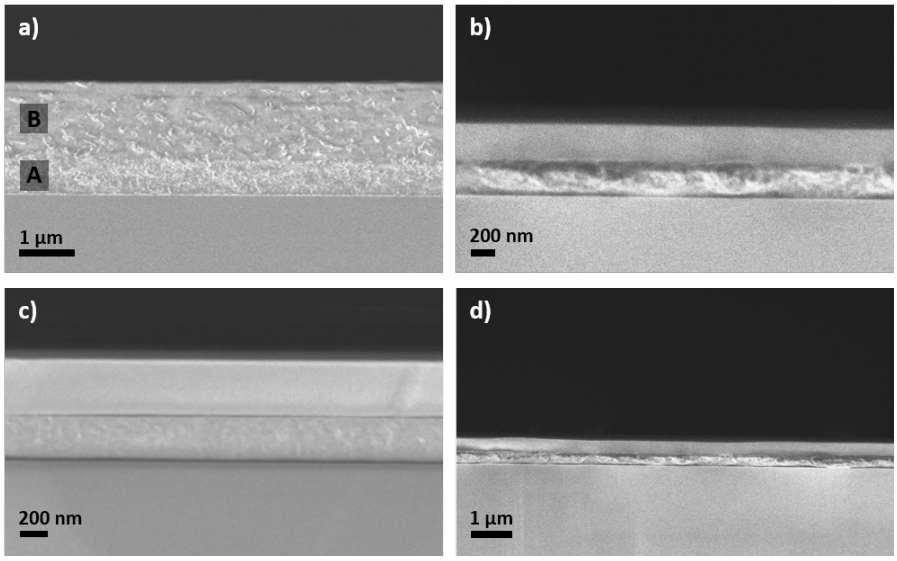

Figure 1.2: SEM images of cleaved cross sections of spincoated bilayers on silicon substrates. a) shows intermixing when an organic is deposited on top of another organic using the same solvent (first layer: 20 mg/ml P3HT in chloroform, second layer: 50 mg/ml PMMA in chloroform), the interface is uneven and the layers are mixed but a clear distinction in contrast can be seen between a lower P3HT-rich region (B) and an upper PMMA-rich region (A) that has picked up flakes of P3HT. b) shows no intermixing when a fluoropolymer is deposited from hydrofluoroethers on top of an organic layer (first layer: 20mg/ml P3HT in chloroform, second layer: 50 mg/ml poly(decafluoromethacrylate) (PFMA) in HFE 7500), c) another example of orthogonal bilayers (first layer: 50 mg/ml PFMA in HFE 7500, second layer: 50 mg/ml PMMA in chloroform), d) same as b) but at lower magnification.

pentacene transistors [25, 28].

1.2.2 Other Non-Organic Solvents

Aside from the fluorinated solvents discussed in the section on *orthogonal processing*, other chemically orthogonality solvents have been suggested. For organic electronics, orthogonal solvents must generally be non-organic. Solubility in organics originates from their lack of polarity, so an orthogonal solvent can be one with significant polarity, such as water. Water-soluble active materials can be used to form organic bilayers [29], but they do not resolve all issues; conventional resists often use an aqueous developer which would damage water-soluble layers. Another solvent option is super critical carbon dioxide ($scCO_2$) which is not polar and a poor solvent for most organic materials. $ScCO_2$ is being used increasingly in a variety of industries as a non-toxic alternative to organic solvents, but a major drawback is the need for specialized equipment to get CO_2 to the necessary temperatures and pressures for super critical behavior.

The **water-soluble** conductive polymer PEDOT is routinely used in organic devices as an injection layer, but use of other water soluble polymers is less common. Gong *et al.* use PEDOT and other polymers to fabricate white polymer light emitting diodes consisting of three layers that are aqueous/organic/aqueous [29]. The device consists of a water-soluble hole transport layer spincoated on top of PEDOT, followed by an organic-soluble emissive blend of two polymers and a metal complex, and finally, a water-soluble electron transporting layer. This is a nice demonstration of the use of orthogonality to achieve multilayer organic devices, but it does not offer the possibility of patterning these devices.

Supercritical carbon dioxide is a poor solvent for most organic materials but has a high affinity for fluorocarbons. Hwang et al. developed a copolymer photoresist [30] composed of tert-butyl methacrylate (TBMA), to provide patternability, and 1H,1H,2H,2H-perfluorodecyl methacrylate, to provide solubility in $scCO_2$. Negative tone images are formed through deprotection of the TBMA and development in $scCO_2$. After pattern transfer into the underlying organic via reactive ion etching, treatment with hexamethyldisilazane is used to re-protect the TBMA so the remaining resist can also be stripped in $scCO_2$. The authors demonstrated patterns down to 1.3 μm and fabrication of OLEDs.

Huang *et al.* developed a process they termed interlayer lithography that patterns an organic resist under a water-soluble active material like PEDOT via lift-off [31]. Further active organic layers can be deposited on top of the PEDOT layer and patterned in the same lift-off step provided they are compatible with the developing solvent. SU-8 photoresist is used in this way to pattern PEDOT and multiple polyfluorenes to 2 μm features on silicon, glass and flexible plastic substrates with lift-off in propylene glycol methyl ether acetate (PGMEA). Leem *et al.* used interlayer lithography to fabricate PEDOT transistors also [32]. Drawbacks include having to expose the active material to UV in the process of exposing the underlying resist, the active material having to be resistant yet permeable to the developer and the resist remaining in place after patterning.

Just as environmental considerations influence which fluorosolvents to use, environmental considerations may also be a factor to consider when it comes to other solvents commonly used in processing organic electronics. Liu et al. sought to avoid the use of chlorinated solvents in the fabrication of P3HT or-

ganic thin film transistors (OTFTs) and developed polythiophene derivatives processible in benign alternatives such as tetrahydrofuran, toluene and xylene [1]. Using this system they fabricate transistors with mobilities up to 0.18 $cm^2V^{-1}s^{-1}$.

1.2.3 Barrier Layers

Protective barrier layers can be used to prevent redissolution of a deposited material. Barrier layer materials must be impervious to the solvents used and non-damaging to the underlying organic. As these requirements are not particularly strict a wide range of materials have potential to be barriers on an equally wide range of organic active materials. A key issue is the removal of the barrier layer after processing which can be difficult when use of organic solvents is not an option. Complications include damage to and contamination of the underlying organic.

DeFranco *et al.* use parylene as a barrier layer [33]. Deposited by chemical vapor deposition, it forms an inert, pin-hole free film impervious to organic solvents. Patterning with conventional organic resists and solvents can then take place on top of the parylene and patterns are transferred to the organic, through the parylene, by a dry etching step. The parylene layer can then be mechanically peeled off leaving the patterned organic. Pentacene, PEDOT and ruthenium tris-bipyridine features down to 1 μm were demonstrated.

Dhar *et al.* use a similar technique but with Cytop as their barrier layer

[34]. Cytop has the advantage of being solution processible from fluorosolvents which are chemically orthogonal to organic materials. Dhar *et al.* demonstrate its use with P3HT and an n-type organic small molecule, naphthalene tetracarboxydiimide, in order to study lateral organic heterojunctions. Chang *et al.* also used a Cytop barrier layer to fabricate lateral organic heterojunctions [35].

Another work uses a 1.2 Å inorganic barrier layer of Al_2O_3 deposited by atomic layer deposition (ALD) [36]. This is deposited on top of poly[1-methoxy-4-(20-ethyl-hexyloxy)-2,5-phenylene vinylene] (MEH-PPV) which is solution processed from toluene. In this case the barrier layer both protects the underlying organic during lithographic processing and improves device function as the Al_2O_3 acts as an electron injection/hole blocking buffer layer in the OLED devices fabricated.

Kuo and Jackson demonstrate a system that used three polymeric barrier layers [37], all formed by spincoating. Water soluble polyvinylalcohol (PVA) was deposited on top of the organic to protect it from organic solvents. A polymethylmethacrylate (PMMA) layer protects the PVA during a later developing step that uses an aqueous base. A cross-linked PVA layer is used to prevent intermixing between the PMMA and a conventional organic resist. Patterning can then be conducted on top of the PVA/PMMA/PVA stack using conventional photolithography. The pattern is transferred through the top two barrier layers and half of the lower PVA layer by a dry etch, then the organic is revealed with a final water etch. Metal contacts can be deposited and the resist stack removed by lift-off in water. This technique is used to fabricate top-contact pentacene transistors with channel lengths down to 6 μm. Aside from complexities arising

from using so many layers, there is no way to precisely time the water etch step such that the organic is exposed but the resist stack does not begin to lift off. Exposure of the organic to water may also be detrimental.

1.2.4 Crosslinking

Crosslinking polymeric active layers after deposition can be used to make them insoluble and it is certainly advantageous that they are then resistant to all solvents (except, possibly, for some swelling). The challenge is to restrict crosslinking to parts of the molecule that are not conjugated because crosslinking that interferes with or interrupts the conjugated π-system can negatively affect electrical and optical properties.

It is worth mentioning the role of **baking** at this point. Baking or annealing a material deposited from solution may well reduce the rate and/or extend of redissolution during deposition of a second layer, but will not eliminate it completely. It is likely that device performance is negatively impacted by the disordered interfaces that result from intermixing, but no extensive study of its effects in organic electronics an be found.

Klarner *et al.* developed a method to end-cap polyfluorene chains with thermally crosslinkable groups [2], as shown in Figure 5.2 a). The vinyl end groups can be crosslinked by annealing at 175-200 °C in an air-free environment to yield an insoluble layer with unchanged emission properties (presumably because the cross-linking density is so low).

Polyfluorenes were also worked on by Muller *et al.* who developed a set of polymers with crosslinkable side chains [3]. The fluorene monomer was copolymerized with moieties to both achieve red, green and blue emission and another oxetane-functionalized moiety (Figure 5.2 b) to make the materials photosensitive. On exposure to UV light, an ionic photo-acid generator produced H+ opening the oxetane ring and initiating cross-linking. As this approach also allows patterning, an OLED with red, green and blue pixels is fabricated via multiple patterning steps. More recently Charas et al. also developed similar polyfluorenes with oxetane sidechains [4] but used an oxetane functionalized phenylene monomer to give the sidechains more mobility, see Figure 5.2 d).

Approaches discussed so far have all dealt with a specific functional polymer, but the utility of the crosslinking approach would be significantly increased if it could be applied more generally. Png *et al.* developed such a technique using a bis(fluorophenyl azide), shown in Figure 5.2 c), as a separate additive to photocrosslink the alkyl sidechains of any conjugated polymer [38]. Interestingly, this approach was then used in the fabrication of bulk heterojunctions (BHJs) for photovoltaic cells, rather than OLEDs or OTFTs as in most other cases. An initial BHJ was deposited with only one phase containing the crosslinker so that the second phase could be washed out and replaced with another material.

Cross-linking that can be applied to any material resulting in resistance to all solvents is an exciting prospect. The key question is whether cross-linking can realistically be extended to other systems without compromising their functional properties, or is it inevitable that the conjugated system will always be interrupted to some small extent? The use of crosslinking for OPV fabrication

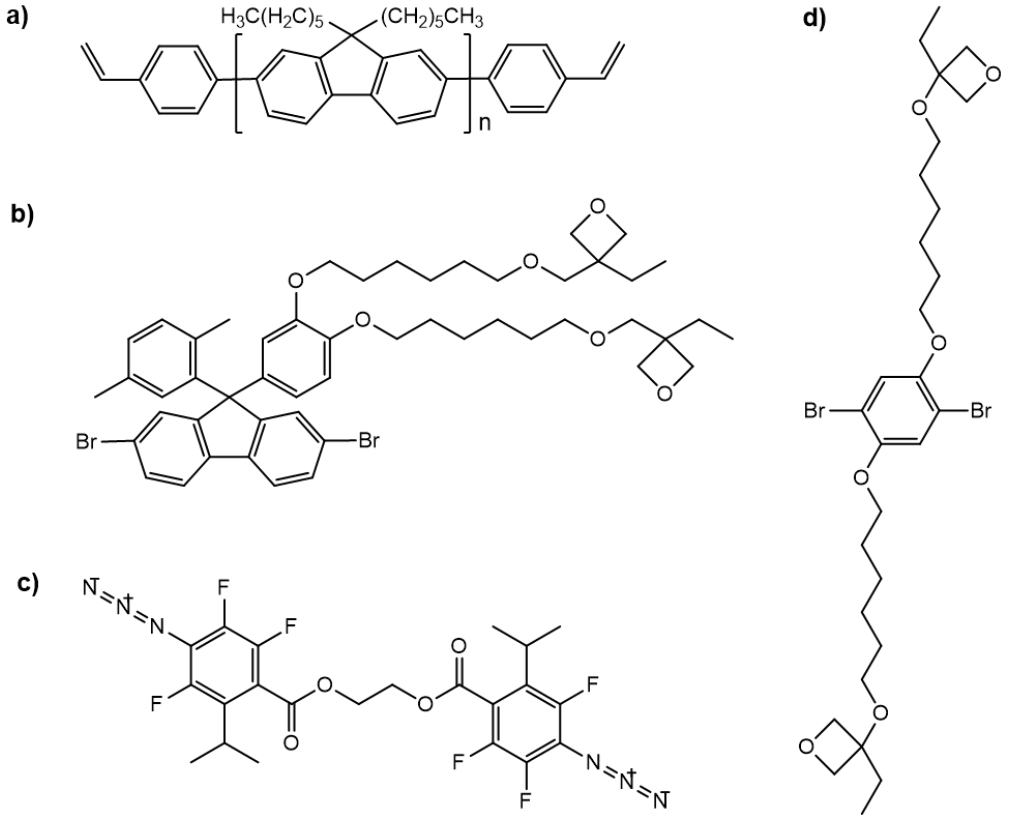

Figure 1.3: Chemical structures of the cross-linkable materials, including a) polyfluorene with thermally cross-linkable end groups, b) oxetane-functioalized moiety used in the synthesis of cross-linkable polyfluorenes by Muller *et al.* c) cross-linking additive ethylene bis(4-azido-2,3,5-trifluoro-6-isopropylbenzoate) and d) oxetane-functioalized moiety used by Charas *et al.* Adapted from [1, 2, 3, 4].

also suggests that the applications of a solution to the solvent problem could go beyond the patterning and multilayer formation discussed in this review.

1.2.5 Self-Patternable Materials

Self-patternable materials are active materials that incorporate some photoresist-like properties such that they are functional but also responsive to light in a way that makes them patternable. Use of self-patternable materials reduces the number of processing steps and therefore offers a route to avoiding redissolution of organics - they can be patterned without spincoating and developing photoresist on top. One way to achieve self-patterning is to induce crosslinking reactions which, in this review, are covered in the section on resistance to solvents. In this section the self-patternable materials discussed respond to light either with a change in solubility or a change in functional properties.

The self-patterning approach was demonstrated by Drury *et al.* using doped polyaniline (PANI) films [39]. A photo acid generator was included in spin-coated films of PANI that, when exposed to light, protonated the PANI rendering it significantly less conductive, as shown in Figure 1.4 a). Unexposed regions with a sheet resistance of 103 $\Omega/\square$ changed to 1014 $\Omega/\square$ after exposure to ultra violet (UV) radiation. The PANI layer was used to form the electrodes of bottom-contact all polymer transistors with 2 μm channel lengths.

Self-patterning of light-emitting active layers can also be achieved by photobleaching. Krebs and Jorgensen adapted polyphenylenevinylene (PPV) to make it photobleachable in air on exposure to UV [5]. Dioctyl- and didodecyl-substituted PPV, as in Figure 1.4 b), are shown to degrade during exposure. The authors hypothesize that this occurs by the cycloaddition of oxygen to the vinylene groups. Krebs and Spanggaard later demonstrated the use of this technique

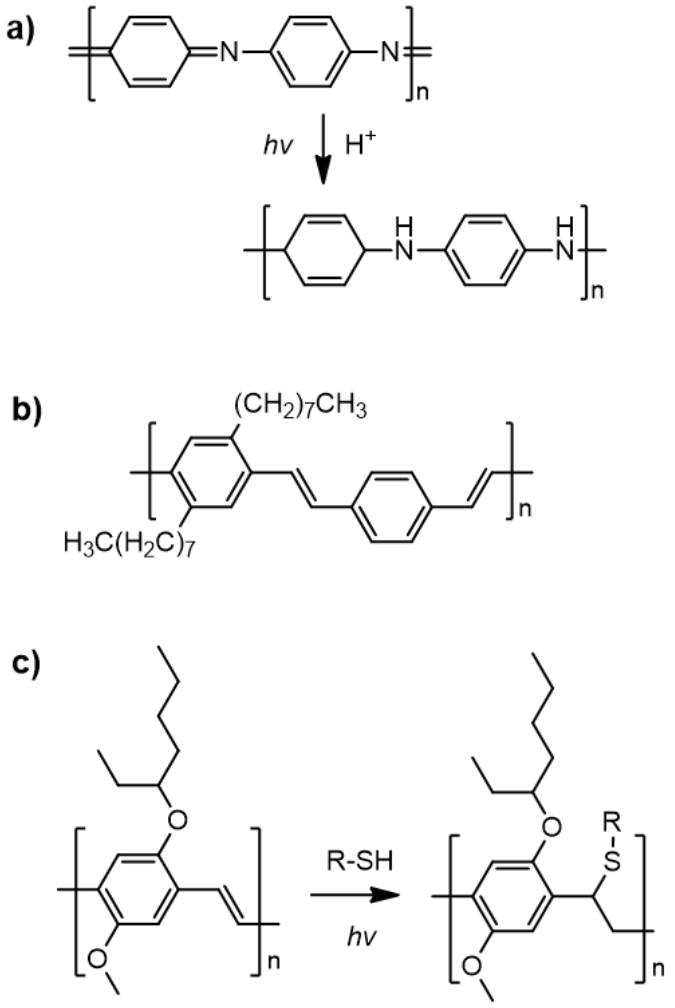

Figure 1.4: Chemical structures and photoreactions of the self-patternable materials, including, a) protonation of PANI, b) structure of photobleachable dioctyl-substituted PPV, and, c) thiol-ene type photobleaching of MEH-PPV. Adapted from [5, 6].

to fabricate and test OLED structures [40]. After photo-bleaching, metal contacts were deposited on top to form complete devices (and the photobleached material remained in place). A later work by Vasilopoulou *et al.* used a similar approach, but interestingly, the emission color could be tuned from red through to green and then blue by varying the exposure dose [6].

Pogantsch *et al.* show that MEH-PPV mixed with dodecanethiol is self-patternable [51]. When exposed, a photo-induced thiol-ene reaction occurs saturating the vinylene units and causing photo-bleaching, see Figure 1.4 c). The authors ingeniously extended this concept to a blend of MEH-PPV and poly(9,9-dioctylfluorene) (PF8) such that the emission color could be tuned from green to blue via patterning.

Unfortunately, the techniques in this section on avoiding solvents are for the most part tailored to specific applications or materials. Shadow masking is restricted to patterning *on* organics; contact printing is material specific due to adhesion forces; barrier layers are material specific due to interlayer interactions; self-patterning properties are restricted to just a few chemical structures. There are also other concerns that would hinder their widespread use: shadow masking is difficult to align to other layers, barrier layers are difficult to remove and very few molecules are self-patternable. To develop more sophisticated and general techniques, solvents are necessary and close attention must be paid to their selection

1.2.6 Contact Printing

Contact printing uses a prefabricated stamp, often made of polydimethylsiloxane (PDMS), with raised features that can vary in size from several hundred microns down to a few microns or even tens of nanometers. The stamp can either be loaded with a material and applied to the substrate for additive patterning, or used as-formed for subtractive patterning. Of great importance is the

control of adhesion forces between the material to be deposited and the stamp, and how they compare to those forces between the material to be deposited and the substrate. These can be tuned to some extent by the use of surface treatments and modification by self-assembled monolayers, often making the stamp specific to a certain material. Limited scope to vary the specificity of these adhesion forces ultimately restricts the range of materials that can be deposited in this way. Also, the effect of subjecting underlying layers to applied pressures is unknown but unlikely to be beneficial.

Loo *et al.* used PDMS, fused silica and gallium arsenide (GsAs) stamps for additive contact printing of gold features on PDMS-coated polyethylene terephthalate (PET) substrates [41]. Gold and a thin layer of titanium were evaporated on the stamp. The gold adheres poorly to the stamp and the titanium improves adhesion to the substrate. 500 nm wide lines were achieved with the GaAs stamp. This technique was used to fabricate top-contact pentacene transistors that were shown to operate comparably to ones fabricated by shadow masking.

Additive contact printing of an organic was shown by Park *et al.* also using a PDMS stamp [52]. The stamp was inked by drop-casting poly-3-hexylthiophene (P3HT) from chloroform and dried with a flow of nitrogen. The P3HT was then stamped onto a prefabricated bottom-contact transistor architecture, the surface being predominantly silicon dioxide. The thickness of the printed P3HT was varied from 100 500 nm but the lateral resolution was not reported. Granlund *et al.* demonstrated subtractive (and additive) patterning of polymers using a PDMS stamp [43]. Poly(3,4-ethylenedioxythiophene) (PEDOT) was spin coated from a water and glycerol mixture on to glass, then pressed against a PDMS

stamp which removed sections leaving lines patterned down to 10 μm. As well as patterning organic layers, contact printing can also be used to form organic bilayer structures. Li and Guo demonstrated forming PEDOT electrodes on pentacene by contact printing [44]. Again, a PDMS stamp was used and top contact pentacene transistors were made with 2 μm channel lengths.

1.2.7 Shadow Masking

Shadow masking uses simple physical masks cut into a metal sheet and avoids solvent use completely. This technique has been the workhorse patterning technique to thermally deposit metal electrodes on top of organics with dimensions of tens of microns. Although it can be used to pattern on top of organic materials via thermal evaporation, it does not solve the problem of fabricating multiple organic layers. Low resolution is the main drawback of shadow masking, but this can be improved by the fabrication of more sophisticated masks. The highest resolution achieved with shadow masking used masks etched into suspended silicon nitride membranes. Metal dots and lines as small as 16 nm across are demonstrated on inorganic substrates [45]. Vazquez-Mena *et al.* recently used similar silicon nitride masks to fabricate 25 nm dots and 75 nm lines on polymer substrates including polyimide, paralyene, polydimethylsiloxane (PDMS) and SU-8 photoresist [46].

Yagi *et al.* used a related approach to form an undercut resist bridge that was in contact with the substrate [47]. They did this using a spin-coated trilayer resist system of polymethylmethacrylate (PMMA) (950k)/PMMA(495k)/MMA

exposed with electron beam lithography. The lower layers had greater solubility in the developer resulting in an undercut profile which cleared completely and formed a bridge if the feature was small enough. An organic semiconductor and metal contacts were deposited by evaporation and the resist bridge structure was left in place. In collaboration with Ante *et al.* this technique was used to fabricate organic transistors with sub-100 nm channel lengths [48].

Another variation on the theme of shadow masking was the demonstration of a strippable mask [49] by Ogihara *et al.* They electrodeposited nickel films onto a conductive indium tin oxide substrate pre-patterned with photoresist. After stripping the resist, organic materials were drop-cast on the nickel mask which has sufficient mechanical strength to then be stripped in one piece. Patterning of carbon nanotubes and titania nanoparticles was demonstrated. Examples did not include any organics, but this technique could presumably be extended to patterning organics.

1.3 Fluorinated Materials: Properties, Applications and Environmental Considerations

Fluorinated materials are central to the orthogonal processing used throughout this work. The unusual properties of fluorinated materials that make them so well suited for *orthogonal processing* derive from the atomic properties of fluorine and how it affects the the C-F bond and intermolecular bonding. Some background on these topics is provided next followed by sections on fluoropolymers

and fluorous solvents to give an idea of how extensively fluorinated materials are used in today's world and how their properties are currently utilized.

1.3.1 Bonding and Intermolecular Forces in Fluorinated Materials

The C-F bond itself is extremely strong [53]. The neon-like configuration it allows fluorine to adopt is particularly stable and unlikely to react further resulting in the characteristic inertness of fluorinated materials. The bond that forms between the most electronegative element, fluorine (3.98), and carbon (2.55) also has a significant dipole moment.

The intermolecular forces between fluorinated materials are of utmost importance in this work because they lead to the very miscibility and solubility properties that underpin *orthogonal processing*. They also determine a number of other useful properties of fluorinated materials [54]. To be more specific, intermolecular forces govern the adhesion of monolayers in Chapter 2, prevent interfacial intermixing in Chapter 3 and determine droplet formation and spreading in Chapter 4.

There are various types of intermolecular forces between molecules including charge-charge interactions, dipole-dipole interactions, charge-dipole interactions, hydrogen bonding and van der Waals dispersion forces [55]. In fluorinated materials charge-charge, charge-dipole and hydrogen bonding do not

normally play a role, leaving polar and dispersive forces.

Considering the significant dipole moment of the C-F bond it might be expected that fluorinated materials have significant polar character, but that is not the case. Due to mutual repulsion of the electronegative fluorine atoms, perfluorinated chains of any length adopt a helical configuration [54] (as opposed to the zigzag configuration of alkyl chains) as shows in Firgure 1.5. In this configuration all dipole moments cancel each other out, as in carbon dioxide, to result in a material that is not polar. As well as eliminating polar intermolecular interactions this configuration also contributes to the inertness of fluorinated materials because the outer negative fluorines provide both electrostatic and steric shielding of the central carbon chain from neucleophilic attack.

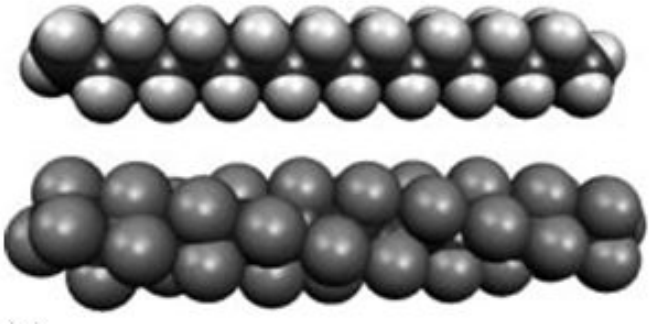

Figure 1.5: A comparison of the zigzag configuration of alkyl chains (upper) with the helical configuration of perfluorinated chains (lower). Adapted from [5, 6].

Dispersive forces, specifically London dispersion forces, exist between all atoms and molecules and are the result of interactions between the molecules' electron clouds resulting in instantaneous dipoles. The magnitude of these forces is proportional to the square of the polarizability [55]. Due to its atomic

structure fluorine has a very low polarizability resulting in significantly reduced London dispersion forces [56]. Hence, in total, fluorinated materials have very weak intermolecular forces compared to other materials.

1.3.2 Fluoropolymers

Fluorine is incorporated into polymer structures for a variety of reasons. Sometimes just one fluorine atom is sufficient, sometimes all hydrogen positions are filled by fluorine atoms. The inclusion of fluorine can lead to significant changes in the material's properties as described above.

Figure 1.6 shows some examples of fluoropolymers. Poly(tetrafluoroethylene) (PTFE, Teflon®) is the most well known and most manufactured fluoropolymer. Infamously stumbled upon at DuPont in 1938, Teflon is one of the most cited accidental discoveries of the 20th century. (When a cylinder thought to contain tetrafluoroethylene gas appeared prematurely empty Plunkett and his team sawed it in half to find a solid white residue with remarkable properties - the gas had polymerized to form PTFE.) PTFE is still produced by polymerization of tetrafluoroethylene gas with annual production at about 10,000 metric tons (small compared to the 80,000,000 metric tons of polyethylene produced annually). At one time used in the Manhattan project to line vessels containing uranium hexafluoide, it is now used extensively to coat anti-stick cookware. Both applications take advantage of PTFE's inertness resulting from being completely fluorinated. It is also very hydrophobic and stable at high temperatures (melting point = 327 °C) [57]. Its extremely low coefficient of friction also makes

it useful for bearings and sliding parts [58]. PTFE's high melting point makes it difficult to process so alternatives such as perfluoroalkoxy (PFA) polymer and poly(vinylidene fluoride) (PVDF) are often used as they have similar properties but are melt-processible and injection moldable. Organization of the alternating CH_2 and CF_2 groups of PVDF also make it piezoelectric [59].

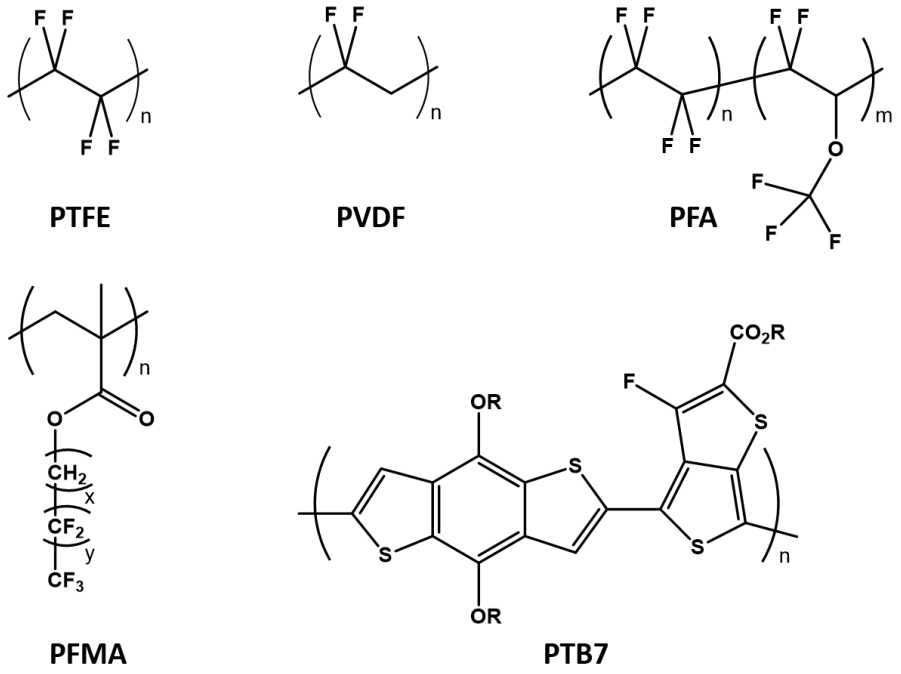

Figure 1.6: The chemical structures of selected fluoropolymers. In PFMA x and y can assume any value but are typically in the ranges $1 \leq x \leq 6$ and $0 \leq y \leq 11$.

Fluorine can be used to modify the electronic properties of semiconducting polymers. Figure 1.6 shows the structure of a benzodithiophene thienothiophene (PTB7) in which a single atom of fluorine has been incorporated. This lowers the highest occupied molecular orbital (HOMO) by 0.1 eV compared to the non-fluorinated analogous polymer, which is desirable in polymer blend solar cell applications [60].

Fluorinated methacrylates have a methacrylate backbone and fluorinated side chains of varying lengths. They are not manufactured in any great quantity, but are used in research because they exhibit typical fluoropolymer properties and are easily synthesized [61]. Consequently they can be adapted and incorporated into polymer brushes [62] and block copolymers [63]. The fluorinated side chains have been shown to align at the surface [64] allowing careful control of the surface energy [65]. Fluorinated methacrylates are used extensively in the work described in this dissertation.

1.3.3 Fluorous Solvents

Fluorous solvents have many of the same properties as fluoropolymers but are small molecules with significantly lower molecular weight. Well-known families of fluorinated solvents include low molecular weight hydrofluorocarbons and hydrofluoroethers (HFEs); although the former are undesirable for environmental reasons. HFEs were originally developed as replacements for chlorofluorocarbon (CFC) refrigerants [66] and have since found other application, e.g. in the electronics industry as cleaning fluids [67]. They are non-toxic [66], have zero ozone depletion potential [68] and are commercially available with boiling points ranging from 61 to 131 °C. This makes them ideal for orthogonal processing and they are the default solvent used throughout this work.

1.4 Summary and Dissertation Outline

The solvent problem, namely that deposited organics remain soluble in organic solvents, restricting subsequent processing steps, has important implications for the fabrication of devices containing organic materials. As the solvent is just a vehicle for deposition or removal, the choice of solvent is often overlooked. Gains can be made in the field if the solvent choice and effects are given more careful consideration. As well as affecting microstructure and properties, it is really the solvents used that determine the processibility of organic materials, including whether they can be patterned or used in multilayer architectures.

The literature review shows that current solutions to the solvent problem are varied and creative. The majority of approaches have been developed for a specific material or device and their abilities are split; some allow for the fabrication of multiple stacked organic layers, others allow for patterning of, or on, organic materials, as summarized in Table 1.1. Considering that the ultimate goal of this area of research is the large scale manufacture of organic-containing or flexible electronics, a comprehensive approach that allows for both multilayer formation and patterning would be preferable.

Orthogonal processing and the use of fluorinated materials offers by far the most widely-applicable and adaptable approach to processing and patterning organic materials. Although the other approaches reviewed, particularly cross-linking, might offer additional benefits, it is orthogonal processing that will form the base of this platform and offer a realistic route to a sound solution. For this reason, orthogonal processing is further developed and investigated in

this dissertation.

The projects described in the following chapters utilize orthogonal processing with fluoropolymers and fluorous solvents to demonstrate new processes and investigate new issues. Chapter 2 looks at how a fluoropolymer active material can be used to make light-emitting monolayers. Chapter 3 uses a fluoropolymer as a barrier layer to allow photolithographic patterning of organic materials with conventional photoresists. Chapter 4 examines the issues related to inkjet printing fluoropolymers for low-end, roll-to-roll compatible patterning of organic materials. Lastly, Chapter 5 investigates the feasibility of developing a fluorinated positive-tone resist for high resolution electron beam patterning.

CHAPTER 2

FLUORINATED POLYFLUORENE MONOLAYERS

Acknowledgment

This project was conducted as a collaboration with Thomas Piachaud and Richard Friend at the University of Cambridge, UK. Some measurements were conducted at Cornell solely by myself (Contact Angle, AFM, NEXAFS), some were conducted at Cornell by Thomas Piachaud and myself (Fluorescence Microscopy, XPS) and some were conducted at the Univeristy of Cambridge solely by Thomas Piachaud (PTDS, photoluminescence, electroluminescence, device characteristics and luminance efficiency). As all measurements contribute to a full picture of the phenomena described in this chapter, much of these data appear in the PhD dissertations of both myself and Thomas Piachaud.

The fluorinated polyfluorene polymers used in this project were synthesized by Jin-Kyun Lee and Seok-Hun partially at Cornell University and partially at Inha University, Korea. The fluorinated fluorene monomer used in some polymerizations was synthesized by Cambridge Display Technologies Ltd. (UK). The XPS measurements were conducted using CCMR equipment with the help of John Shu. The NEXAFS measurements were taken at the National Synchrotron Light Source (NSLS) at Brookhaven National Lab.

2.1 Abstract

The emissive layers of polymer light emitting diodes are typically deposited via spincoating which limits their thickness to 10 nm or more. Incorporating thinner layers into devices has not been investigated for lack of a fabrication technique compatible with conjugated polymers. In this chapter a new solution processing technique is described that allows reliable fabrication of monolayers of fluorinated polyfluorenes, electroluminescent conjugated polymers, that can be incorporated into stacked devices. The monolayers formed are consistently measured to be 1-2 nm thick and, remarkably, are found to be continuous and pin-hole free, making them suitable for use in devices. When incorporated into polymer light emitting diodes, light emission is observed from solely the 1-2 nm thick monolayer, representing a significant confinement of the recombination zone.

2.2 Introduction

A polymer light emitting diode (PLED) is a type of organic light emitting diode (OLED) in which the emissive layer is a film of amorphous, electroluminescent polymer which emits light in response to an electrical current. Use of polymeric active materials in devices is attractive due to their ability to be solution processed allowing low cost manufacture of large area, low-weight, flexible electronics via roll-to-roll fabrication. This advantage is balanced, however, by a frustrating lack of precise control over the deposition of the polymer. There is a need to gain better control over their lateral and vertical placement and their microstructure once deposited. Progress is being made in the areas of patterning

methods [19] and synthesis of specialized polymers [22] for this purpose.

The aim of the work described in this chapter is to reduce the thickness of the electroluminescent conjugated polymer layer to its ultimate limit - a monolayer - then characterize it and observe its behavior in a device. Normally, conjugated polymers are deposited via spin-coating, but it is difficult to form continuous films less than 10 nm thick [69], especially with rigid rod-like conjugated polymers. Molecular beam epitaxy can deposit monolayers of conjugated small organic molecules [70], but not conjugated polymers. Some other techniques to form conjugated polymer monolayers have been demonstrated. Yu et al. used evaporation from a solvent mixture to form self-assembled sheets of P3HT [71] while Onoda and Yoshino [72] and Fou et al. [73] used layer-by-layer assembly to form alternating layers of charged conjugated polymers. However, these techniques are restricted to quite specific polymers and form essentially different structures to those studied here which are single monolayers with the conjugated backbone lying flat on the substrate.

Here a simple solution processing technique is developed that can form a single monolayer of conjugated polymer on a variety of substrates at room temperature. Briefly, as illustrated in Figure 2.1, after spincoating a (thick) bilayer consisting of a conjugated fluoropolymer on a conjugated non-fluorinated polymer underlayer, the majority of the fluoropolymer layer is rinsed away with a selective fluorinated solvent leaving just a monolayer behind. The method relies on the use of orthogonal processing, as described in Section 1.2.

Light-emitting polymers (LEP) were first successfully incorporated into light-emitting diodes in 1990 by Burroughes *et al.* [74] who observed yellow-green emission from poly(*p*-phenylene vinylene) (PPV) in a diode structure. A

Figure 2.1: Monolayer fabrication steps

plethora of PPV derivatives have been synthesized in the years since [75, 76, 77] to achieve better performance, and emission in the red, green and blue regions of the spectrum have been demonstrated. PPV derivatives remain one of the most-studied groups of light-emitting polymers to this day, the only other group which has shown as much diversity and resilience are polymers based on a fluorene unit.

Polyfluorenes (PFO), are named so because they fluoresce, although they *normally* do not contain any fluorine atoms. These are a class of conjugated electroluminescent polymer that appeared in 1991 [78] and have since been explored extensively [79]. Their basic structure is shown in Figure 2.2 where alkyl sidechains are often added to the conjugated backbone to allow solubility in organic solvents. The non-fluorinated polyfluorene used in this work (Aryl-F8) has additional aryl rings in the sidechain and emits in the blue region of the spectrum [80].

Fluorinated polyfluorenes (FPF) have the standard polyfluorene backbone but with fluorinated sidechains to give solubility in fluorinated solvents. These materials were developed by the Ober Group and have been fully characterized and previously incorporated into organic devices [27, 50]. Further characterization found that their optical properties are very similar to that of their

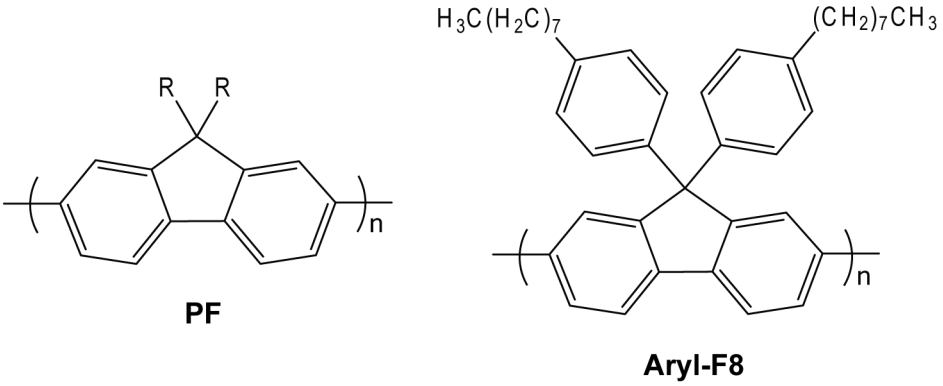

Figure 2.2: The chemical structures of polyfluorene (PFO) where typically R = $(CH_2)_xCH_3$ and poly(9,9-di-*n*-(aryl-4-octyl)fluorenyl-2,7-diyl) (Aryl-F8).

non-fluorinated analogs [81]. The structures of the FPFs used in this study are shown in Figure 2.3. Co-monomers are incorporated into the polymer to tune the emission wavelength to green (FPF-G) and red (FPF-R), then the monomer ratios are adjusted to optimize solubility in the fluorinated solvents.

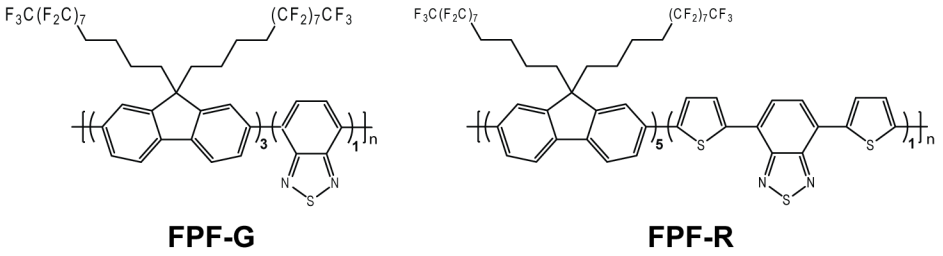

Figure 2.3: The chemical structures of green- and red-emitting fluorinated polyfluorenes.

The behavior of these monolayers in devices is also of significant interest and they can easily be incorporated into PLED devices with stacked architectures. The typical device structure used is shown in Figure 2.4. As hole mobility in LEPs is typically higher than electron mobility, recombination (resulting in

light emission) typically occurs close to the LEP/anode interface. Since the first PLED demonstration in 1990 [74] the device architecture has evolved to incorporate multiple organic layers, as shown in Figure 2.4, in order to improve device efficiency. An electron transporting/hole blocking layer (ETL) is inserted between the anode and the LEP. This serves two roles and is chosen such that it has optimal energy levels. First it increases injection of electrons by creating an intermediate step in the LUMO level and thereby reducing the energetic barrier to electron injection. Second, the deep HOMO level, it was anticipated, would cause a build up of holes in the LEP which would in turn increase the probability of recombination and possibly improve device performance. An analogous hole transporting/electron blocking layer (HTL) is sometimes inserted between the LEP and the cathode but this has a smaller effect on device performance as hole mobility is already higher.

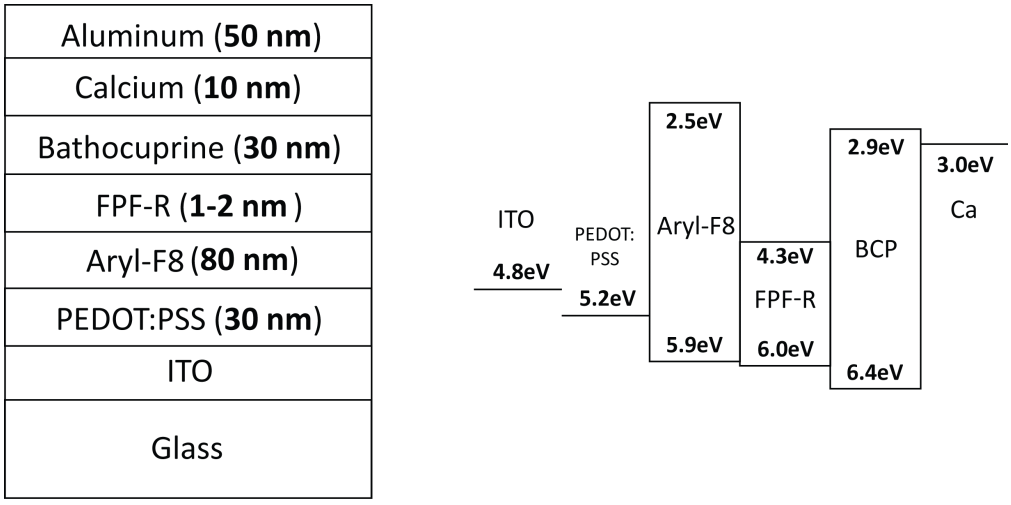

Figure 2.4: Device structure and band diagram of a PLED that incorporates a hole blocking layer and FPF monolayer.

When suitable materials were selected, light emission from these devices is observed from just the 1-2 nm thick monolayer. This represents an unprece-

dented reduction in the width of the recombination zone in a PLED which is typically 20 - 100 nm wide [82]. Variation of the recombination zone has been studied extensively in OLEDs [83] where it has been found that the position, width and number of recombination zones can have a significant effect on device performance and efficiency.

Utilizing a fluoropolymer in this project is necessary not only for the formation of these monolayers but it also aids in differentiating the monolayer from the non-fluorinated underlayer during characterization. Accurate characterization of something with such small dimensions that is also chemically similar in nature to the underlayer is not trivial. However, this approach still provides a rare and valuable opportunity to probe the interface between two conjugated polymers.

2.3 Experimental Methods

Materials

Both the red and green semiperfluoroalkyl polyfluorenes (FPF-R and FPF-G) were synthesized in house, according to the previously described method [50]. The monomers used in these syntheses were largely synthesized in house, but some of the monomer used in fluorinated polyfluorene synthesis was gratefully received from Cambridge Display Technologies.

(Aryl-F8) was also received from Cambridge Display Technologies and used as received (M_n = 386k, PDI = 2.7). Poly[(9,9-di-n-octylfluorenyl-2,7-diyl)-alt-(benzo[2,1,3]thiadiazol-4,8-diyl)] (F8BT) was purchased from American Dye

Source Inc. and used as received. 1,3,5-bis(trifluoromethyl benzene) (BTFMB), pentafluorobenzene (5FB) and xylenes were purchased from Sigma Aldrich and used as received. Test grade silicon wafers were purchased from Wafer Reclaim Services Inc.

Monolayer Formation

The standard method of monolayer formation used in this project is defined as follows: A solution of 10 mg/ml Aryl-F8 in xylenes is spincoated at 2000 rpm for 45 seconds on a 1 cm X 1 cm silicon chip. Next a solution of 10 mg/ml FPF in 5FB is immediately spin coated at 2000 rpm for 45 seconds on top of the Aryl-F8. The sample is then spin rinsed with 50 μl of BTFMB twice. (In the spin rinse the solvent was dispensed on the sample which was then spun at 2000 rpm for 30 seconds.)

Variations on the standard method were used where noted. The Aryl-F8 under layer was sometimes exchanged for F8BT. The fluorinated solvents used to spincoat and rinse the FPF could be 5FB or BTFMB. All solutions used had concentrations of 10 mg/ml. An alternative method of monolayer formation was tested in which a spincoated film of Aryl-F8 was submerged in a 1 mg/ml solution of FPF in 5FB for 30 seconds.

Equipment

Contact angle measurements were performed using a VCA Optima tool and software, at room temperature in a cleanroom environment. A Zeiss 710 Confocal Microscope was used to perform the fluorescence microscopy. All samples

were excited with a 405 nm laser and observed with a 10x objective. AFM was performed using a Veeco Icon AFM in non-contact mode. All NEXAFS experiments were performed at the National Synchrotron Light Source (Brookhaven National Lab) on beamline U7a.

2.4 Results and Discussion

The physical aspects of the monolayers were first investigated to learn more about their thickness, chemical composition and microstructure. Next their electroptical properties were characterized to determine if their light emission differs at all to the bulk material. Finally, monolayers were incorporated into stacked PLED device structures and the electrical characteristics of these devices were characterized. Based onl these data, a mechanism of formation of these monolayers is proposed.

2.4.1 Physical Characterization

Preliminary Experiment

To initially gain an idea of whether these monolayers form as expected, some simple contact angle measurements are made. The results are shown in Table 2.1. Uncoated, the contact angle of the underlying F8BT layer is 97°. With addition of the FPF-R monolayer the contact angle increased significantly to 110° which is typical of all fluoropolymers. The third sample confirms that some of the FPF-R remains adhered to the underlying F8BT layer after the rinse step, al-

Table 2.1: Contact Angle Measurements

Substrate	Underlayer	Monolayer	Formation Method	Contact Angle (±2°)
Si	F8BT	-	-	97°
Si	F8BT	FPF-R	-	115°
Si	F8BT	FPF-R	BTFMB rinse	112°
Si	F8BT	FPF-R	BTFMB 60s soak	110°

All values represent static water contact angles and are an average of three repeats.

BTFMB = bis(trifluoromethyl)benzene.

though the slightly reduced value suggests the coverage may not be 100%. The fourth sample, which was soaked in bis(trifluoromethyl)benzene (BTFMB) for 60 seconds, shows that the monolayers are remarkably stable over a significant time scale.

Fluorescence Microscopy

The aryl-F8 underlayer and the FPF monolayer all absorb radiation at 405 nm but each emit radiation of different wavelengths. This allows the aryl-F8 and the FPF monolayers to be imaged separately using fluorescence microscopy as in Figure 2.5. Images of five samples are split into four showing the red, green and blue channels separately, and a sum of all the channels. The gain for each channel is kept constant across all samples. The scratches at the bottom left of the images serve to confirm that the signal observed is due to light emission from the polymer film and is not due to amplified noise.

Sample 1 is a film of aryl-F8 so emission is seen in the blue channel only and none in the red and green channels, as expected. Sample 2 is a bilayer of

aryl-F8 with a layer of FPF-G on top so that we now see emission in both the blue channel, from the aryl-F8, and the green channel, from the FPF-G layer. It appears that when there is significant emission from the red or green channels the intensity of the blue channel is somewhat decreased. The reason for this is unclear, but may indicate that photons emitted from the underlayer is absorbed by the upper layer. Sample 3 is a monolayer of FPF-G on top of aryl-F8 prepared via the standard method. Again, emission is observed in the blue channel and the green channel, and the green channel signal is fainter where less material is present. This image confirms the presence of FPF-G after rinsing and indicates that it is uniform at this length scale. Similar results are observed for Samples 4 and 5 which show a bilayer and monolayer, respectively, of FPF-R on aryl-F8 so emission is now observed in the red channel instead of the green channel. All evidence supports the formation of monolayers of FPF on aryl-F8.

Fluorescence microscopy can also be used to compare methods of forming the monolayers, as shown in Figure 2.6. Samples 1 and 2 are formed via the standard method where the final spin-rinse step was performed using pentafluorobenzene (5FB) for Sample 1 and bis(trifluoromethyl)benzene (BTFMB) for Sample 2. The green channel signal from the monolayer is slightly stronger in Sample 2 than Sample 1 suggesting that a BTFMB rinse results in a slightly thicker (or denser) monolayer than a 5FB rinse does. In general 5FB is found to be a better solvent for both FPF materials than BTFMB. The monolayer of Sample 3 is formed by a different method: a spincoated film of aryl-F8 is simply immersed in a dilute solution of FPF in 5FB. Fluorescence microscopy shows that this solution method seems to form a thicker (or denser) monolayer similar to that of Sample 2. Samples 4 - 6 are analogous to Samples 1-3 except the monolayers are formed with FPF-R so emission is observed in the red channel.

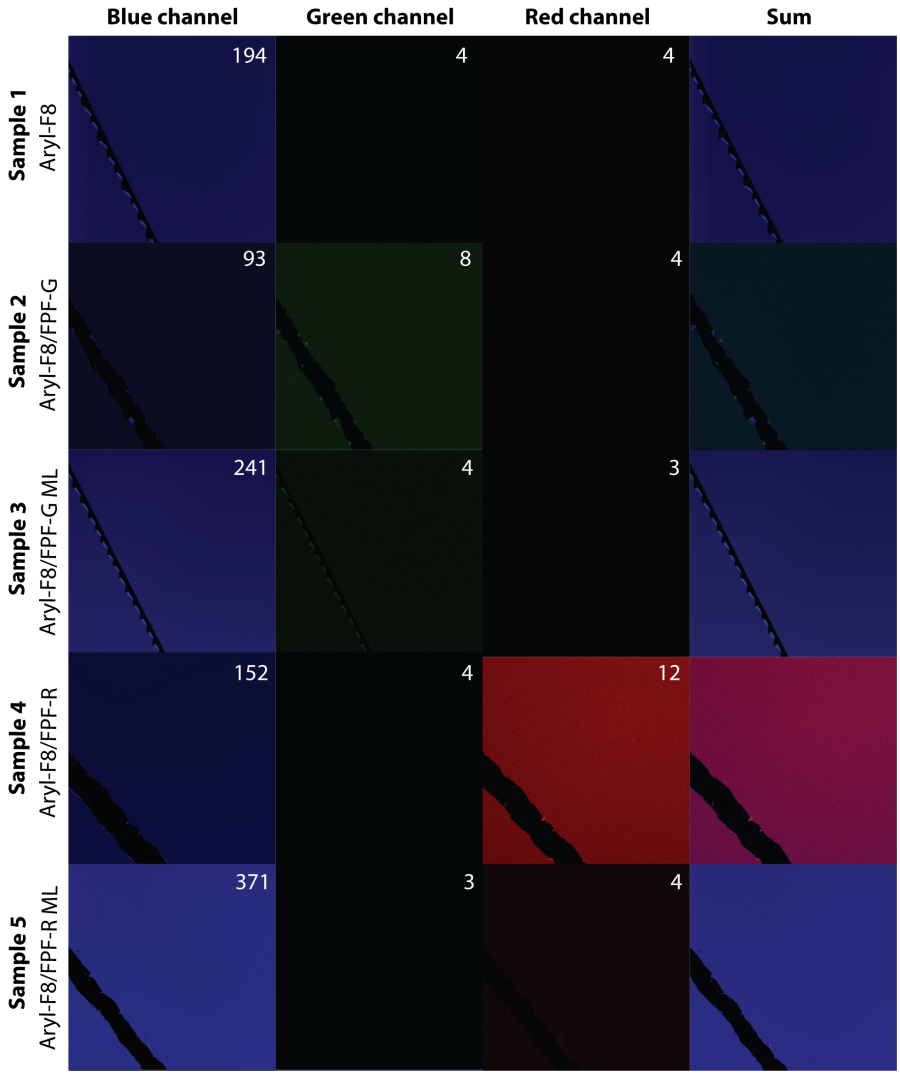

Figure 2.5: Fluorescence micrographs excited at 405 nm. Emission signals observed in three channels: blue (420-440 nm), green (560-570 nm) and red (690-700 nm). The sum represents addition of all channels. Intensity was recorded (averages indicated in white) and false color added later. Sample 1 is a spincoated film of aryl-F8. Samples 2 and 3 are a bilayer and monolayer, respectively, of FPF-G on aryl-F8. Samples 4 and 5 are a bilayer and monolayer, respectively, of FPF-R on aryl-F8. Each image field is 500 μm by 500 μm.

The red monolayers follow the same trend as the green; a 5FB rinse results in a fainter monolayer while a BTFMB rinse and the solution formation method result in slightly brighter monolayers.

Atomic Force Microscopy (AFM)

Figure 2.7 shows AFM images of the same (scratched) sample at each of the steps of monolayer formation. It can be seen that spincoating FPF on top smooths out the features of the underlying F8BT (which is relatively rough for a spin-coated film as it has been annealed). The features of the F8BT then re-emerge when the majority of the FPF layer is rinsed off to leave just the monolayer. The intermediate rms roughness value for the monolayer does support its existence, but also suggests that its thickness is not uniform as it acts to smooth the features of the F8BT underlayer.

X-ray Photoemission Spectroscopy (XPS)

X-ray Photoemission Spectroscopy (XPS) is a surface sensitive technique that reveals the elemental composition of the top ~7 nm of the polymer surface. Figure 2.8 compares XPS scans of F8BT, FPF-R and a monolayer of FPF-R on F8BT. The presence of similar fluorine peaks in the scans of both FPF-R and the monolayer again support the existence of the monolayer. It can be seen that the carbon 1s peak is a single peak in the F8BT sample but forms two peaks in the FPF-R and FPF-R monolayer samples. When carbon is bonded to fluorine its peak is shifted where the extent of the shift depends on the number of fluorine atoms bound to the carbon. For carbon not bonded to any fluorine the peak is at ~285

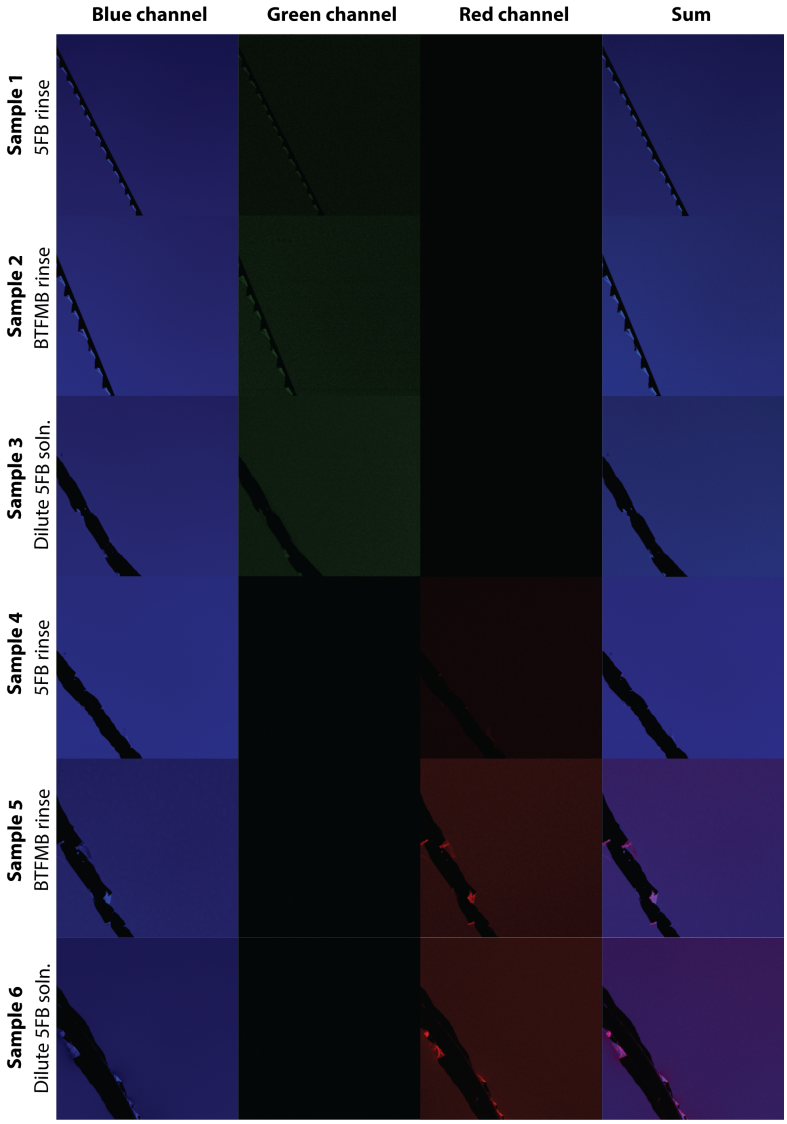

Figure 2.6: Fluorescence micrographs comparing the effect of formation method on monolayer brightness. The channels are set up as in Figure 2.5 and the gain for each channel is kept constant across all samples, allowing comparisons. Each image field is 500 μm by 500 μm.

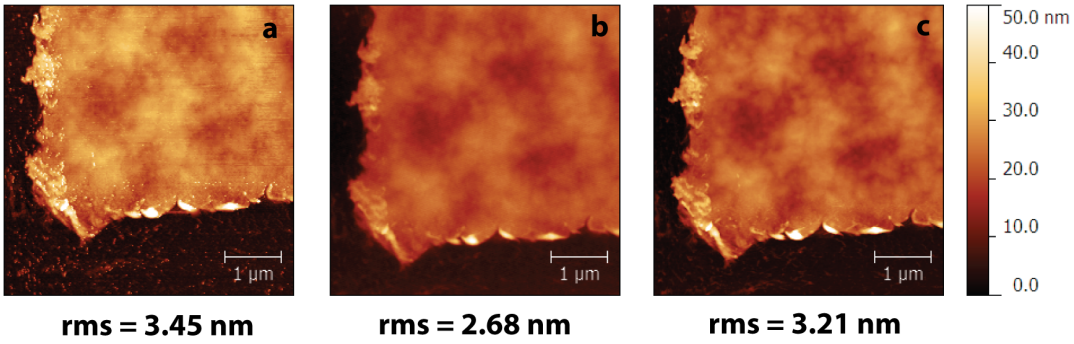

Figure 2.7: AFM images taken at the same location of the same sample at different stages during the monolayer formation process. Namely, a) after spincoating F8BT and scratching it to mark a position, b) after spincoating FPF-G on the F8BT, and c) after rinsing in BTFMB to leave a monolayer of FPF-G on the F8BT.

eV. When bonded to one, two or three fluorine atoms the peak shifts to ~289 eV, ~293 eV and ~296 eV, respectively. What we see in this XPS scan are peaks corresponding to carbon bonded to no fluorine and to two fluorine atoms, which agrees with the chemical structures of the two polymers. As the peak area is proportional to the amount of that element present, these scans indicate that in bulk FPF-R about half the carbon atoms are not bound to fluorine and half are bound to two fluorine atoms, as expected.

Meanwhile, in the monolayer sample the carbon 1s peak representing carbon not bonded to any fluorine is approximately three times the area of the peak representing carbon bonded to two fluorine atoms. The scan samples both the monolayer *and* a portion of the F8BT underlayer. This confirms that the monolayer thickness is indeed less than the sampling depth (~7 nm), but determining the thickness more precisely than that from these data is not possible due to the difficulty of accurately determining the sampling depth (equivalent

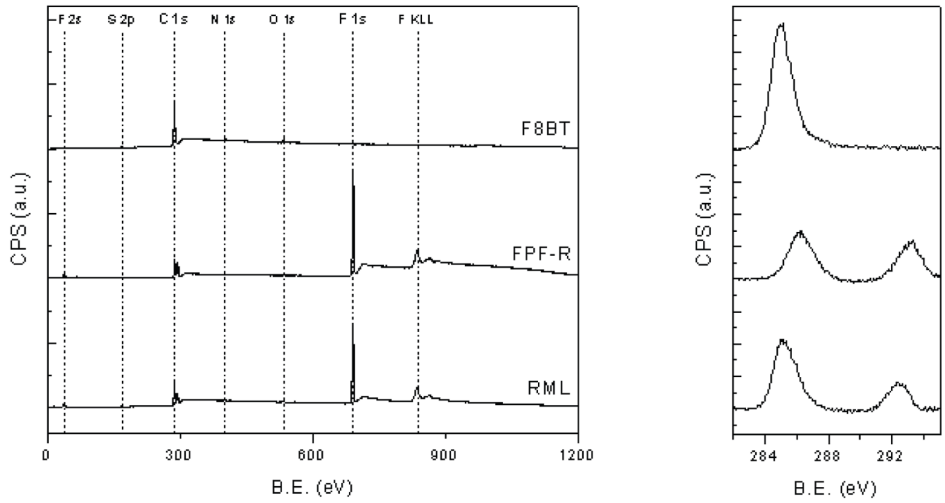

Figure 2.8: XPS scans of F8BT (upper), FPF-R (middle) and a FPF-R monolayer on F8BT (lower). Wide scans are shown on the left and high resolution carbon 1s scans are shown on the right.

to the electron mean free path) which varies between polymers.

Angular resolved XPS (AR-XPS) is commonly used to determine the thickness of surface layers of distinct chemical composition, and that was considered here. However, to accurately determine the surface layer thickness the sample must exhibit one signal (peak) that is exclusively from the substrate, and one signal (peak) that is exclusively from the surface layer, and ideally these peaks should be close to each other on the energy axis [84]. The split carbon 1s peak is almost ideal for this purpose except that one peak comes from the surface layer (fluorinated monolayer) and the other peak comes from *both* the substrate and the surface layer.

Near Edge X-ray Absorption Fine Structure (NEXAFS)

NEXAFS is a surface characterization technique somewhat similar to XPS. A beam of electromagnetic radiation is incident upon a sample resulting in the emission (or promotion to excited but bound states) of photoelectrons *and* emission of secondary electrons due to Auger processes. It is these Auger electrons that are detected [85] yielding detailed information about the types of bonding present in the top 1-2 nm and, by varying the incident angle of radiation, revealing any preferential orientation of each type of bonding.

Figure 2.9 shows NEXAFS scans of the carbon edge of a film of Aryl-F8 and a film of FPF-G. It can be seen that the experimental data can be modeled well by the sum of a modified error function and a series of Gaussian peaks [86]. Quantitative data describing the peaks in given in Table 2.2. Each peak corresponds to a different type of carbon bond while the step corresponds to promoting an electron into the vacuum. The position of the step function is fixed across all samples. The peaks are identified by considering the chemical structure and by comparing the scan to those of known materials. Watts *et al.* published data on the NEXAFS of common conjugated polymers [87] and others on polymers with perfluorinated segments [88, 89, 90, 91].

The scan for Aryl-F8 contains five peaks (A, B, C, D1 and G) very similar to that of a simple polymer like polystyrene [86], while the FPF-G scan contains these same peaks plus four others (D2, E, F and H) thought to arise from perfluorinated chain segments. In the Aryl-F8 scan, the prominent initial A peak is attributed to the C=C π^* energy level and is particularly strong, presumably due to the benzene rings in the side chains of Aryl-F8. Peaks B, C, D1 and G are attributed to C-H σ^*, the C-C π^* 2, the C-C σ^* and the C-C σ^* 2, respectively, as

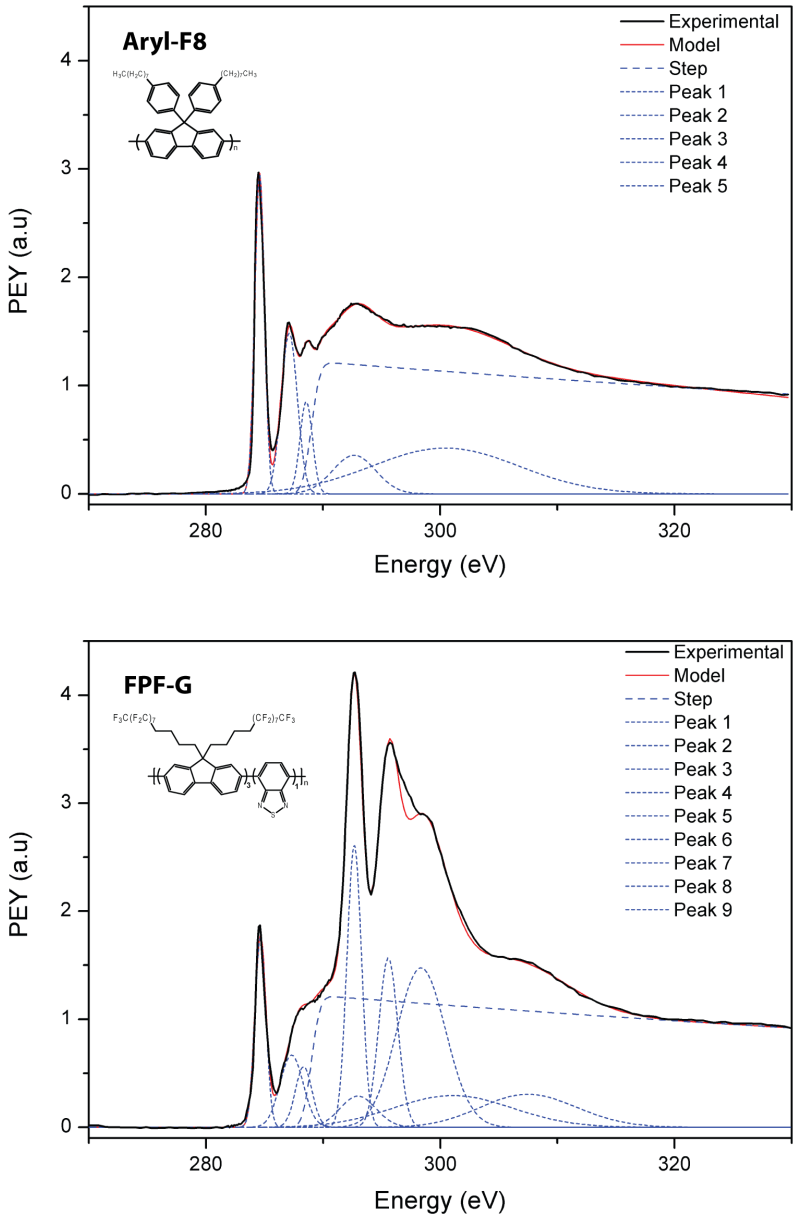

Figure 2.9: NEXAFS scans of 20 nm thick Aryl-F8 (top) and 20 nm thick FPF-G (bottom) films spincoated on silicon. The modified error function and Gaussian peaks are shown that, when added together, form a model fit to the experiment data.

Table 2.2: NEXAFS model specifications

			Aryl-F8		FPF-G		
Label	Position (eV)	Feature	Height	FWHM	Height	FWHM	Bond Assigned
-	289.0	Mod. Erf.	1.200	2.000	1.200	2	Vacuum
A	284.6	Gaussian	2.959	0.957	1.758	1.095	C=C π*
B	287.3	Gaussian	1.484	1.623	0.706	2.199	C-H σ*
C	288.3	Gaussian	0.852	1.250	0.537	1.486	C=C π* *2*
D1	292.6	Gaussian	0.356	4.316	0.356 *	4.316*	C-C σ*
D2	292.7	Gaussian	-	-	2.595	1.425	C-F σ*
E	295.6	Gaussian	-	-	1.552	1.808	C-F ?
F	298.4	Gaussian	-	-	1.457	4.653	C-F σ* *2*
G	300.4	Gaussian	0.422	14.78	0.294	11.98	C-C σ * *2*
H	307.1	Gaussian	-	-	0.333	9.245	C-F ?

** fixed to be the same as the Aryl-F8 scan.*

they appear at the recognized positions. The peak width is also seen to increase with increasing energy, as normally observed.

Assigning peaks in the FPF-G scan is more complicated for two reasons. First, few NEXAFS studies of polymers with perfluorinated sections have been conducted, and those that do exist do not agree in their peak assignments or they leave peaks un-assigned [88, 89, 90, 91]. Secondly, it appears that there are several overlapping peaks in the 290 - 300 eV region. Also peak D becomes inexplicably larger in the FPF-G scan - there is not a great deal more C - C σ bonding in FPF-G compared to Aryl-F8. This might be explained by the D peak being a sum of the C-C σ resonance and at least one other peak. Also, peaks generally become wider with increasing energy. However, the D peak is narrower than would be expected, which could be explained by it being the sum of two (or more) Gaussian peaks.

First, consider the FPF-G peaks that also appear in the Aryl-F8 scan and can be rationalized as follows. The A peak is strong due to the conjugated backbone, but smaller than in Aryl-F8 due to the lack of benzene rings in the side chains. The B peak is reduced in size because many C-H bonds have been replaced by C-F bonds in the sidechains. The B peak height is reduced by approximately the same proportion as the A peak, as to be expected if they are attributed to the same bond. The D1 and G peaks are assumed to be present, but buried under other peaks. Therefore, in the Aryl-F8 fit, the D1 and G peak positions are fixed at the same energy as in the Aryl-F8 scan, and the D1 peak height and FWHM are also fixed as there is no other way to determine these parameters. Having subtracted these peaks from the data, the remaining data can be fit by four more Gaussian peaks. There is reasonable consensus in the literature that peaks D2 and F are a result of C-F σ* bonds [89]. Peak E is often left un-assigned, but sometimes is attributed to another C-C σ* transition. In this case, however, that does not seem to make sense as it only appears in the FPF-G scan and not the Aryl-F8 scan. It therefore seems logical to conclude that both peaks E and H are also a result of the C-F bonding.

Figure 2.10 shows NEXAFS scans of *monolayers* of FPF on Aryl-F8. The PEY signals are very similar to that of a thick layer of FPF and show no evidence of the underlying Aryl-F8. The similarity of the scans for FPF-G and FPF-R monolayers is also striking, although maybe not surprising as the two materials contain very similar types of carbon bonding. These scans confirm once again the presence of the fluorinated monolayer on top of Aryl-F8 and imply that the monolayer thickness must be at least as great as the sampling depth of NEXAFS.

NEXAFS data was also collected with varying angles of incidence in order

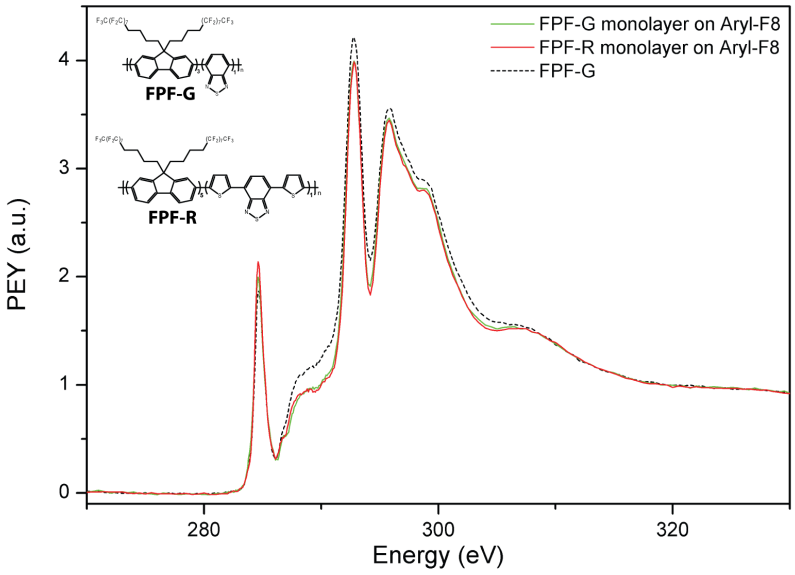

Figure 2.10: NEXAFS scans of monolayers of FPF-G (green solid line) and FPF-R (red solid line) formed by the standard method on 20 nm thick layers of Aryl-F8. The scan of a 20 nm thick film of FPF-G is included for comparison (black dashed line, same as in Fig 2.9).

to obtain bond orientation information. After normalization, this resulted in scans such as the one shown in Fig 2.11 for a monolayer of FPF-G on Aryl-F8. The intensity of the initial C=C π* peak can be seen to decrease with increasing angle which indicates that this bond has a preferred orientation. After fitting Gaussian functions to these peaks quantitative calculations (Appendix A) we determined that these C=C π bonds preferentially lie flat to the surface with an order parameter of S = 0.20. (Where S = 1 would indicate perfect order and S = 0 would indicate random order.) The biphenyl rings in polyfluorenes have been observed to be preferentially oriented before [87, 92, 93]. The Gaussian functions do not fit the experimental peak shape perfectly, although this is what others generally use. A better fit might be obtained with a combination of a

Table 2.3: NEXAFS C=C π^* peak order

Sample	Order Parameter, S
FPF-G monolayer on Aryl-F8	0.204
FPF-R monolayer on Aryl-F8	0.204
FPF-G monolayer on F8BT	0.115
FPF-R monolayer on F8BT	0.194
Aryl-F8	0.039
F8BT	0.166
FPF-G	0.170
FPF-R	0.163

Lorentzian function and a Gaussian function with some skew as well. However, it is unlikely that an improved fit would significantly alter the order parameter value calculated.

Similar ordering of the C=C π^* peak is observed in other samples and is summarized in Table 2.3. It is believed that the similarity of the order parameter values for the molecules in the monolayers and underlayers is significant and indicates that the two are aligning. This alignment would allow overlap of the π-conjugated systems in the two polymers hence providing a force of adhesion to anchor the FPF monolayer to the underlying PFO layer.

It was initially imagined that the extent of ordering of the biphenyl rings might be improved by annealing either the underlayer or the monolayer. NEXAFS data were collected for a series of samples that had undergone a variety of different annealing times and temperatures. However, none of these conditions yielded a detectable change in the extent of ordering (Appendix A). Order

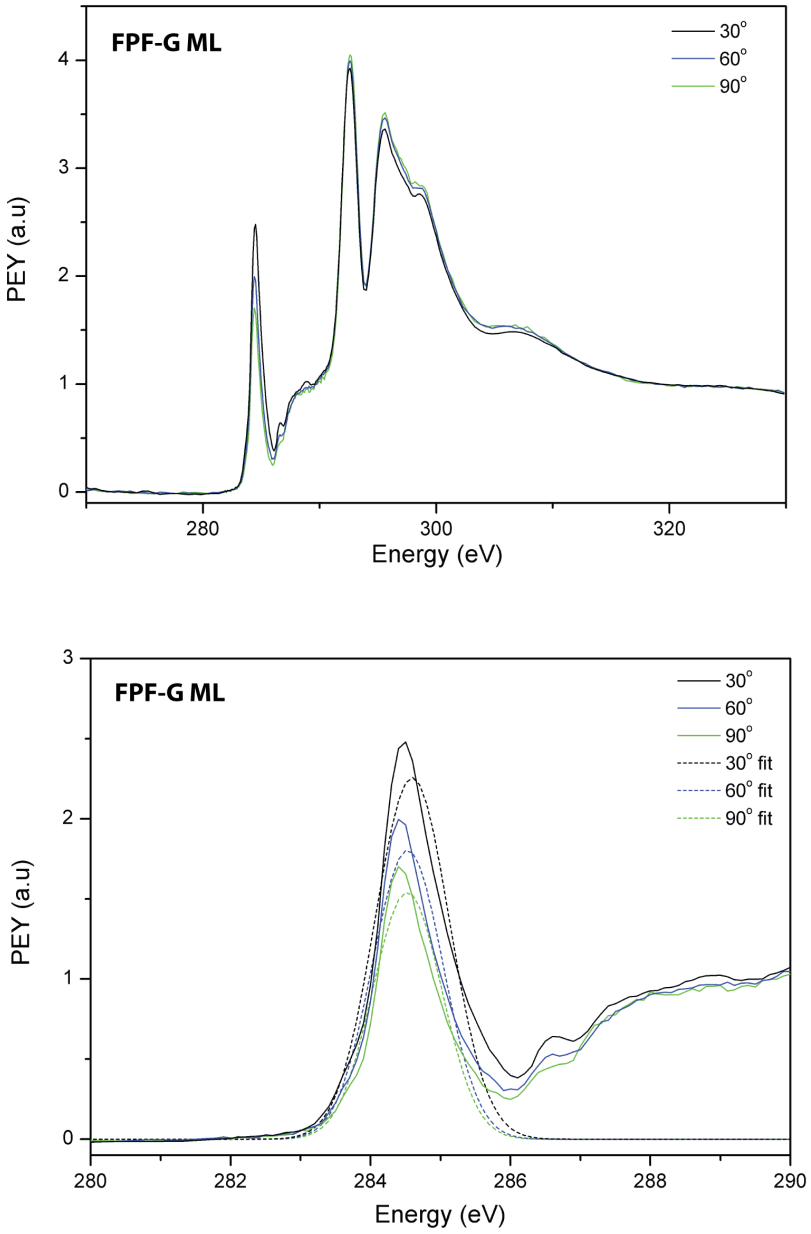

Figure 2.11: NEXAFS scans of a monolayers of FPF-G formed by the standard method on Aryl-F8 taken at incident angles of 30 (black), 60 (blue) and 90 (green) degrees. The lower plot is an enlargement of the C=C π^* peak showing Gaussian peaks (dashed lines) fitted to the experimental data.

parameters were also invariant to monomer ratio and underlayer thickness.

2.4.2 Optical Characterization

Photoluminescence

Figure 2.12 shows photoluminescence spectra of the pure polymers studied in this work. FPF-G and FPF-R show strong emission in the green and red regions of the spectrum while Aryl-F8 emits in the blue region, as expected. This difference in emission wavelength is one of the properties that allows the polymers to be distinguished from each other when stacked in bilayers.

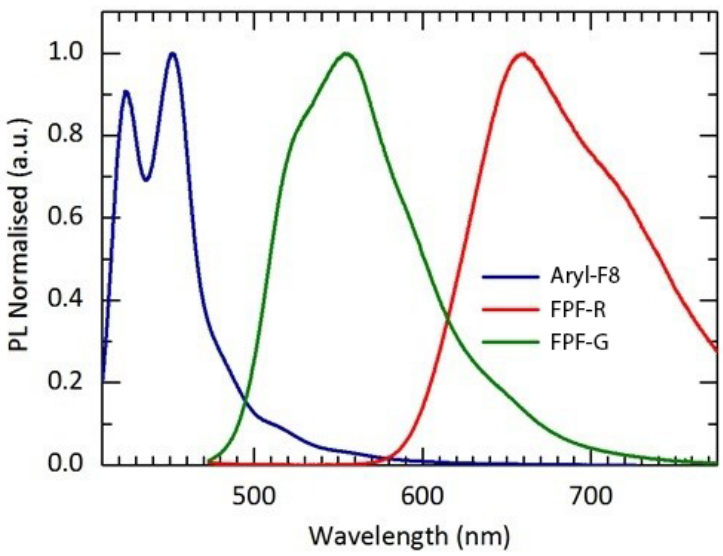

Figure 2.12: Photoluminescence spectra of 20 nm thick layers of FPF-G, FPF-R and Aryl-F8.

Electroluminescence

Figure 2.13 compares electroluminescence spectra from devices with thick emissive layers to that of devices with monolayers. The spectrum for the device with thick FPF-R shows one peak in the red region of the spectrum, however the device with an FPF-R monolayer shows several smaller peaks in the blue region in addition to the main peak in the red region. This indicates that in this device there is light emission from the underlying Aryl-F8 layer in addition to emission from the FPF-R monolayer. The case is different for the devices containing FPF-G layers. In the device with a thick layer of FPF-G a peak is seen in the green region of the spectrum, as expected, and a very similar peak is seen in the device with just a monolayer of FPF-G. This is quite remarkable - that all the emission in this device is from the monolayer and none is from the underlying Aryl-F8 shows that the monolayer must be completely continuous and free of pin-holes. It was later found that the emission from Aryl-F8 in the FPF-R monolayer device was due to incomplete monolayer formation and is only included here for illustration purposes. Devices with FPF-R monolayers that emitted from solely the monolayer were also fabricated.

Photothermal Deflection Spectroscopy (PTDS)

Photothermal Deflection Spectroscopy (PTDS) is a sensitive technique to measure the absorption of photons by a material. Figure 2.14 shows the absorption spectra of five samples. Aryl-F8 shows a strong absorption in the blue region. The four other samples are layers of FPF on Aryl-F8 so they all show the same peak in the blue region, in addition to other features. The FPF-G samples show a peak in the green region and the FPF-R samples show an absorption that ex-

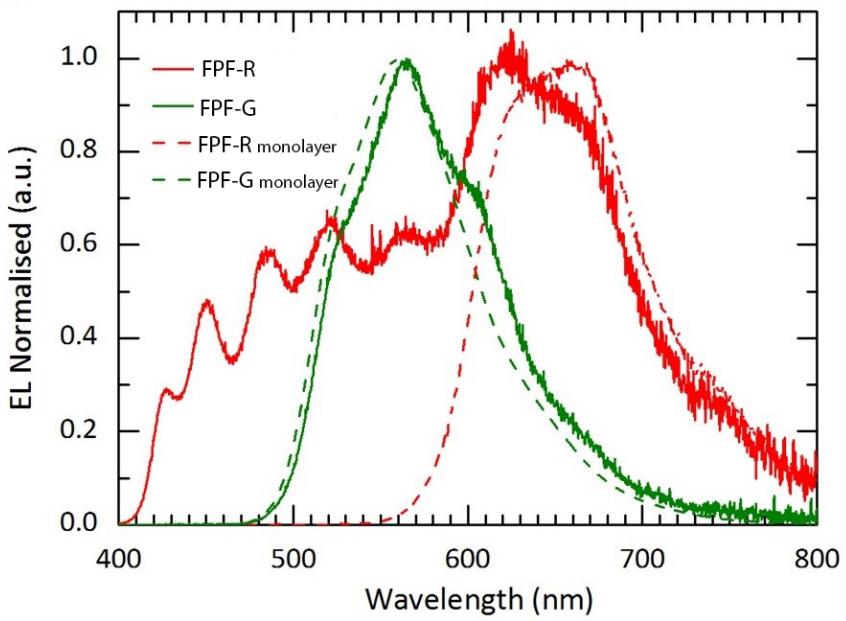

Figure 2.13: Electroluminescence spectra from four separate devices. Two with thick emissive layers ITO / PEDOT:PSS /80 nm Aryl-F8 / 20 nm FPF / BCP / Ca / Al (dashed lines) and two with monolayer emissive layers ITO / PEDOT:PSS /80 nm Aryl-F8 / 1-2 nm FPF monolayer / BCP / Ca / Al (solid lines)

tends to the red region of the spectrum.

It can be seen that the spectra for the monolayer samples of FPF-G and FPF-R show less absorption in the green and red regions respectively than the samples with thick layers of FPF-G and FPF-R. The reduction in absorption is presumably a result of there being less material present in the monolayer. If the assumption is made that the amount of material is directly proportional to the strength of absorption, PTDS provides a very accurate method of measuring the thickness of the monolayers. Using this method it is determined that both the FPF-G and FPF-R monolayers are 1 - 2 nm thick.

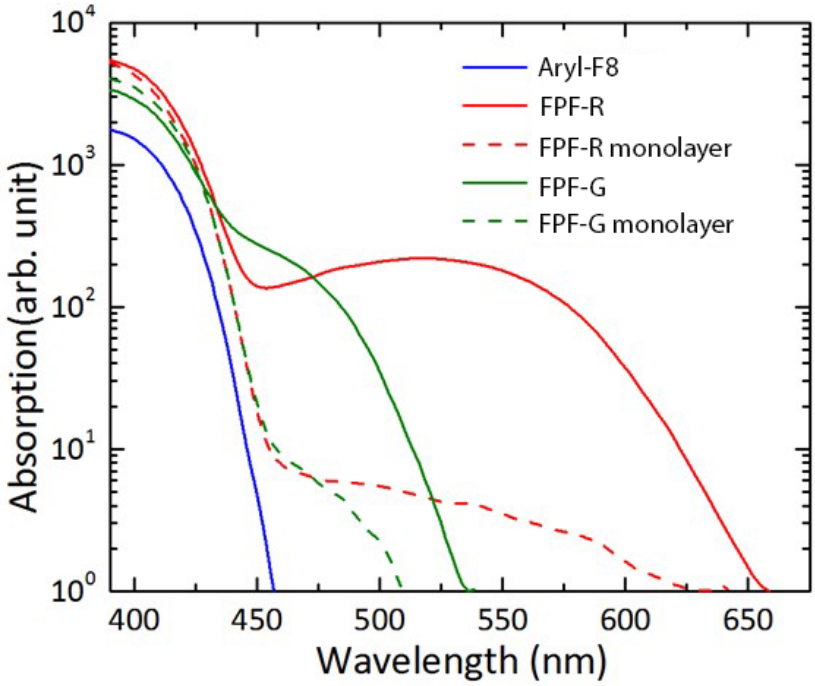

Figure 2.14: Photothermal Deflection Spectroscopy scans of five samples. Aryl-F8 alone (solid blue), bilayers of 20 nm of FPF-R or FPF-G on 80 nm of Aryl-F8 (solid red and green respectively) and finally, monolayers of 1-2 nm thick FPF-R and FPF-G monolayers on 80 nm of Aryl-F8.

2.4.3 Device Fabrication and Characterization

With reasonable confidence that these monolayers form, we began investigating incorporating them into PLED devices. The standard device structure is shown in Figure 2.4 and all devices fabricated are variations on this structure. The electrodes and transport layers are kept the same and only the middle emissive layers - the Aryl-F8 and FPF - are varied.

Electrical Characteristics

The current-voltage plot of three devices is shown in Figure 2.15. All devices show curves typical of PLEDs indicating that they are operating as expected. However, it can be seen that the turn-on voltage (V_{on}) is relatively high and the on/off current ratio is modest. The high V_{on} could indicate interfacial contamination between one or more layers in the stacked device.

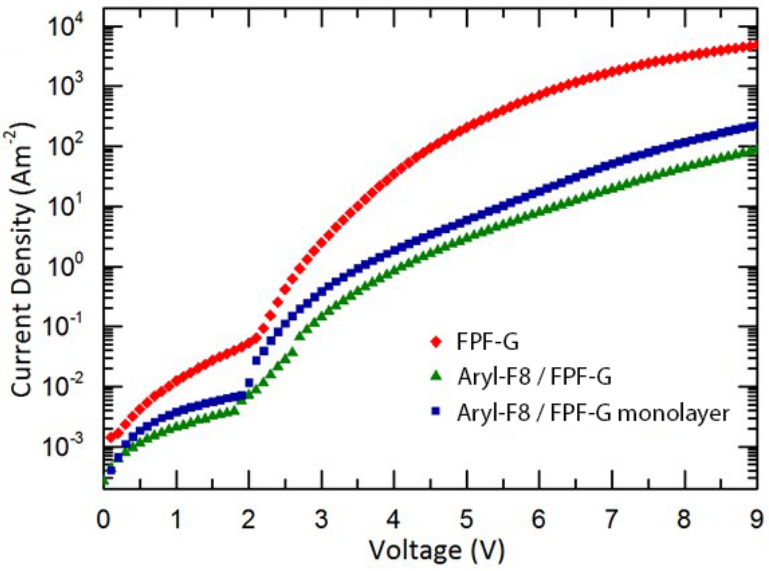

Figure 2.15: Electrical Characteristics of three separate devices with different emissive layers, 20 nm thick FPF-G (red), 80 nm Aryl-F8 / 20nm FPF-G (green) and 80 nm Aryl-F8 / 1-2 nm FPF-G monolayer (blue).

Luminescence Efficiency

Figure 2.16 shows a plot of the luminance efficiency variation with current flowing through the device. First, note that the samples *with* Aryl-F8 exhibit peak luminance at lower currents than for the device with just a thick layer of FPF-G.

The second observation is that the peak luminance of the device with a monolayer of FPF-G is significantly lower than that of the device with a thick layer of FPF-G. Although at one point it was thought recombination might be increased by the monolayer resulting in an increase luminance efficiency, it seems that this is not the case and a thinner emissive layer simply results in lower luminance efficiency.

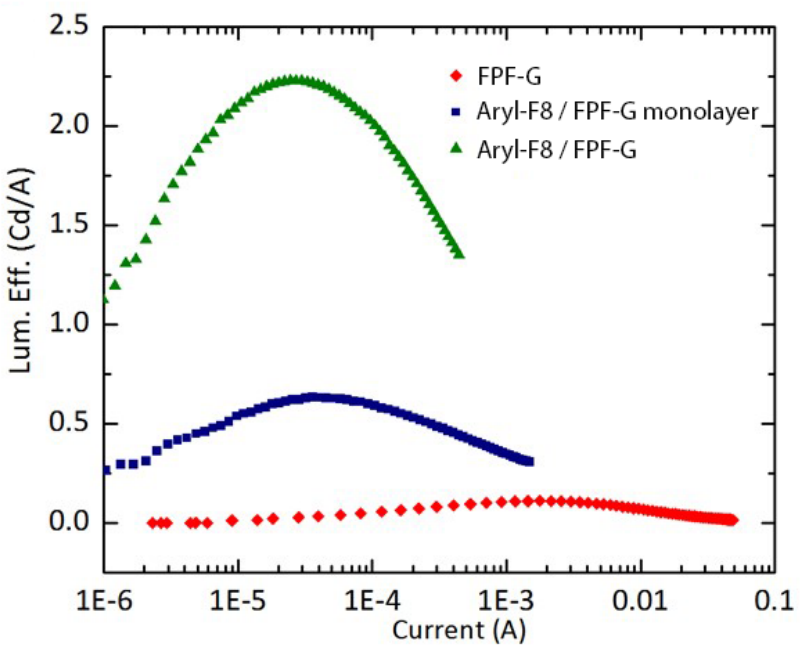

Figure 2.16: Luminanace efficiency of three separate devices with different emissive layers. One with 20 nm thick FPF-G (red), one with 20nm FPF-G on 80 nm Aryl-F8 (green) and one with a 1 - 2 nm monolayer of FPF-G on 80 nm of Aryl-F8.

2.4.4 Theory of Monolayer Formation

It is evident that the formation of these monolayers is very dependent on the materials used. A comprehensive list of material combinations tested is given

Table 2.4: Monolayer formation conditions

Underlayer	Monolayer	Solvent	Formation Method	Monolayer Formed?	Method
Aryl-F8	FPF-R/G	5PF	BTFMB rinse	Y	NEXAFS
Aryl-F8	FPF-R/G	5FB	BTFMB soak	Y	NEXAFS
F8BT	FPF-R	BTFMB	BTFMB rinse	Y	NEXAFS
Polystyrene	FPF-R	BTFMB	BTFMB rinse	Y	NEXAFS
PMMA	FPF-R	BTFMB	BTFMB rinse	N	NEXAFS
Si	FPF-R	BTFMB	BTFMB rinse	Y	NEXAFS
F8BT	FPF-R	5FB	BTFMB rinse	Y	NEXAFS
Polystyrene	FPF-R	5FB	BTFMB rinse	Y	NEXAFS
PMMA	FPF-R	5FB	BTFMB rinse	Y	NEXAFS
Si	FPF-R	5FB	BTFMB rinse	Y	NEXAFS
FPF-R	F8BT	xylenes	xylenes rinse	N	NEXAFS
Si	F8BT	xylenes	xylenes rinse	N	NEXAFS

in Table 2.4 that summarizes results obtained over this 3 year project.

It was also observed that monolayers cannot be 'stacked up' or improved in any way by repeating the standard monolayer formation method on an already formed monolayer. The order parameter, S, was found to be unaltered by annealing, 'stacking' layers, or increasing the amount of time the FPF solution sits before being spun off.

These observations lead to the hypothesis that there are two conditions essential to the formation of these monolayers:

1. During the spincoating and/or rinsing steps, a certain solution must be in contact with the underlayer such that there is a high-energy interface between the two phases. In this project there is a high-energy interface

between the organic substrate and the fluorinated solvent due to their chemical orthogonality. The energy of this interface can be lowered by the fluoropolymer segregating to this interface and orientating itself such that the fluorinated parts and organic parts essentially act as a surfactant. Thus, the fluoropolymer in solution is pushed to the high-energy interfaces forming a uniform ultra-thin film over all these surfaces.

2. Once at the interface, the monolayer-forming polymer chains can form some kind of intermolecular bonds to the substrate to anchor them in place and hence resist being washed off. In this project, the NEXAFS data indicate that, at least some portion of, the conjugated parts of the polymers in the monolayer and substrate are aligned leading us to suspect that adhesion is via π-stacking.

Note that it is the first condition that ensures the monolayer is continuous and pin-hole free, while the second condition ensures the layer is just one molecule thick. Although in this system adhesion via π-stacking is probable, it is conceivable that other types of intermolecular bonding could contribute to the anchoring of the monolayer. This might explain why monolayers are observed to form on some other non-conjugated substrates. It is also worth mentioning that the first condition (polymers in solution adhering to orthogonal polymer substrates) has been observed in other systems, namely biomolecules appearing to adhere to fluoropolymers [94], and has also been used by other researchers in the fabrication of monolayers of non-conjugated, non-fluorinated polymers on fluorinated polymers [95].

2.5 Conclusions

There are several key conclusions about the monolayers that can be drawn from the various characterization methods used in this project:

1. **The monolayers exist.** This is confirmed by the presence of fluorine on the surfaces examined by XPS and NEXAFS and the fluorescence observed by fluorescence microscopy.
2. **Monolayers are one molecule thick.** The layer thicknesses calculated from the PTDS data are so small they can only correspond to the dimension of one molecule.
3. **Monolayers are continuous and without pinholes.** This is illustrated by the electroluminescene data which show that monolayer devices only emit in the monolayer color. If the monolayers were not continuous alternative pathways would exist resulting in emission in the underlayer (blue) region also.
4. **The biphenyl rings of the FPF polymer in the monolayer are preferentially oriented**. This is indicated by the variation of peak intensity with angle in the NEXAFS data and is surprisingly consistent amongst differing samples. It is also notably robust, not being significantly affected by variations in annealing and processing.
5. **When incorporated into devices, light emission comes solely from the monolayer.** This is again evident from the electroluminescence data with no emission in the blue region from the underlying layer.

All other methods produce results in agreement with and supporting the above conclusions, but do not contribute additional facts about the monolay-

ers. With these considerations in mind, the proposed mechanism of monolayer formation is consistent with the available data.

If the proposed mechanism is correct, it not only explains how FPF forms monolayers on PFO-type materials, but predicts that it is much more general. If the two criteria for formation are met, a monolayer is likely to form in any polymeric material system. Combinations of conjugated polymers are particularly well suited because their conjugation provides an inherent adhesion mechanism via π-stacking.

CHAPTER 3

PATTERNING ORGANIC MATERIALS USING FLUOROPOLYMER BARRIER LAYERS

3.1 Abstract

Organic electronic materials cannot be processed using conventional photoresists because they may be damaged or removed by the solvents involved in this process. In this work a fluorinated methacrylate polymer is used as a barrier layer to protect organic materials during processing. Additive and subtractive process routes are demonstrated that achieve 1 μm features in common organic semiconductors such as P3HT and F8BT. Red, green and blue light emitting polymers are used to illustrate that aligned two- and three-component patterns can also be achieved through the additive process and results are examined using SEM and fluorescence microscopy. It is also demonstrated that the additive process can be modified to allow patterning of gold on top of P3HT. Finally, new issues in the patterning of organic materials are raised by a deeper examination of resist sidewall profiles and the consequences of pattern layout. In all, this approach is found to be a robust and flexible process with significant processing advantages over previously proposed solutions.

3.2 Introduction

The types of materials incorporated into electronics are continuing to diversify beyond the traditional inorganic semiconductors and metals. The drive to man-

ufacture low-cost, large-area, flexible and bio-compatible electronics has created interest in organic active materials in new electronics applications. However these delicate organic materials cannot usually be processed with conventional fabrication methods as they are easily damaged or even removed by the organic solvents used to spincoat, develop and strip the photoresists that are used in the patterning stages of these processes.Therefore new patterning methods need to be developed that are compatible with (i.e. non-damaging to) active organic materials. Other patterning methods including shadow masking [18], inkjet printing [96] and microcontact printing [42] have been investigated for this purpose but often lack the desired resolution or potential for large-scale manufacture. The industry is already very familiar with photolithographic patterning hence a photolithographic method of patterning organics would be preferable.

Specialized materials systems have previously been developed to allow photolithographic patterning of materials for organic electronics. In 2009 it was demonstrated that a fluorinated resist could be processed in super-critical CO_2 ($scCO_2$) to pattern both PEDOT:PSS and a light-emitting polymer down to 5 μm [97]. However, this approach comes with the significant disadvantage of requiring a chamber for the high-pressure, high-temperature conditions necessary for the developing and stripping stages. Later it was shown that fluorinated photoresists could also be processed in fluorinated solvents [23, 24]. This removes the need for a high-pressure chamber and enables pattern formations down to about 1 μm in certain circumstances; however, the process was generally restricted to a negative-tone subtractive one, resist sensitivity was low compared to commercial resists and side wall profiles were often not steep enough to perform lift-off procedures.

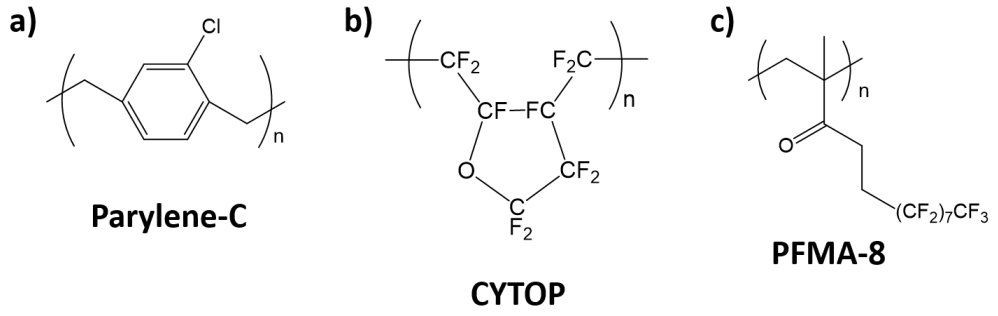

Figure 3.1: The chemical structures of a) Parylene-C, b) CYTOP and c) PFMA-8.

To solve this problem while maintaining the advantages of a commercial resist several researchers have investigated using a combination of an inert barrier layer with a conventional resist. In 2006 DeFranco *et al.* used Parylene-C (structure shown in Figure 5.2) as a barrier layer in additive and subtractive patterning down to 1 μm resolutions [33] although the authors admit that as Parylene is deposited via chemical vapor deposition, stripping it was sometimes problematic. In 2009 Kuo *et al.* demonstrated a four-layer polyvinyl-alcohol-based method to pattern electrodes on PEDOT:PSS down to 6 μm channel lengths [98] but this process seems un-necessarily complex. More recently, Dhar *et al.* used CYTOP, a commercially available fluoropolymer, as a barrier layer in the fabrication of organic lateral heterojunctions [34] yet the interface showed significant roughness and patterning at higher resolutions was not investigated. Chang *et al.* used a very similar CYTOP process to also fabricate organic lateral heterojunctions in addition to lines down to 2 μm resolution [35].

In this work a fluorinated methacrylate polymer, PFMA-8, is used as a barrier layer underneath a commercially available photoresist. There are several advantages to using PFMA-8 over the techniques cited above. PFMA-8 is fully

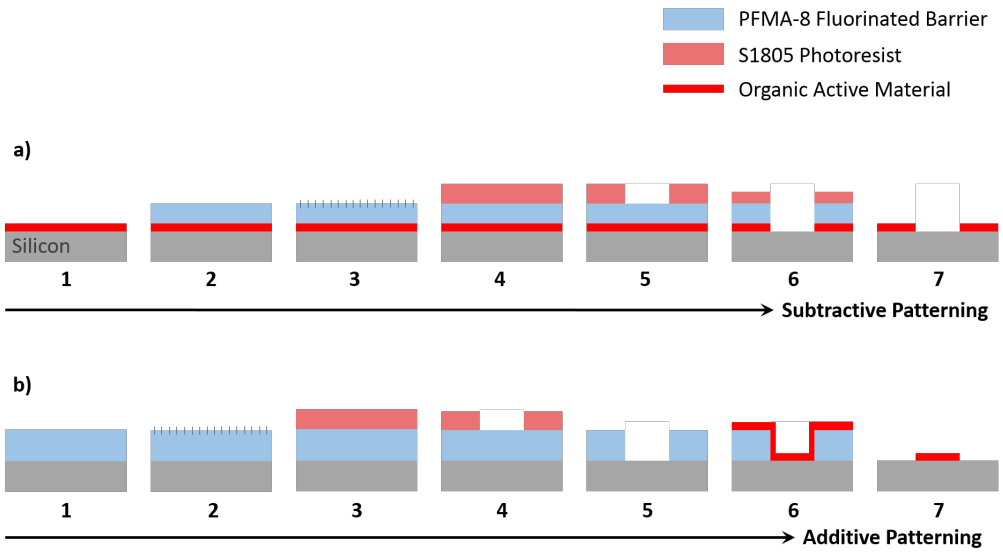

Figure 3.2: Schematic diagram showing the steps involved in a) subtractive and b) additive patterning of organics using a fluorinated barrier layer. Subtractive process flow: 1 = spincoat organic active material from organic solvent, 2 = spincoat barrier layer from fluorinated solvent, 3 = short oxygen plasma etch, 4 = spincoat photoresist, 5 = expose and develop photoresist, 6 = oxygen plasma transfer etch, and 7 = strip resist stack in fluorinated solvent. Additive process flow: 1 = spincoat barrier layer, 2 = short oxygen plasma etch, 3 = spincoat photoresist, 4 = expose and develop photoresist, 5 = oxygen plasma transfer etch, 6 = spincoat organic active material from organic solvent, and 7 = lift off in fluorinated solvent.

solution processible in hydrofluoroether (HFE) solvents. It can be spincoated from and stripped in HFEs which have previously been shown to be non-damaging to organic materials, due to their lack of interaction. In particular they do not alter the electronic properties of organic semiconductors [23]. Many different photoresists could be used in combination with a PFMA-8 barrier layer depending on the patterning requirements. In this work Microposit^{TM}1800 photoresist from Shipley (Rohm and Haas) was chosen as it does not require any bake steps so can be processed entirely at room temperature. For features greater than 1 μm a post apply bake is not necessary, and the resist chemistry is

such that it does not require a post exposure bake step.

The process flows used in this work are shown in Figure 3.2. Briefly, in the subtractive process a fluorinated barrier layer is used to protect the underlying organic active material to be patterned while a photoresist is processed on top of the barrier which is stripped at the end. In the additive process the barrier layer is patterned then doubles as a lift-off layer in the final stages. Fluoropolymers are notoriously difficult to adhere other materials to and this was found to be a problem when spincoating photoresist on top of the PFMA-8 barrier layer. Various methods of functionalizing the fluoropolymer surface have been reported [95, 99, 100]. For this process flow a short oxygen plasma etch was found to be most convenient.

In all, this approach gives much greater flexibility than previous methods while also maintaining the advantages of a conventional resist. Patterns down to 1 μm can be made in positive- or negative-tone, via an additive or subtractive process, with high sensitivity, steep sidewall profiles, and all at room temperature. This work also examines several issues in greater depth than previous works have, including the feasibility of multi-component patterns, pattern shape restrictions and the cross sectional profile of the patterned organic active material.

3.3 Experimental Methods

3.3.1 Materials

1*H*,1*H*,2*H*,2*H*,-heptadecafluorodecyl methacrylate was purchased from Oakwood Chemicals and used as received. S1805 Microposit^{TM}photoresist and MIF 726 Developer were provided by the Cornell Nanofabrication Facility. Poly(3-hexylthiophene-2,5-diyl) (P3HT) and poly[(9,9-di-n-octylfluorenyl-2,7-diyl)-alt-(benzo[2,1,3]thiadiazol-4,8-diyl)] (F8BT) were purchased from American Dye Source Inc. and used as received. 1,1,1,2,3,3,3-hexafluoro-4-(1,1,2,3,3,3-hexafluoropropoxy)-pentane (HFE 7600) was purchased from 3M Inc. Chloroform was purchased from Sigma Aldrich and used as received. Silicon substrates were purchased from WRS Materials Inc.

3.3.2 Methods

General Poly(1*H*,1*H*,2*H*,2*H*-heptadecafluorodecyl methacrylate) (PFMA-8) was synthesized by radical polymerization as described previously [101]. All spin-coated solutions were filtered with a 0.2 μm Nylon or Teflon filter. A set of photomasks was designed with complementary patterns and fabricated using a Heidelberg DWL laser mask writer. Silicon substrates for multi-component patterns had gold alignment marks thermally evaporated on to them using a standard lithography and lift-off process. All patterns were then aligned to these marks.

Subtractive patterning The organic active material (P3HT, F8BT, PFO or PF-

R) is first spincoated at 2000 rpm on bare silicon from a 5 mg/ml solution in chloroform to give an approximately 20 nm thick film. Next a 10 wt% solution of PFMA-8 in HFE 7600 is spincoated on top at 1000 rpm to give a 600 nm thick barrier layer. A PT72 Reactive Ion Etcher is used to perform a 10 second oxygen plasma etch with 50 sccm O_2 gas flow, 150 W power and 60 mT pressure is used to modify the PFMA-8 surface to aid adhesion. The S1805 photoresist is *immediately* spincoated on top at 2000 rpm. The photoresist is exposed through a specially designed photomask on a GCA AS200 Stepper with 365 nm radiation for 0.1 sec at 200 mW cm^{-2} to give a dose of 20 mJ cm^{-2}. The patterns are developed in standard MIF 726 developer for 10 seconds using an automated Hamatech processing station for improved reproducibility. The PT72 is used again to etch through the barrier layer and into the organic active material using 50 sccm O_2 gas flow, 150 W power and 60 mT pressure for 150 seconds. The barrier layer and any remaining photoresist are stripped in HFE 7200 for 30 seconds.

Additive patterning A 10 wt% solution of PFMA-8 in HFE 7600 is spincoated on bare silicon at 500 rpm to give a 800 nm thick barrier layer. A PT72 Reactive Ion Etcher is used to perform a 10 second oxygen plasma etch with 50 sccm O_2 gas flow, 150 W power and 60 mT pressure to modify the PFMA-8 surface to aid adhesion. The S1805 photoresist is *immediately* spincoated on top at 5000 rpm. The photoresist is exposed through a specially designed photomask on a GCA AS200 Stepper with 365 nm radiation for 0.1 sec at 200 mW cm^{-2} to give a dose of 20 mJ cm^{-2}. The patterns are developed in standard MIF 726 developer for 10 seconds using an automated Hamatech processing station. The PT72 is used again to etch through the barrier layer and remove the photoresist using 50 sccm O_2 gas flow, 150 W power and 60 mT pressure for 150 seconds. The organic active material (P3HT, F8BT, PFO or PF-R) is then spincoated at

2000 rpm on the patterned PFMA-8 layer from a 5 mg/ml solution in chloroform to give an approximately 20 nm thick film. The sample is then submerged in HFE 7200 for 180 minutes to dissolve the PFMA-8 and lift off unwanted organic active material. It is found that agitation by pipette aided the speed and extent of liftoff but that sonication is too aggressive causing delamination of the organic active material patterns also.

Patterning gold on P3HT P3HT is spincoated on bare silicon from a 5 mg/ml solution in chloroform. The standard additive process is then followed with a few alterations. The exposure dose is increased to 30 mJ cm^{-3} as less than this resulted in underexposed patterns (possibly caused by an increase in scattering from the rougher/darker surface of P3HT). The transfer etch was reduced to 50 seconds with 50 sccm O_2 gas flow, 150 W power and 60 mT pressure. This removed the majority of the barrier layer but left a small amount covering all the P3HT. The remainder was then removed with a rinse in HFE 7200 as this is selective to the PFMA-8 barrier and would not eat into the underlying P3HT as an oxygen plasma etch would. 25 nm of gold is then thermally evaporated at 2.3 $x10^{-6}$ Torr.

Fluorescence microscopy A Zeiss 710 Confocal Microscope was used to perform the fluorescence microscopy. All samples are excited with a 405 nm laser and observed with a 10x objective. All images are the sum of three channels: blue (420-440 nm), green (560-570 nm) and red (690-700 nm) and the gain is kept constant throughout (except where noted) to allow comparisons to be made.

3.4 Results and Discussion

3.4.1 Preliminary Experiments

It is first necessary to establish that the presence of a barrier layer does not interfere with the functioning of the S1805 photoresist. For this purpose contrast curves were recorded for samples with and without the barrier layer present as shown in Figure 3.3. They show that the resist behavior is not greatly altered by the barrier layer, and even appears to be somewhat more sensitive.

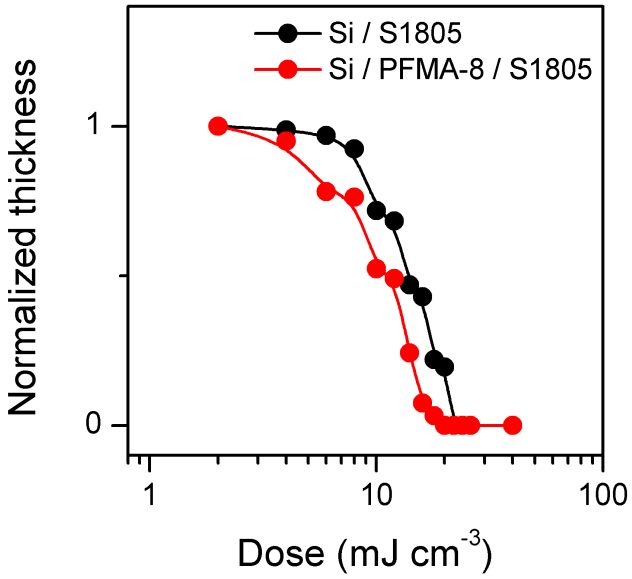

Figure 3.3: Contrast curves for 400 nm thick S1805 photoresist a) without and b) with a 600 nm thick PFMA-8 barrier layer exposed with 365 nm radiation and developed for 10 seconds in MIF 726.

In order to design sensible process flows it is also useful to know how the polymer film thicknesses are affected by spincoating conditions and etch parameters. Figure 3.4 shows spin curves for PFMA-8 and etch rates of PFMA-8

and S1805. Thicknesses ranging from 200 nm to 800 nm could be attained via spincoating with 5 and 10 wt% solutions and the PFMA-8 was found to etch approximately twice as fast as the S1805 in an oxygen plasma etch.

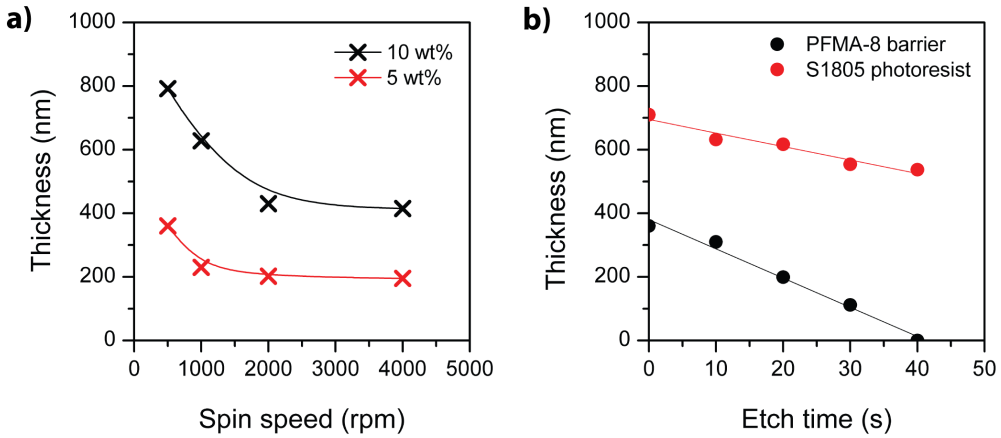

Figure 3.4: Process parameters of PFMA-8 where a) shows a spin-speed curve for two concentrations of PFMA-8 in HFE 7600, and b) shows etch rates of PFMA-8 and S1805 in an oxygen plasma with 50 sccm O_2, 150 W and 60 mT. Under these conditions the etch rate of PFMA-8 is 9.2 nm/sec and the etch rate of S1805 is 4.2 nm/sec.

3.4.2 Patterning

Figure 3.5 shows patterns of the resist on top of the fluorinated PFMA-8 barrier layer after patterning. Features from 10 μm down to 1 μm are shown and feature size is not significantly distorted or increased by the transfer etch into the PFMA-8 barrier layer. The rounding of the 1 μm squares is a result of the feature shape on the mask.

Figure 3.6 shows the side wall profile of the resist as the pattern is transferred in to the PFMA-8 barrier layer. In the additive process flow, the S1805

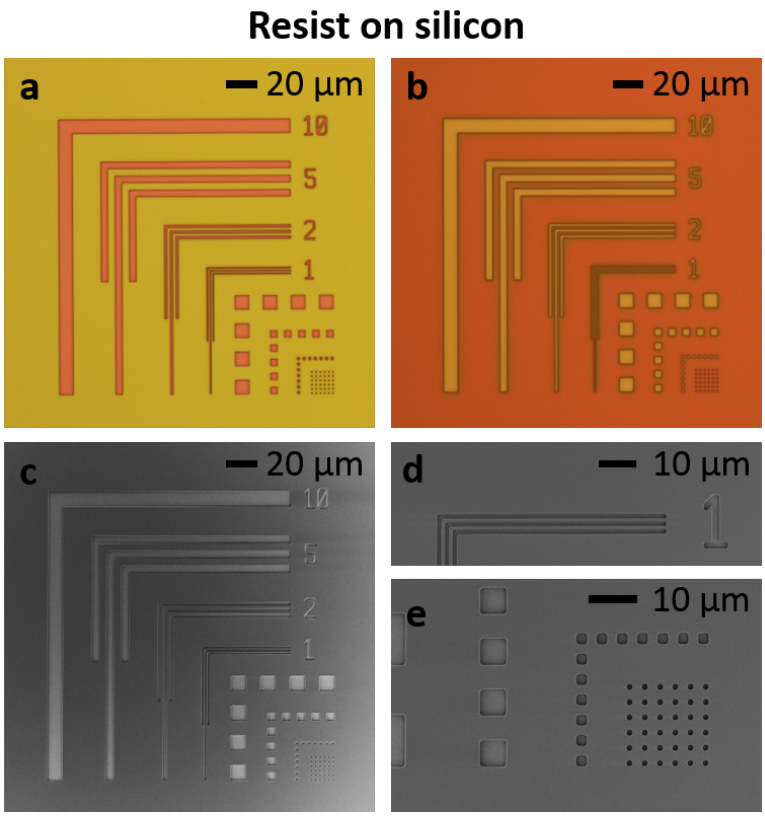

Figure 3.5: Patterned resist stack on silicon. Optical micrographs of S1805 on PFMA-8 a) after development of the S1805 and b) after the transfer etch into PFMA-8 which is cleared to the silicon. Scanning electron microscope (SEM) images of S1805 on PFMA-8 after the transfer etch showing c) the whole test pattern, d) 1 μm lines and e) 5 μm, 2 μm and 1 μm squares.

and PFMA-8 barrier layer were spin coated slightly thinner and thicker, respectively, for improved lift-off. The guide lines show that feature width is only slightly reduced by the (anisotropic) transfer etch. The final sidewall profile is relatively steep in the additive process and even slightly undercut in the subtractive process.

Figure 3.7 shows test patterns in various organic materials made via the subtractive process route. The materials are first spincoated on silicon and covered by a spincoated barrier layer of PFMA-8. A brief oxygen plasma etch is used to

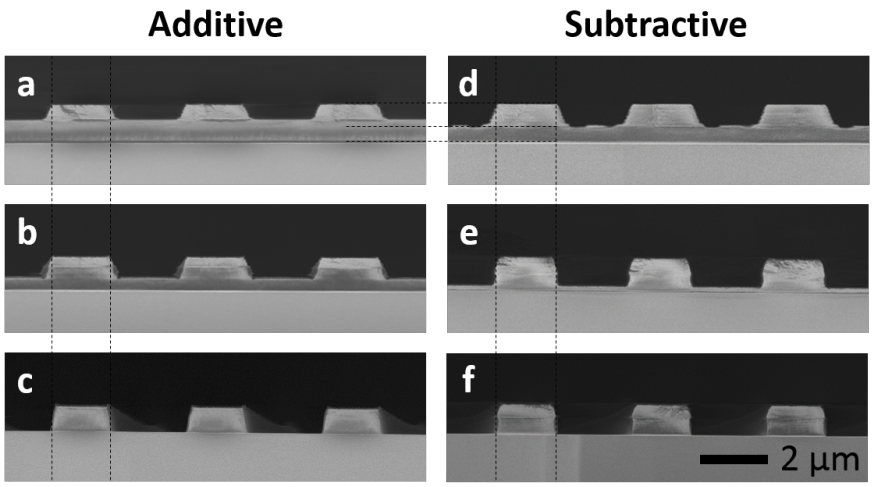

Figure 3.6: SEM images of the cross sections of patterned resist stack on silicon. a-c) shows the recipe used in additive patterning while d-f) shows the recipe used in subtractive patterning. a) and d) show images after development, b) and e) are after partial etching and c) and f) after complete etching. Dashed black guide lines are included to aid comparison of dimensions between images.

modify the PFMA-8 surface to allow the S1805 photoresist to adhere to it when it is spincoated on top. After exposure and development of the S1805, patterns are dry etched through the PFMA-8 barrier layer and into the underlying organic active material in a single step, using an oxygen plasma recipe. Patterns down to 1 μm or 2 μm are well formed in P3HT and three light emitting polymers (LEPs) that emit in the red, green and blue. Fluorescence images of the patterns in LEPs show light emission from the parts protected by the barrier layer and are dark in the areas that have been removed by the dry etch.

Patterning via an additive route is also possible and Figure 3.8 shows patterns of P3HT and F8BT on silicon made via the additive route. A PFMA-8 barrier layer is first spin coated on to bare silicon and its surface is modified

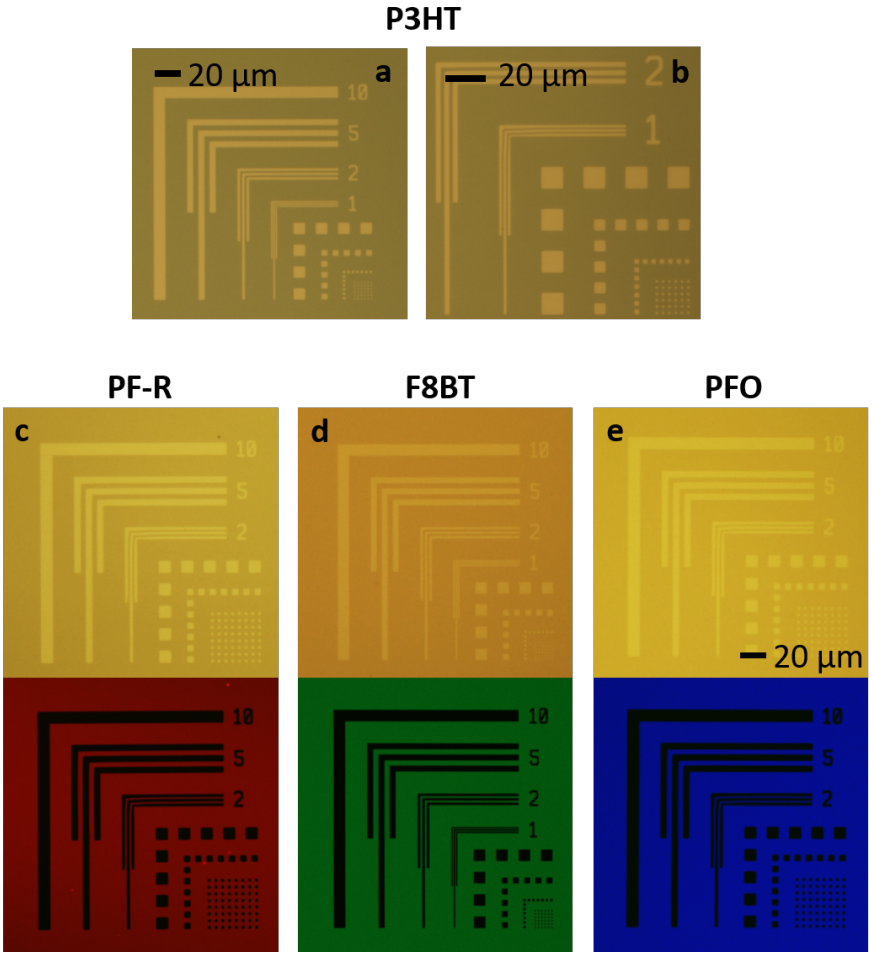

Figure 3.7: Materials patterned using the subtractive process flow. Optical micrographs of test patterns of P3HT at a) low and b) higher magnification, c) PF-R, d) F8BT and e) PFO. In the optical micrographs the darker regions are where the material remains and lighter regions are where the bare silicon has been revealed. Corresponding fluorescence micrographs are shown for PF-R, F8BT and PFO.

with a short oxygen plasma etch. S1805 photoresist is then spincoated, exposed and developed on top. Patterns are transferred into the barrier layer with a second oxygen plasma etch. This etch should be timed to also remove *all* the S1805 resist which would otherwise contaminate the organic active material put down subsequently. The organic active material to be patterned is then spincoated on

top of the patterned resist stack from an organic solvent. Finally, the sample is submerged in HFE 7600 fluorinated solvent, dissolving the PFMA-8 barrier layer and lifting off all unwanted organic active material. Well-formed features down to 1 μm remain on the silicon substrate and it is noted that adhesion between the organic active material and the silicon substrate is strong enough to resist being washed off by the fluorinated solvent.

It can be seen in the patterns formed by the additive process that the deposited organic active materials do not have uniform thickness and material aggregates around the edges of features. This 'edge effect' is also seen with other organic patterning methods [23]. The effect is particularly evident in the fluorescence micrographs where the brightness around feature edges is so much greater than at their center that they appear completely empty. This is not the case and emission from these regions is visible when the gain is increased, but it is indicative of the severity of this problem, which appears to be worse for the LEPs than for P3HT. The issue is investigated later with SEM and potential causes and remedies are discussed.

The lift-off step takes 30 - 60 minutes depending on process parameters. Figure 3.9 illustrates what happens during lift-off to a sample that has patterned S1805 on top of a PFMA-8 barrier layer on silicon. The patterns have *not* been etched into the PFMA-8 layer. The sample is submerged in HFE 7600 and imaged at intervals. After 30 seconds the solvent front (indicated by a black arrow) can been seen moving into the PFMA-8 layer dissolving it out from underneath the insoluble S1805 layer. The front continues to advance until it has dissolved all the PFMA-8 layer. This appears to happen at 4 minutes but the S1805 layer generally took longer to detach fully, usually coming off as a single piece or in

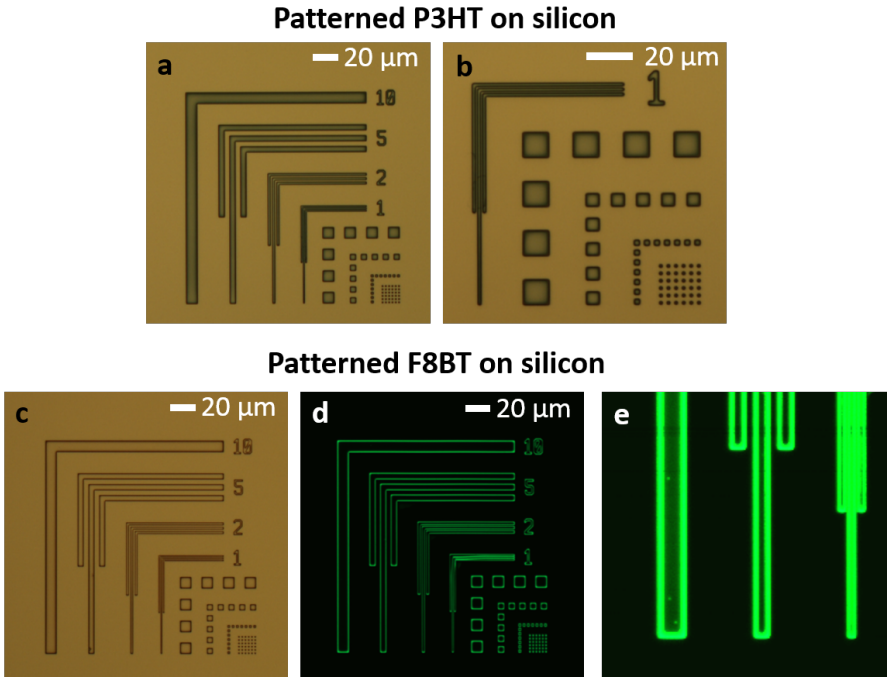

Figure 3.8: Materials patterned using the additive process flow. Optical micrographs of test patterns of a) P3HT, b) P3HT at higher magnification and c) F8BT on silicon. A corresponding fluorescence micrograph of the F8BT test pattern is shown in d) and e) shows a magnified part of the same pattern imaged at higher gain so that the feature interiors are visible.

large sections.

The additive process can be repeated and aligned to earlier patterns to achieve multiple component patterns. Figure 3.10 shows two component patterns of F8BT and PFO, and F8BT and PF-R. In both cases the F8BT was patterned first, then a PFMA-8 barrier layer was put down to protect these features while S1805 was spincoated on top and windows were opened up to pattern the second LEP. Features down to 1 μm are reproducible and well aligned throughout. Figure 3.10 also shows a three-component red, green and blue pattern where the F8BT, then PFO, then PF-R were patterned.

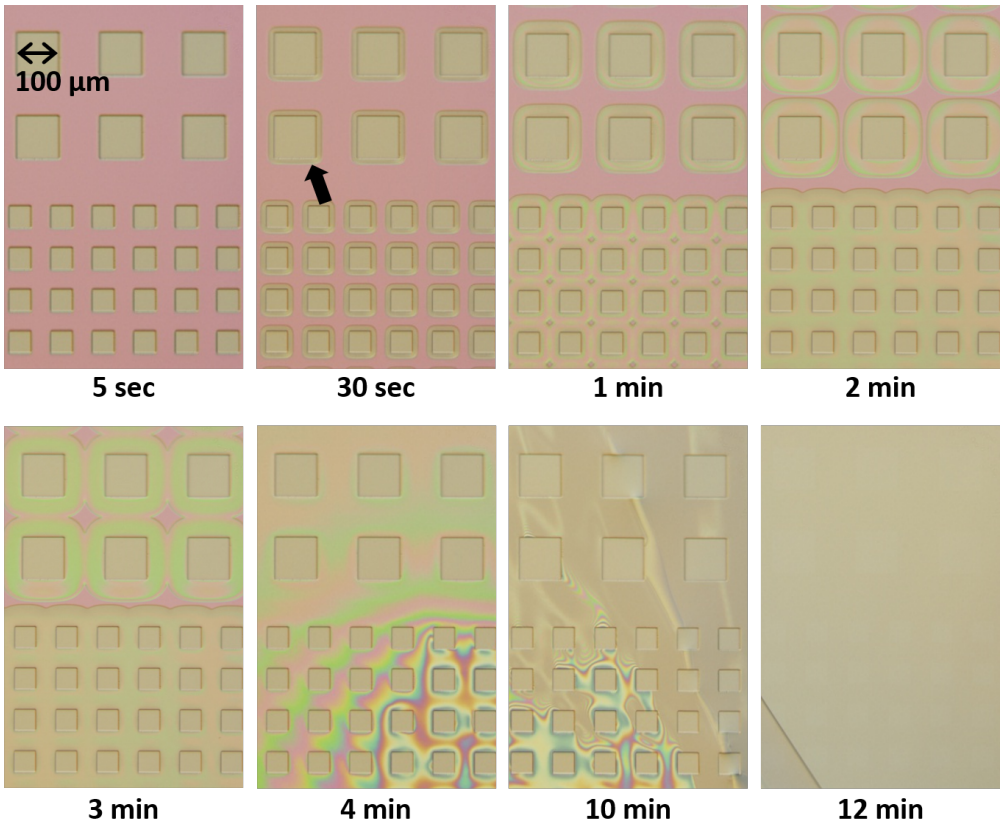

Figure 3.9: The resist lift off process. Exposed and developed patterns of S1805 with a barrier layer of PFMA-8 on silicon are submerged in HFE 7600 solvent and imaged at intervals showing the progress of the solvent front (indicated by a black arrow at 30 seconds) moving into the underlying PFMA-8 and resulting in the complete lift off of the intact S1805 resist layer.

For the fabrication of organic electronic devices it is often necessary to pattern metal electrodes on top of organic active materials. The additive patterning process can be adapted for this and the resulting patterns of gold on P3HT are shown in Figure 3.11. P3HT is spincoated on silicon and a protective PFMA-8 barrier layer in spincoated on top of this. The surface is modified with a short oxygen plasma etch and S1805 photoresist is spincoated on top, as in the normal additive process route. However, the (anisotropic) transfer etch is timed so that it does *not* go through the whole of the barrier layer leaving approximately 50

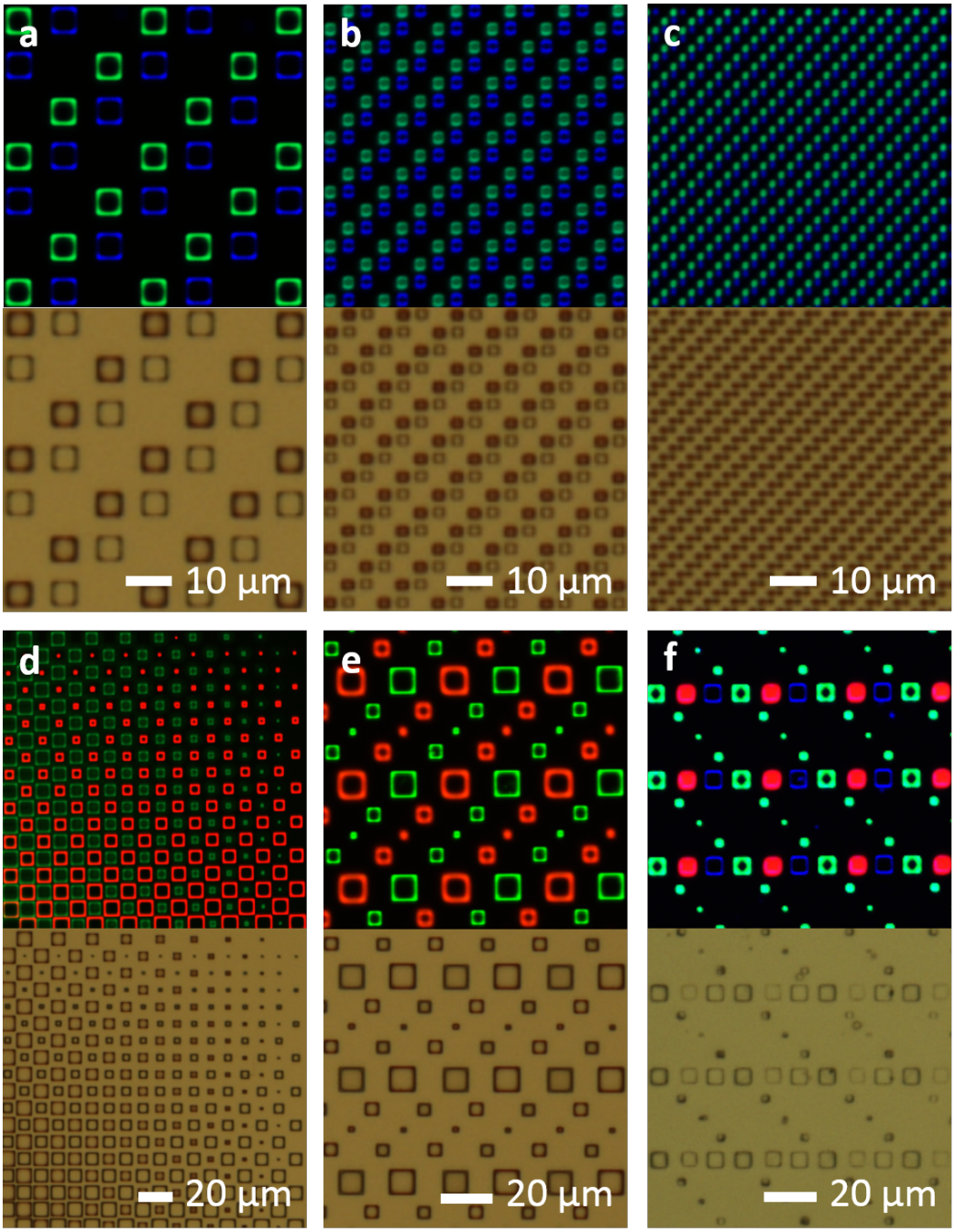

Figure 3.10: Two- and three-component patterns via multiple repeats of the additive process flow. Fluorescence micrographs with corresponding optical micrographs of patterns of F8BT and PFO with a) 5 μm, b) 2 μm and c) 1μm features. Then patterns of F8BT and PF-R with d) features ranging from 8 μm down to 1 μm and e) 10 μm, 5 μm and 2 μm features. Finally, e) shows a pattern of F8BT, PFO and PF-R with 5 μm, 2 μm and 1 μm features.

nm of PFMA-8 on top of the P3HT. This remaining PFMA-8 is then removed with a short (isotropic) wet etch, or solvent rinse, in HFE 7600. This fluorinated solvent reveals the P3HT surface at the bottom of the pattern's features, but does not damage the underlying P3HT, and enough PFMA-8 remains in all other areas to allow lift-off. Gold is then thermally evaporated onto the sample which is subsequently immersed in HFE 7600 to dissolve the remaining PFMA-8 and lift-off the unwanted gold.

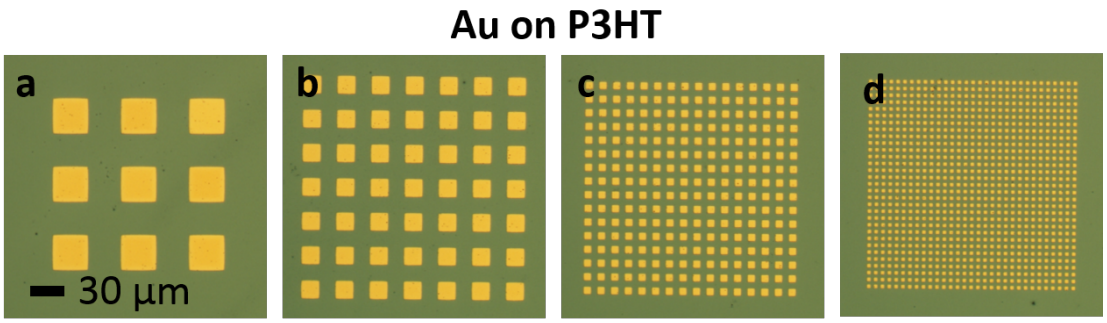

Figure 3.11: Patterns of gold on P3HT patterned via an adapted additive process. Optical micrographs of a) 30 μm squares, b) 15 μm squares, c) 6 μm squares, and d) 3 μm squares of gold on P3HT.

As observed earlier, the additive process results in patterns of organic active materials that have significant accumulations of material at the edges. This can be seen in more detail in Figure 3.12 that shows SEM cross sections of the additive patterning process. When spincoated on bare silicon this F8BT solution gives a 20 nm thick layer of F8BT. When spincoated on the patterned PFMA-8 it appears to form a film about this thickness in the center of features, but becomes considerably thicker in the 300 nm closest to the edge reaching a maximum thickness of 200 nm. Note that it coats the rest of the PFMA-8 (which

was recently subjected to surface modifying etch conditions) in a thin layer of F8BT which appears to rupture unevenly along the top edge of the resist during lift-off leaving some precarious 400 nm tall fan-like structures standing along the edges of the final patterns. The 'edge effect' is presumably caused by the combination of surface energies used in this material system.

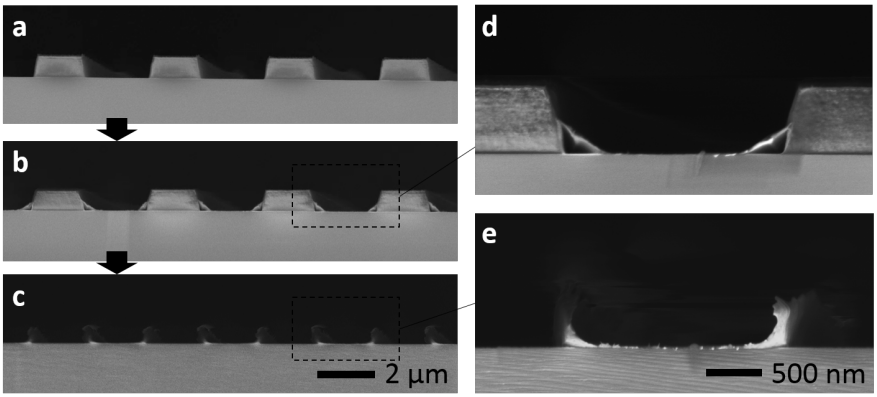

Figure 3.12: SEM images of resist cross sections during the additive process flow. 2 μm-wide lines are shown a) after development and etching, b) after spincoating of F8BT and c) after lift-off. With higher magnification images of the patterns d) after spincoating F8BT and e) after lift-off.

It is hard to anticipate whether the additive process could be used to put features of two different LEPs next to, or even inside of, each other. Figure 3.13 shows the result of some trials. Once the first LEP has been patterned and windows have been opened up in the resist/fluoropolymer stack for the second polymer there arises a problem: as the second LEP solution is spincoated on the sample it will contact part of the existing patterns along the edge of the features. If both LEPs are soluble in the same solvent the first could be dissolved by the solution of the second. However, the cross section of these areas would only be about 20 nm tall and which has not been a problem in other similar patterning

methods [101]. Unfortunately it can be seen that in this case it is a problem - both the fluorescence and optical micrographs show evidence of the first LEP (F8BT) having been washed away by the subsequent patterning steps, while the second LEP (PFO) features have formed normally.

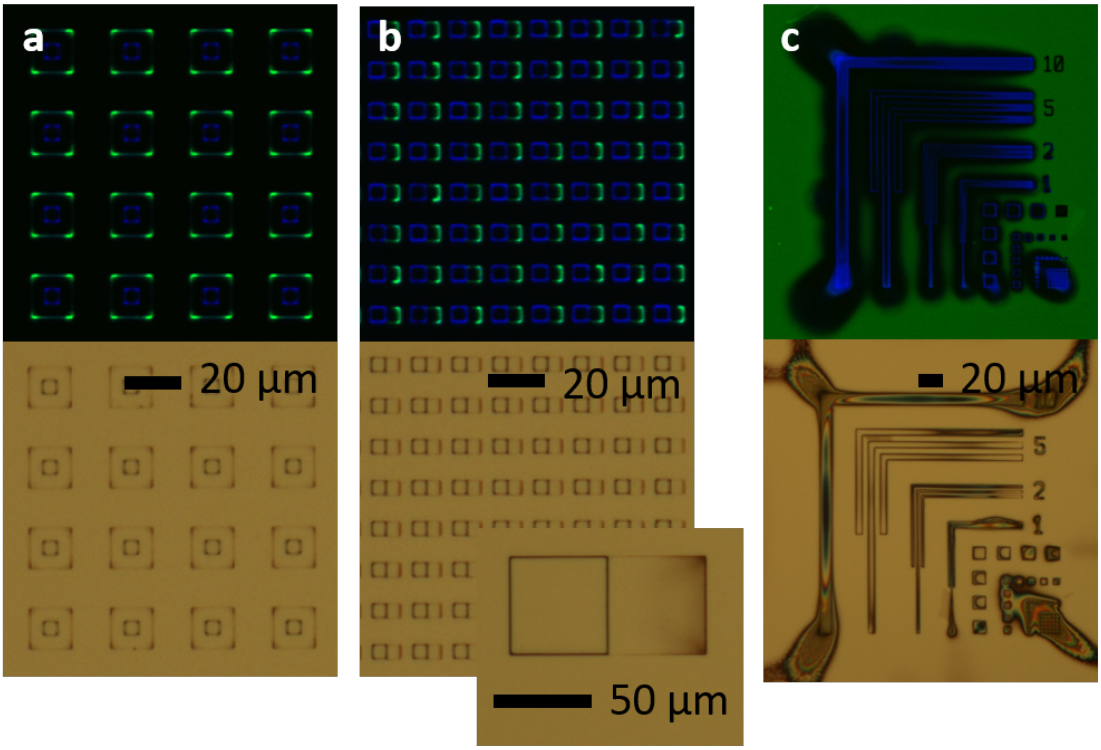

Figure 3.13: Two component patterns with features close to each other. In all cases the F8BT was patterned first, then the PFO. a) and b) show the result of two repeats of the additive process. The inset shows a similar but larger feature. c) shows the result of attempting combined additive and subtractive patterning in which the F8BT was first subtractively patterned then PFO was additively patterned into the gaps created.The corresponding optical micrograph is of a repeat of a similarly processed test pattern, but not exactly the same one.

Another way to obtain features of two LEPs next to each other would be to combine the additive and subtractive processes. The results of this trial are

also shown in Figure 3.13. The F8BT is patterned subtractively first, then the *same* resist is used to perform a lift-off step after depositing the PFO. However it can be seen that this method suffers the same problem and the solvent used to spincoat the second LEP washes away parts of the first LEP. This is indicated by dark areas where there should be F8BT in the fluorescence micrograph.

3.5 Conclusions

This project sought to investigate the use of a fluorinated methacrylate polymer as a barrier layer to protect organic active materials during patterning. It was found not to significantly alter the sensitivity of a commercial resist which could be deposited on top after an oxygen plasma surface functionalization step. Using this approach patterns of common organic active materials such as P3HT and F8BT could be patterned additively or subtractively down to 1 μm resolutions. Patterns combining up to three different organic active materials were achieved via repeating the additive process. Features in these patterns however had to be separated by 1 μm or more and not overlap otherwise the solvent used to deposit later materials would partially wash away the first. Additive patterning was also found to result in non-uniform thicknesses with significant accumulations of material along the edge of features.

In general this technique provides a robust and highly reproducible route to patterning organic materials that offers significantly more flexibility and improved processibility over previously proposed solutions. However, by examining the patterning process in more depth it raises new issues that researchers in this area would benefit from being aware of, and others that beg to be inves-

tigated further. For example, given these results patterns need to be carefully designed such that overlapping features are minimized or eliminated, unless a better solution can be found. It would also be interesting to investigate the ”edge effect” further to see if it could be tempered by altering the concentration or solvent used to deposit the organic materials, or whether a surface modification before deposition could help.

CHAPTER 4

INKJET PRINTING OF FLUOROPOLYMERS

4.1 Abstract

With the rise of functional printing there is a need to understand the inkjet printability of broad classes of materials. Fluorinated materials and solvents have some unusual properties, but this study finds them to be reliably inkjet printable. The fluorinated ink used had Reynolds and Weber numbers of 9.2 ± 1.8 and 20.3 ± 3.0, respectively, and printed line widths on silicon was varied from 45 μm to 90 μm by controlling printing parameters. A key advantage of printing from fluorinated solvents is that they can be printed on other organic layers without damaging or dissolving the underlayer. Test patterns were demonstrated on PMMA, P3HT, pentacene and F8BT. This naturally suggests their application to patterning organic semiconductors by selectively protecting some areas, so this technique is demonstrated with the fabrication of an array of 2 μm channel length P3HT transistors with patterned active areas.

4.2 Introduction

This chapter seeks to investigate the printability of fluoropolymers. Manufacture via printing, known as functional printing, is set to become increasingly

This chapter has been published previously and is adapted from Ref. [7] with permission from Springer Publishing.

important in the near future as it enables fabrication of new strucutres, or fabrication of existing structures at significantly reduced cost (via roll-to-roll processing). If fluoropolymers are to be included in these new structures, or used in their fabrication, there is a need to understand their printability.

Inkjet printing involves the generation of a drop of liquid that is subsequently deposited on a substrate after which it solidifies. Most people are somewhat familiar with the technique as inkjet printers for graphical printing have become common household items over the last two decades. Figure 4.2 illustrates the basic process. First a voltage is applied to the piezoelectric element causing it to contract and raising the membrane so that ink is drawn in to the ejection cavity. The voltage is then changed rapidly so that the piezoelectric element elongates and the membrane is lowered sending a pressure wave through the ink in the ejection cavity. When this reaches the nozzle a small drop is formed and ejected. The membrane is then relaxed before the cycle is repeated.

One of the main attractions of printing techniques is their compatibility with roll-to-roll (R2R) processing. R2R processing would use similar equipment to that used in the printing of newspapers, but applied to the electronics industry. Large-area electronic devices (e.g. LEDs that cover the entire ceiling) could be printed on continuous flexible polymer films at high speed, and therefore potentialy at low cost. The possibility of R2R processing was recognised early in the development of organic electronics, but large scale uptake has been delayed by issues such as alignment, low device performance and questionable compatibility of other processing steps.

The function of printing techniques in R2R processing is largely coating/deposition of films, and low-resolution patterning of films. There are vari-

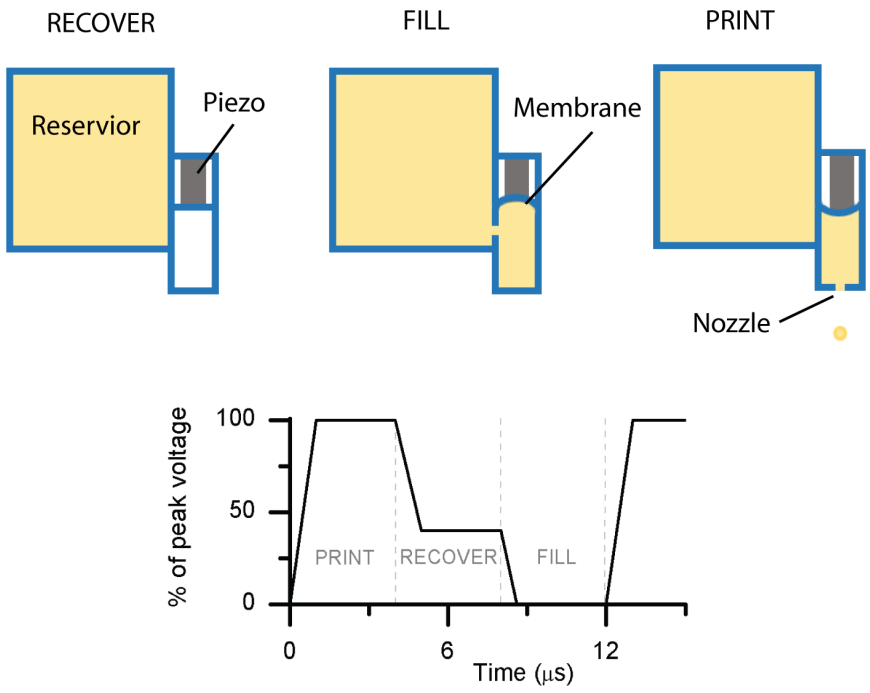

Figure 4.1: Schematic of the drop ejection process in an inkjet printer

ous printing techniques that can perform these functions and that are compatible with R2R processing, including: slot die, gravure, doctor blade... and inkjet. A review of the literature shows no study of the deposition of fluoropolymers by any of these techniques. This chapter is concerned with deposition of fluoropolymers specifically by inkjet printing. Although inkjet is a representative printing technique capable of both deposition and patterning, this investigation only scratches the surface of an area that could become extensive, and of potentially significant industrial importance if R2R processing sees widespread implementation.

The inkjet printing market is expected to double between 2011 and 2017 [102] as a result of growth in functional printing. Growth in the traditional graph-

ics sector has saturated, so the expansion of possibilities in functional printing (largely as a result of academic research) conveniently coincides with the industry looking for alternative areas of potential growth. Hence, this is an exciting time to have been involved with this topic of research.

Traditional graphics printing consists of deposition of pigment on paper. Functional printing has much greater scope encompassing the deposition of any liquid (solution, melt, suspension etc.) onto any substrate [103]. This affords a far broader range of end applications including, for example, plastic electronics [104], biosensors [105], and tissue engineering [106]. Large scale adoption of functional printing will see inkjet printing transition into a manufacturing process and can even be thought of as a stepping stone to widespread implementation of 3D printing [107].

Functional printing necessitates the ability to deposit a much wider range of materials than the dye-based aqueous suspensions used for the majority of graphical printing [108]. Printing of different materials involves many considerations and already inkjet printing of various materials have been studied including polymers [109], organic semiconductors [110], metal [111] and [112] ceramic nanoparticles and proteins [113]. This list does not include the use of any fluoropolymers or fluorinated solvents, but due to their unusual properties [57], inkjet printing of such fluorinted materials is expected to differ to that of non-fluorinated systems. This makes investigating their inkjet printability interesting from a fundamental point of view, as well as for more applied purposes.

It is expected that inkjet printing of fluorinated materials will differ in several ways to that of conventional ink. Fluorinated materials' properties that are expected to affect their inkjet printability include their low surface tension,

high density, inertness and immiscibility with non-fluorinated materials. These could affect each of the three stages of the printing process: drop ejection, interaction of the drop with the substrate and drop solidification. Low surface tension would be expected to reduce the energy barrier that must be overcome to eject a drop and aid wetting of any substrate (but this could be a concern if resolution is limited due to excessive spreading).

Several potential applications of inkjet printed fluoropolymers can be envisaged which derive from their inertness and chemical orthogonality. For example, fluorinated polymers could be deposited on top of organic polymers to form bilayers with no interfacial intermixing. This would allow them to be used as barrier layers to protect underlying organic materials from aggressive processing steps, or for patterning applications if only selected areas are protected. Another possibility is to use their difference in surface energy to direct the shape of subsequently deposited non-fluorinated inks in a quasi-chemical-patterning approach. Fluorinated photoresists and imprint resists previously developed for the patterning of organic semiconductors [23, 24], and biomolecules [101] could also be deposited via inkjet printing before subsequent processing steps.

To study the inkjet printability of fluorinated materials, a polymer system was selected for study. This had the advantage of being an easily varied and controlled system, while also leading to potential patterning applications. A model system consisting of poly(1*H*,1*H*,2*H*,2*H*-heptadecafluorodecyl methacrylate) (PFMA-2C8F) dissolved in 1,1,1,2,3,3,3-hexafluoro-4-(1,1,2,3,3,3-hexafluoropropoxy)-pentane (HFE 7600), the structures of which are shown in Figure 4.2, is used as a starting point. Solutions of PFMA-2C8F in HFE 7600 are hereinafter referred to as fluoro-ink.

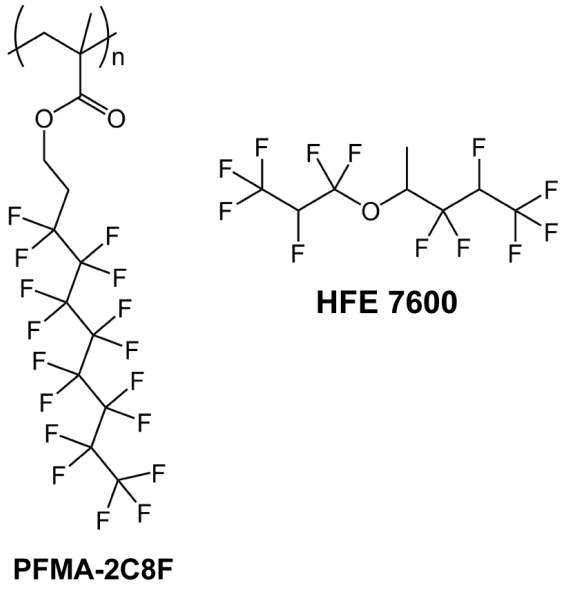

Figure 4.2: The chemical structures of PFMA-2C8F and HFE 7600.

Commercially available hydrofluoroethers have boiling points ranging from 61 °C (HFE 7100) to 131 °C (HFE 7600). HFE 7600 was selected for this study as its higher boiling point is better suited to inkjet printing. Table 4.1 compares the properties of HFE 7600 to those of other common solvents. In can be seen that HFE 7600 has a high density and very low surface energy, as expected for a highly fluorinated material. The viscosity of HFE 7600 is comparable to that of solvents typically used in organic inks and its vapor pressure is high considering its mass yet another indicator of its weak intermolecular forces.

In this study relevant contact angles were first measured and used to predict the surface energy of PFMA-2C8F. Next the effects of systematically varying basic printing parameters are investigated. Test patterns were demonstrated on a range of substrates including some organic semiconductors and finally, to demonstrate a potential application, fluoro-ink was used to pattern the organic

Table 4.1: Comparison of solvent properties

	Surface energy	Kinematic viscosity	Density	Boiling point	Vapor pressure
Units	mJ m^{-2}	x10^{-6} m^2 s^{-1}	g cm^{-3}	°C	kPa
Water	72.8	1.00	1.00	100	2.33
m-Xylene	31.1	0.94	0.86	139	1.10
Formamide	58.2	2.91	1.13	210	0.01
HFE 7600	18.0	1.07	1.54	131	0.93

Values taken from manufactures' Material Safety Data Sheets (MSDS)

semiconductor in an array of organic thin film transistors.

4.3 Experimental Methods

4.3.1 Materials

1*H*,1*H*,2*H*,2*H*-heptadecafluorodecyl methacrylate monomer was purchased from Oakwood Chemicals and used as received. 1,1,1,2,3,3,3-hexafluoro-4-(1,1,2,3,3,3-hexafluoropropoxy)-pentane (HFE 7600) was obtained from Orthogonal Inc. Silicon substrates were purchased from WRS Materials Inc. Poly(methyl methacrylate) (PMMA) and pentacene were purchased from Sigma Aldrich and used as received. Poly(3-hexylthiophene-2,5-diyl) (P3HT) and poly[(9,9-di-n-octylfluorenyl-2,7-diyl)-alt-(benzo[2,1,3]thiadiazol-4,8-diyl)] (F8BT) were purchased from American Dye Source Inc. and used as received.

4.3.2 Methods

Poly(1*H*,1*H*,2*H*,2*H*-heptadecafluorodecyl methacrylate) (PFMA-2C8F) was synthesized by radical polymerization as described previously [101]. All fluoro-ink was filtered using a 0.2 μm Nylon filter before being loaded in Dimatix 10 pL print cartridges. All printing was done using a Fujifilm Dimatix DMP-2800 printer which is a drop-on-demand system.

The following substrates were prepared for contact angle measurements and substrates for the test patterns shown in Figure 4.8. One silicon wafer was dipped in BOE 6:1 for 1 min to remove the native oxide, rinsed with deionized water and measurements were made immediately. Another silicon wafer was treated with hexamethyldisilazane (HMDS) using a YES Vapor Priming Oven. Another silicon wafer was treated with trichloro(1H,1H,2H,2H-perfluorooctyl)silane (FOTS) using an MVD 100 molecular vapor deposition tool with a 10 minute RF clean followed by a 15 minute reaction time. SPR 220, a typical photoresist from Shipley, was spincoated at 2000 rpm on to another silicon wafer followed by a 60 second bake at 115 °C. 5 wt% PFMA-2C8F was dissolved in HFE 7600, filtered with a 0.2 μm Nylon filter and spincoated at 2000 rpm on to another silicon wafer followed by a 60 second bake at 115 °C. 8 mg/ml PMMA-2C8F was dissolved in Annisole, filtered with a 0.2 μm PTFE filter and spincoated at 2000 rpm on to another silicon wafer. 5 mg/ml P3HT was dissolved in chloroform, filtered with a 0.2 μm PTFE filter and spincoated at 2000 rpm on to another silicon wafer. 5 mg/ml F8BT was dissolved in *m*-xylene, filtered with a 0.2 μm PTFE filter and spincoated at 2000 rpm on to another silicon wafer. 30 nm of pentacene was deposited on another silicon wafer by organic vapor deposition at a pressure of 1.8 x 10^{-6} Torr and a rate of 1

Å s^{-1} while the substrate was heated to 60 °C.

All contact angle measurements were made using a VCA Optima contact angle tool. Each static contact angle measurement was repeated three times and the mean of these readings is reported. Surface energy calculations were made using the built in software.

Viscosity measurements of the fluoro-ink were performed using a 25 ml calibrated Ostwald viscometer according to standard procedure. The viscometer constant was 0.0157.

To fabricate the P3HT transistors, a highly doped (Boron, 0.001 Ω cm) silicon wafer was coated with a 50 nm thick aluminium oxide dielectric using atomic layer deposition on an Oxford ALD FlexAL. (The breakdown voltage of the oxide was later measured to be 37 V). Electrodes were defined by liftoff in the following way. SPR 220-4.5 was spincoated at 3000 rpm, baked for 90 seconds at 115 °C and exposed on a GCA AS200 stepper with 365 nm UV light before a post exposure bake of 115 °C for 90 seconds. Patterns were developed on a Hamatech automated developing station using MIF 726 for 60 seconds. 25 nm of gold was then evaporated with a 3 nm chromium adhesion layer before a lift off step in acetone. 5 mg/ml solution of P3HT in chloroform was then spincoated over the whole wafer. Next a pattern of 15 wt% fluoro-ink was deposited on the P3HT such that the PFMA-2C8F drops deposited were aligned and centered over the middle of the channel. A 30 second oxygen plasma etch on a PlasmaTherm PT72 reactive ion etcher was used to remove the majority of the P3HT, leaving P3HT only in active areas protected by PFMA-2C8F droplets. The remaining PFMA-2C8F droplets were stripped by a 30 second dip in HFE leaving the patterned P3HT undamaged on finished devices. Electrical measurements were

made using a Karl Suss PSM6 submicron prober and two Keithley 236 source measurement units.

4.4 Results and Discussion

4.4.1 Inkjet Printing

Contact angle measurements

A preliminary study of static contact angle measurements was made to determine the surface energy of PFMA-2C8F while also giving insight into how HFE 7600 and fluoro-ink interact with various substrates compared to other solvents. Figure 4.3 shows contact angles of some common solvents on a spincoated film of PFMA-2C8F and of HFE 7600 wetting various substrates. All values are recorded in Table 4.2 which also shows the results of calculations to predict each substrate's surface energy. Water, m-xylene and formamide all have relatively high contact angles on PFMA-2C8F, in agreement with the literature [114], while HFE 7600 wets it well. HFE 7600, due to its low surface energy, has very low contact angles on all substrates tested. The contact angles of water, m-xylene and formamide were used in combination to calculate surface energies using both the geometric and harmonic mean methods [115], where the harmonic mean method is more accurate for low surface energies [116]. Values calculated compare well with those that exist in the literature. The surface energy of PFMA-2C8F, taking the value from the harmonic mean method, is found to be 13.1 mJ m^{-2}. This is very low and comparable to Teflon which has

Table 4.2: Contact angle measurements and calculated surface energies

					Calculated surface energy, mJ m^{-2}					
	Static contact angle, °				Harmonic			Geometric		
	Water	*m*-Xylene	Formamide	HFE 7600	d	p	total	d	p	total
Silicon	72.7	3.9	66.8	13.6	23.0	13.4	36.4	16.1	14.6	30.7
HMDS	84.1	9.9	62.8	15.0	64.3	8.1	72.4	21.1	8.7	29.8
FOTS	107.1	68.1	90.2	19.8	17.7	4.4	22.1	10.8	3.3	14.1
SPR 220	75.2	11.6	52.1	13.3	29.7	15.0	44.7	22.3	14.4	36.7
PFMA-2C8F	117.8	78.1	109.8	*	10.4	2.7	13.1	6.0	1.1	7.1

* Measurement not possible as solvent dissolved the substrate.

a surface energy of 18.4 mJ m^{-2}. These calculations also give an indication of the contributions to the surface energy from dispersive (d) and polar (p) intermolecular forces which are both found to be low for PFMA-2C8F, as expected. It is also observed that static contact angles on silicon increase with increasing concentration of PFMA-2C8F in HFE 7600. Measurements of 0, 5, 10, 15 and 20 wt% fluoro-ink result in values of 14, 21, 20, 26 and 32° respectively. However, the effect of solidification at the drop surface (film formation) may distort these contact angle measurements.

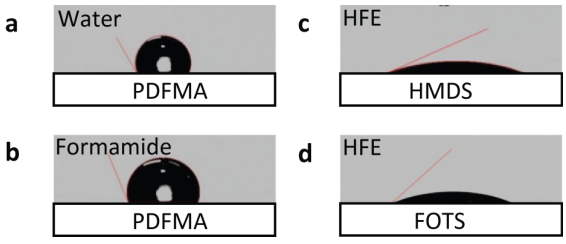

Figure 4.3: Contact angles.

Effect of varying printing parameters

An initial test of inkjet printing a 15 wt% fluoro-ink found it to be facile, robust and stable for several minutes. Figure 4.4a shows an image of six nozzles simultaneously ejecting typical fluoro-ink droplets. We speculate that the ease of printing is a result of fluoro-inks low surface energy. Wetting of the printhead around the nozzles by the fluoro-ink does not pose a significant problem and only occurs in very small areas. A ligament is observed behind the ejected drop which is not unusual in inkjet printing of polymer solutions [117] and is discussed in more detail below.

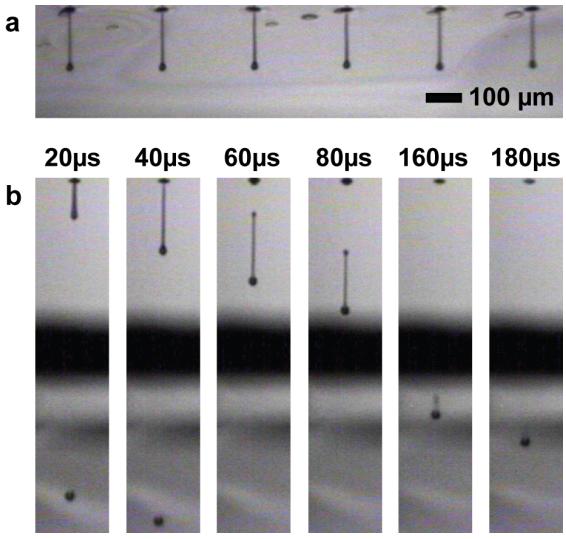

Figure 4.4: Drops being ejected.

During continuous inkjet printing, a periodically varying voltage (waveform) is applied to the piezoelectric printhead. The waveform used in this study is shown in Figure 4.2 where t = 0 is the point at which the voltage first becomes positive. At t = 0 a drop is forced out of the print nozzle and at t = 20 μs can be seen protruding 100 μm or so out of the printhead (Figure 4.4 b). The drop

is ejected in full by t = 60 μs and is initially composed of a large leading drop followed by a ligament of much thinner diameter. It is interesting to note that although the surface energy of fluoro-ink is extremely low it still provides sufficient driving force to make the ligament contract and re-join the drop by t = 180 μs. This occurs at 0.75 mm below the printhead. As long as the printhead height above the substrate exceeds this no satellite drops or splatter are observed.

The inkjet printability of a liquid can be quantified using the Reynolds (Re) and Weber (We) numbers [103] defined as,

$$Re = \frac{va}{\eta} \tag{4.1}$$

$$We = \frac{v^2 \rho a}{\gamma} \tag{4.2}$$

where v is the drop velocity, a is the drop radius, η is the kinematic viscosity, ρ is the ink density, and γ is the surface energy of the ink. 15 wt % fluoro-ink was found to have a density of 1.508 g cm^{-3}. Taking γ to be the mean of the values for PFMA-2C8F and HFE 7600 gives $Re = 9.2 \pm 1.8$ and $We = 20.3 \pm 3.0$ where the errors are dominated by the uncertainty in a and γ. To assess the inkjet printability a third parameter, Z, is defined

$$Z = \frac{1}{Oh} = \frac{Re}{\sqrt{We}} \tag{4.3}$$

where Oh is the Ohnesorge number. Z must fall in the range $1 < Z < 10$ for an ink to be printable [103]. Using the values for 15 wt % fluoro-ink gives $Z = 2.0 \pm 0.5$ which meets the requirement for printablilty and puts 15 wt% fluoro-ink in the

printable fluid region when these quantities are mapped out as in Figure 4 of Reference 2.

The viscosity of fluoro-ink can be controlled by varying its concentration. The relationship departs from linearity at higher concentrations as the assumption of no interaction between macromolecules in solution becomes invalid (Fig. 5a). Fluoro-inks with concentrations ranging from 10 wt% to 18 wt% were printable. Below 10 wt%, the fluoro-ink dribbles out of the nozzle, presumably because the surface tension is not great enough to form a barrier across the nozzle. Above 18 wt%, a droplet cannot be ejected because the energy barrier is too high. A concentration of 15 wt% was found to be optimal for jetting and all further studies were conducted with this ink.

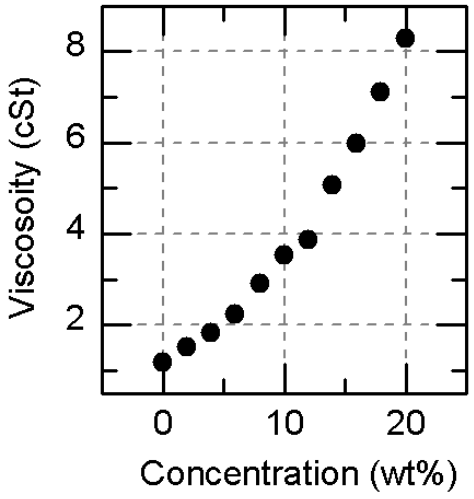

Figure 4.5: Variation of fluoro-ink viscosity with concentration

The highest resolution features achieved were 45 μm-wide lines. This is limited by the print cartridge dimensions and not the properties of the ink. It is expected that higher resolution features would be possible using a print cartridge with smaller nozzle diameter. Line width was influenced by a number of

printing parameters including drop spacing, height of the printhead above the substrate and peak jetting voltage. Adjusting drop spacing results in the greatest control and widest range of possible line widths as plotted in Figure 4.6a and in the micrographs of Figure 4.7. Drop spacings greater than 45 μm result in discontinuous lines. The (maximum) thickness of lines also decreases with increasing drop spacing suggesting that the volume of ink per unit length is decreasing. This makes sense as a single droplet is spread over a greater length when drop spacing is increased.

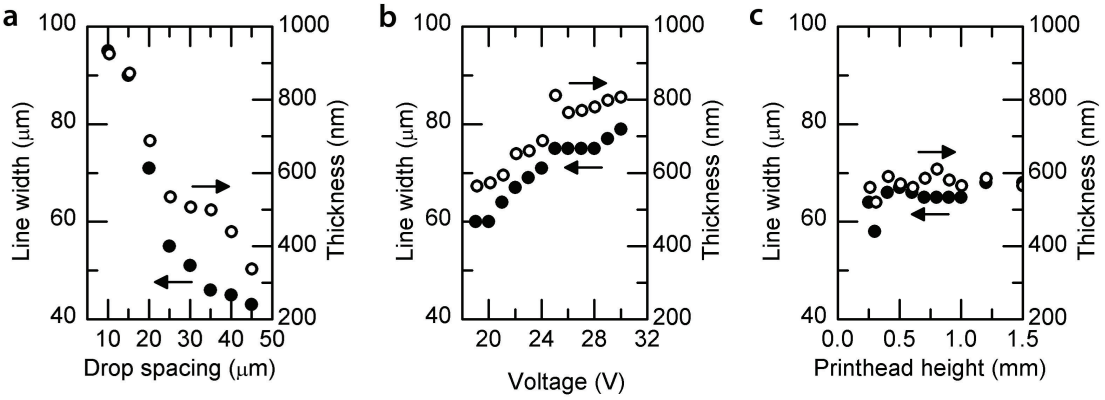

Figure 4.6: Effect of varying a) drop spacing, b) peak ejection voltage, and c) printhead height on printed line dimensions.

Increasing peak jetting voltage also increased line width, as shown in Fig. 4.6b. Again, the maximum thickness follows the line width, but in this case indicates that at higher peak voltages the volume of the droplet ejected increases, while being spread over the same length. However, variation of peak voltage does not achieve as wide a range of line widths as varying drop spacing. Below 19 V, no drop is ejected and above 30 V there is significant splatter. The effect of peak voltage on the shape of drop ejected is shown in Figure 4.4d. At a print-

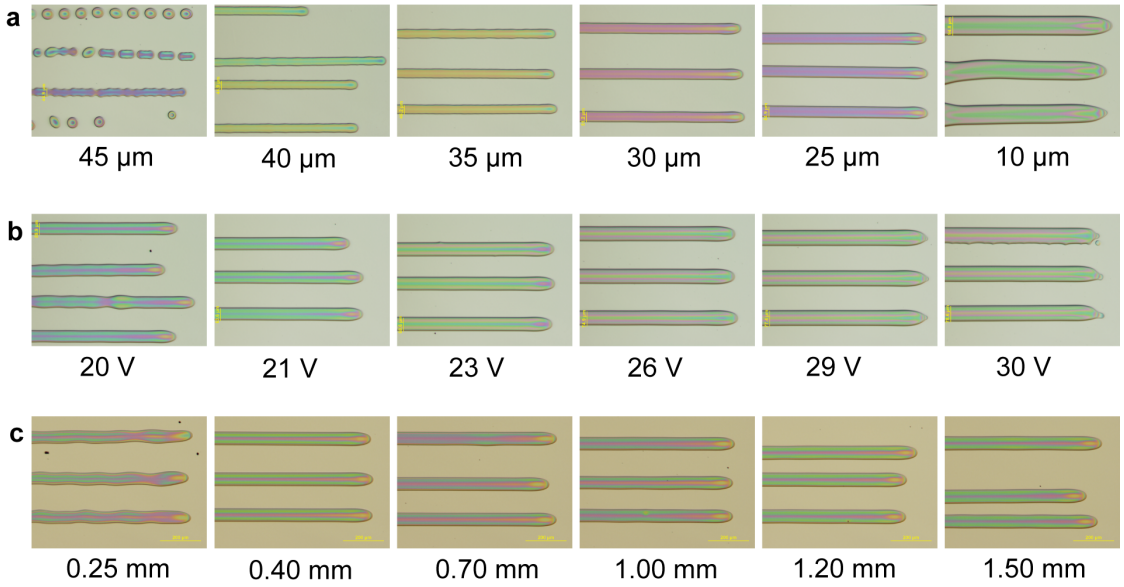

Figure 4.7: Micrographs taken in reflection mode of lines printed of 15 wt% fluoro-ink printed on silicon with varying a) drop spacing, b) peak ejection voltage, and c) printhead height.

head height of 1 mm and peak voltages below 28 V, the ligament contracts to form satellite drops which rejoin the main drop before impacting the substrate.

4.4.2 Printing on Organic Materials

A key advantage of fluoro-ink is that it can be printed onto underlying organic layers without damage and without causing any other alterations. The solvents used to print conventional organic inks are likely to penetrate into and partially dissolve underlying organic layers, but this is not a problem when using highly fluorinated solvents.

One potential application of inkjet printed fluoro-inks is their use for pat-

terning organic semiconductors. They can be printed on top of organic semiconductors without any intermixing, used to selectively protect underlying areas, and later stripped without damaging the organic semiconductor. This ability to create non-interacting multi-layers of inkjet printed materials comes at a time when functional printing is seeking to produce structures of increasing complexity. Note also, that this patterning technique is compatible with roll-to-roll processing and hence of interest in the fabrication of low-cost, large area electronics on flexible substrates.

Fluoro-ink can be printed on various organic thin films including organic semiconductors. Test patterns on silicon and thin films of PMMA, pentacene, poly(3-hexylthiophene-2,5-diyl) (P3HT) and poly[(9,9-di-n-octylfluorenyl-2,7-diyl)-alt-(benzo[2,1,3]thiadiazol-4,8-diyl)] (F8BT) are shown in Figure 4.8. Very similar patterns and resolutions are observed on each substrate despite variations in surface chemistry. In agreement with the contact angle measurements of HFE 7600, the fluoro-ink patterns appear to wet each substrate similarly (due to its low surface energy). The similarity of patterns on different substrates suggests drop spreading is capillary driven rather than impact driven although spreading might be affected by the formation of a solid film on the surface of the droplet due to evaporation of the solvent. However, excessive spreading that would limit resolution is not observed.

After solidification the thickness of a drop varies slightly with radius, as indicated by the colored rings seen in all the micrographs of the test patterns in Figure 4.8. This variation is caused by the coffee stain effect and is observed to be more significant at lower concentrations of fluoro-ink. However the cross section SEM of fluoro-ink on PMMA shown in Figure 4.9 confirms that thick-

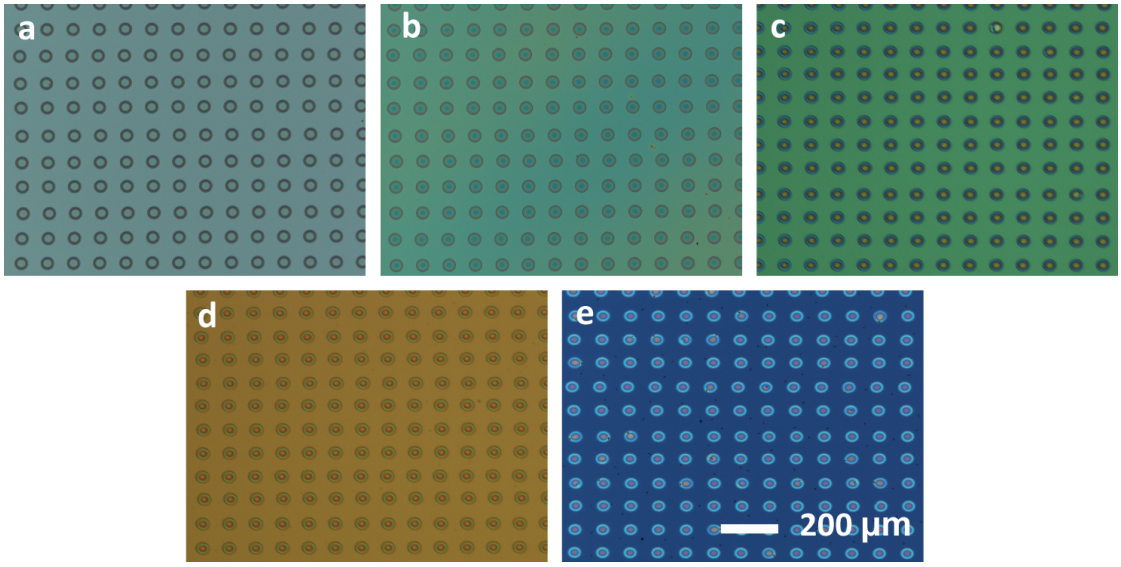

Figure 4.8: Demonstration patterns of fluoro-ink drops on a) silicon, b) PMMA, c) P3HT, d) F8BT and e) pentacene.

ness variation is not significant for 15 wt % fluoro-ink. Two distinct layers can clearly be seen in the higher magnification image and there is no evidence of intermixing or solvent damage to the underlying PMMA layer.

4.4.3 Device Fabrication and Characterization

To establish the utility of fluoro-inks for patterning organic semiconductors, an array of P3HT transistors with 2 μm channel lengths was fabricated. Fluoro-ink was printed on top of the P3HT and used as an etch mask to pattern the active region. It has been shown that performance of bottom contact P3HT transistors can be improved by patterning the organic semiconductor [118] and this provides a straight-forward, high-throughput method of doing so that is also

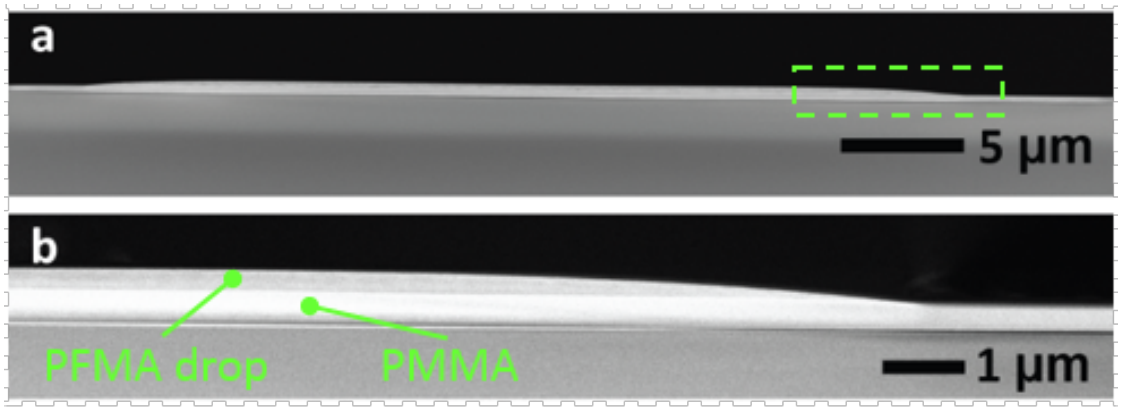

Figure 4.9: SEM cross sections of a fluoro-ink drop on a PMMA film (on silicon substrate) where a) shows the whole drop and b) is an enlargement of the section indicated by a dashed box in a).

roll-to-roll compatible. A schematic of the device is shown in Figure 4.10.

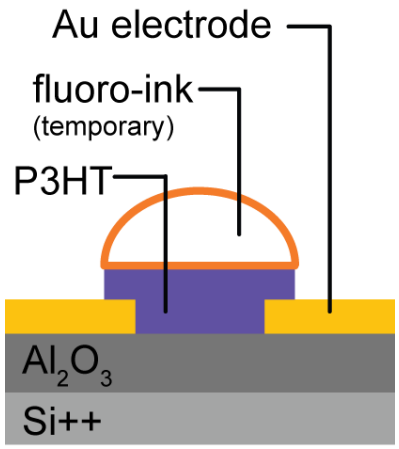

Figure 4.10: Device architecture.

An images of an array of 3 x 6 finished devices is shown in Figure 4.11a, while 4.11b shows a close-up of a finished device (with patterned P3HT and no fluoro-ink drop). Fig 4.11c shows the device during fabrication as P3HT covers

all areas and the fluoro-ink drop has been placed on top of the active region to protect it during the subsequent oxygen plasma step.

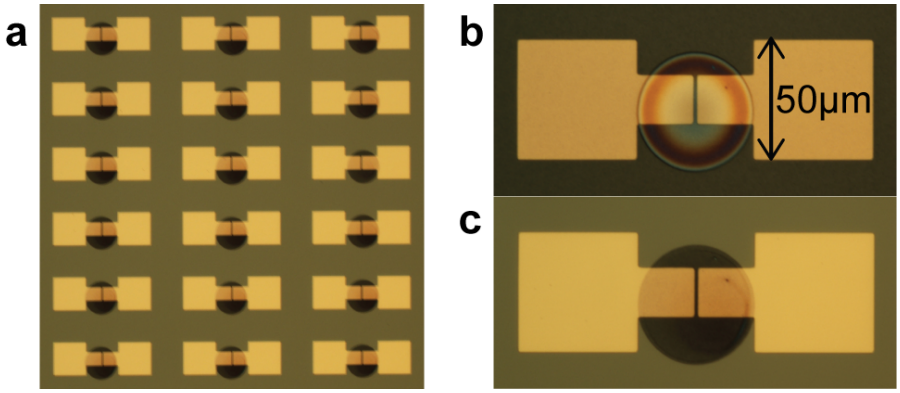

Figure 4.11: Micrographs of a) an array of patterned TFTs, b) the device during fabrication and c) the final device.

Electrical characteristics of a typical device are shown in Figure 4.12. The mobility was extracted and found to be 0.029 $cm^2\ V^{-1}\ s^{-1}$ with an on/off current ratio of 10^3 . There is no evidence that the electrical characteristics of the organic semiconductor were altered by the deposition of fluoropolymer on top of it, nor by submersion in HFE 7600 during stripping.

4.5 Conclusions

Although fluorinated materials have some unusual properties, namely very low surface energies, they can be reliably inkjet printed. This has been demonstrated using a model fluoropolymer ink (fluoro-ink). The surface energy of the fluoropolymer, PFMA-2C8F, was found to be 13.1 mJ m^{-2}. Fluoro-ink inkjet prints robustly and controllably, albeit with some differences to printing of conven-

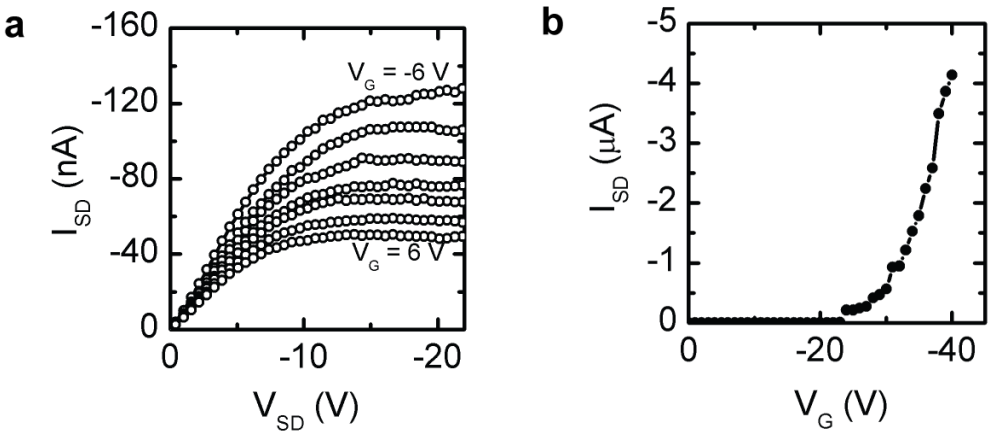

Figure 4.12: Electrical characteristics of a typical inkjet patterned device.

tional inks. The Reynolds and Weber numbers for the 15 wt% fluoro-ink used throughout were found to be 9.2 ± 1.8 and 20.3 ± 3.0, respectively. A ligament is formed during drop generation but does retract into the main drop as long as the printhead is greater than 0.75 mm from the substrate. Lines with widths varying from 45 μm to 90 μm were achieved by varying the drop spacing; peak voltage and printhead height showed lesser effects on line width.

Fluoro-ink can be printed on other organic thin films without the fluorinated HFE 7600 solvent damaging the underlayer. Test patterns were demonstrated on a range of organic substrates and cross section SEM images show no evidence of intermixing with an underlying PMMA layer. This makes fluoro-inks ideal for patterning organic semiconductors in a straightforward, high-thoughput, roll-to-roll compatible method. To demonstrate this application fluoro-ink was used to pattern the active areas of an array of P3HT transistors with 2 μm channel lengths.

This work establishes that inkjet printing of fluorinated materials is both

possible and useful. The ability to print multilayer organic structures without them interacting is key and we hope it will motivate future work on dispersing or dissolving other materials in similar solvents for inkjet printing applications.

CHAPTER 5

TOWARDS A POSITIVE-TONE FLUORINATED E-BEAM RESIST

5.1 Abstract

The chapter describes the development of a positive-tone e-beam resist fully processible in fluorinated solvents thus enabling the fabrication of sub-100 nm channel length top-contact organic thin film transistors. Several fluorinated methacrylate resists are tested and show promising results. A switch from positive- to negative-tone behavior is observed at relatively low doses due, it is hypothesized, to the loss of fluorinated side chains. Clearing of the last 15 - 20 nm of resist was identified as a major problem. Using the resist at negative-tone doses a process for device fabrication, although not ideal, is developed. Several significant findings are made which lay the groundwork for eventual creation of the desired resist.

5.2 Introduction

Organic materials such as the polymeric semiconductors used in organic electronics cannot be patterned with conventional resists as the solvents used will damage or dissolve them. Fluorinated polymers and solvents are chemically orthogonal (i.e. non-interacting) to these organic materials and provide the perfect material system to develop new patterning materials, an approach our group has named *orthogonal processing*. Ideally, orthogonal processing should include a family of resists capable of patterning organic materials at all desirable resolu-

tions with the option of choosing positive- or negative-tone process flows. The progress made so far is summarized in Figure 5.1. A non-chemically amplified fluorinated methacrylate copolymer photoresist that achieves 1 μm resolutions can be switched between positive- or negative-tone behavior by altering the copolymer composition and developer solvents [24]. Although this resolution is probably sufficient for all manufacturing requirements of organic electronics, higher resolution patterning may be useful in the design of experiments to, for example, study the relationship between electronic properties and the microstructure of organic semiconductors. Hence, a fluorinated resorcinerene was shown to be patternable by exposure to an electron beam (e-beam) to achieve negative-tone patterning [23] of features down to 80 nm. Note that it is relatively easy to attain negative-tone behavior in fluorinated systems by simply inducing the detachment of the fluorinated side chains causing a loss of solubility in fluorinated solvents (although this can lead to problems in stripping the resist). A resist that allows high resolution positive-tone patterning is anticipated to be more difficult to develop, but that is the aim of this work as it may also have more interesting applications, such as the fabrication of sub-100 nm channel length *top* contact organic thin film transistors (OTFTs).

Poly(methyl methacrylate) (PMMA), shown in Figure 5.2, has been the work-horse resist used for the majority of e-beam patterning for decades [119, 120]. It is easily spin coated, exhibits positive-tone behavior, has good sensitivity, acceptable resolution and acceptable etch resistance. The approach taken here to develop an orthogonal e-beam resist is to start with PMMA and add sufficient fluorination to make it processible in fluorinated solvents. To maintain a similarity with PMMA it is decided that the fluorination should be added in the form of a side chain off the carboxylate group of PMMA and

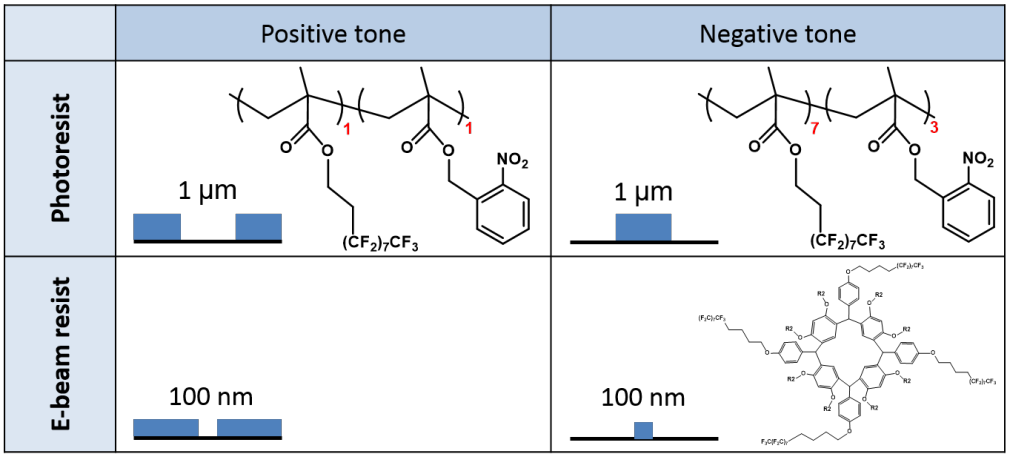

Figure 5.1: Summary of the orthogonal family of resists developed to date.

separated by an alkyl spacer of at least $(CH_2)_2$ from the oxygen. As for the length of the fluorinated sidechain, previous work in the Ober Group on developing orthogonal photoresists utilized copolymers of poly(1*H*, 1*H*, 2*H*, 2*H*,-heptadecafluorodecyl methacrylate (PFMA-2C8F) [23, 24] shown in Figure 5.2. It has the same backbone as PMMA, a fluorinated side chain long enough to give it good solubility in fluorinated solvents and is easily synthesized from the commercially available monomer. PFMA-2C8F is therefore used as a starting point in this investigation, before branching out to experiment with other fluorinated methacrylate polymers.

In 1977 Kakuchi *et al.* briefly investigated the e-beam patternability of a poly(fluorobutyl methacrylate) shown in Figure 5.2 and found it to be more sensitive than PMMA [121]. Strahan *et al.* [122] also more recently investigated the e-beam patternability of some fluorine-containing polymethacrylates. Their motivation was different - they sought to develop a resist with greater sensitivity by replacing the α-CH_3 with an electron-withdrawing α-CF_3 group in order

to increase the backbone scission efficiency of the polymer. The polymers they looked at, shown in Figure 5.2, therefore contained much less fluorine than that required to give solubility in fluorinated solvents, but they still report some findings of relevance to this work. Quoting directly from their publication and referring to the polymers in Figure 5.2:

"[D] was envisioned as a means to determine the effect of fluorine incorporation in a position believed not to effect chain scission.

and later,

A surprising find was the similarity of the G(s) values for [C] (2.75) and [D] (2.80). It was hypothesized that [D] would have a lower scission efficiency than [C] due to the lack of a α*-*CF_3 *substituent; The effect of the -*CH_2CF_3 *alkoxy substituent on the G(s) warrants further study.*

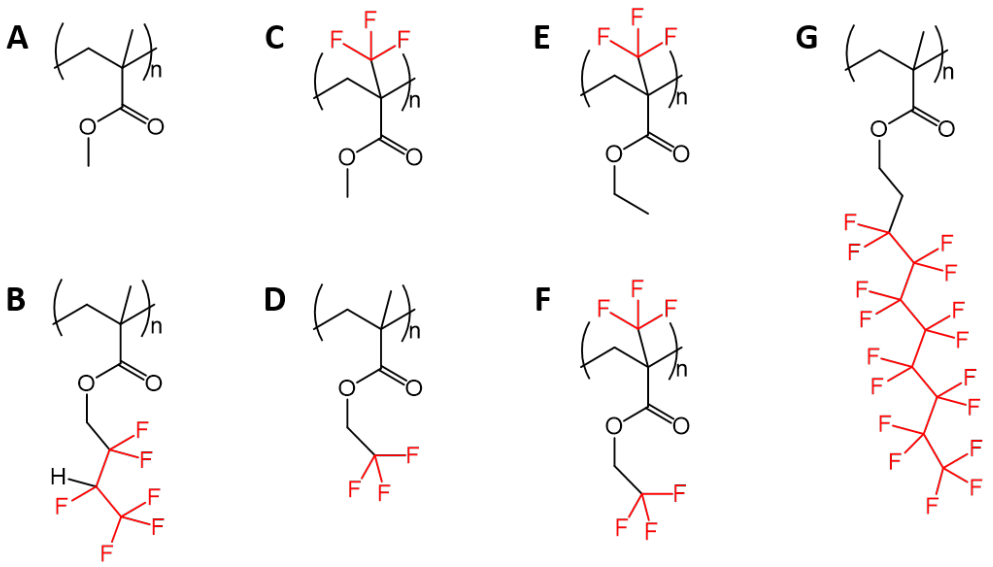

Figure 5.2: The chemical structures of A) PMMA, B) the PFMA investigated by Kakuchi *et al.*, C-F) the PFMAs investigated by Strahan *et al.* and G) PFMA-2C8F.

Attaining high sensitivity is not one of the goals of this work as an orthogonal e-beam resist is anticipated to only be used for small experimental exposures. The aim of this work is rather to understand the changes in solubility in fluorinated solvents of these fluorinated methacrylates polymers. Throughout this work hydrofluoroethers (HFEs) are the solvent of choice as they have previously been shown to be suitable for processing of organic electronic materials [23], and other commercially available fluorinated solvents are used at limited times.

The solubility of a successful orthogonal positive-tone resist needs to be carefully balanced. It must be sufficiently soluble in a strong fluorinated solvent to allow good spin coating, and it must maintain this solubility throughout in order to allow resist stripping at the end of the process. However, it must be insoluble enough in a weaker fluorinated solvent to resist being dissolved during the development step. Meanwhile, the e-beam exposure must increase the solubility of the exposed resist allowing these regions to be dissolved in the weaker solvent during the development step, hence forming patterns.

The solubility of PFMA polymers in fluorinated solvents is largely governed by the fluorinated side chain. There are many fluorinated methacrylates that could potentially function as an orthogonal positive-tone e-beam resist, some are shown in Figure 5.3. Varying the length of the alkyl spacer and the length of the side chain is expected to affect the polymer's solubility in fluorinated solvents as well as the probability of side chain scission. Understanding these relationships is key to attaining a good resist so several PFMA structures were investigated. The choices were made according to what monomers were commercially available and in order to test certain hypotheses. All PFMA polymers

were synthesized in the same way resulting in similar molecular weights and dispersities, as detailed in the Experimental Methods section, therefore allowing comparisons to be made between different PFMA polymers (i.e. assuming that variation in molecular weight or dispersity were not the cause of observed differences in solubility or resist sensitivity).

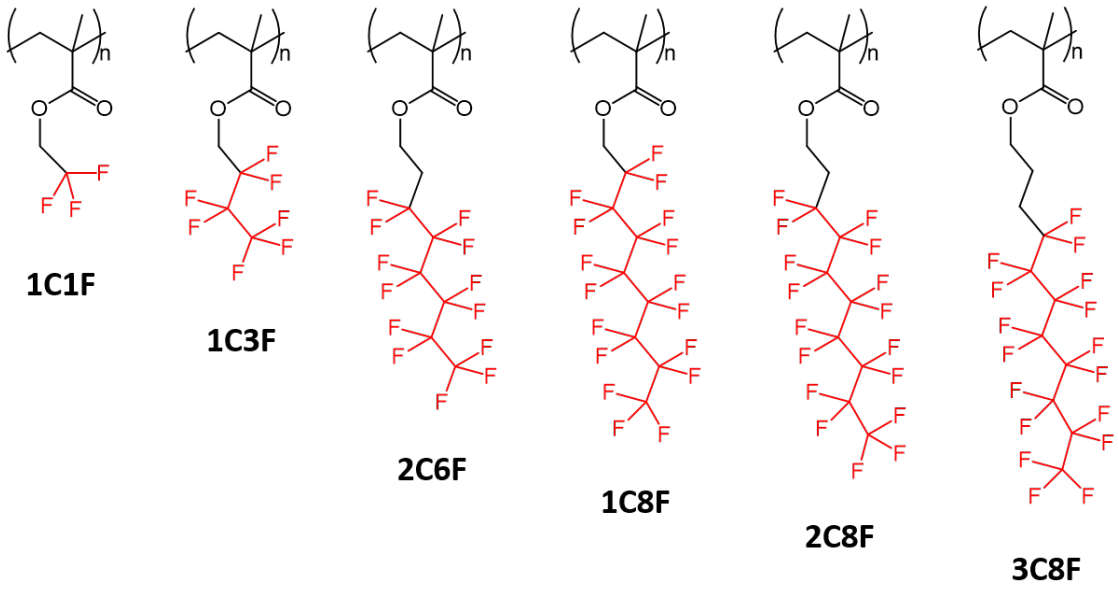

Figure 5.3: The chemical structures of the poly(fluorinated methacrylate) (PFMA) polymers used in this study.

It is envisioned that this resist would enable a variety of experiments that examine the fundamental relationships between organic active material microstructure and the electronic behavior of devices fabricated from it. One such possible experiment is described here. Pentacene [123] and P3HT [124] have long been the basic test materials for the fabrication of OTFTs made from small molecule and polymeric semiconductors, respectively. Pentacene OTFTs have already been fabricated with channel lengths down to 30 nm [125] but the bot-

tom contact configuration is not ideal as the presence of pre-fabricated electrodes can alter the growth of the organic semiconductor on top. A top contact configuration, as show in in Figure 5.4 is preferable as the organic semiconductor is first deposited undisturbed, then electrodes are formed on top. Several routes to top-contact OTFTs have been proposed [24, 37, 126] but these all use photolithographic methods which limits channel lengths to 1 μm or greater. As shown in Figure 5.4 b) a 1-2 μm channel in a pentacene device would incorporate a great variety of microstructural features between the two electrodes. In order to really isolate and probe certain microstructural features the contacts need to be defined by e-beam patterning. This would allow, for example devices to be fabricated in which the channel sits entirely in a single pentacene grain. This might allow a better experimental measurement of the intrinsic mobility of charge carriers in pentacene. It would also be interesting to compare the performance of such a device with one that is intentionally positioned to have a grain boundary in the channel region, as illustrated in Figure 5.4 c).

5.3 Experimental Methods

5.3.1 Materials

The monomers, 1*H*,1*H*-trifluoroethcyl methacrylate, 1*H*,1*H*-heptafluorobutyl methacrylate, 1*H*,1*H*,2*H*,2*H*-tridecafluorooctyl methacrylate, 1*H*,1*H*- heptadecafluorononyl methacrylate, 1*H*,1*H*,2*H*,2*H*-heptadecafluorodecyl methacrylate, and 1*H*,1*H*,2*H*,2*H*,3*H*,3*H*-heptadecafluoroundecyl methacrylate, were purchased from Oakwood Chemicals and used as received. HFE 7600, HFE 7500

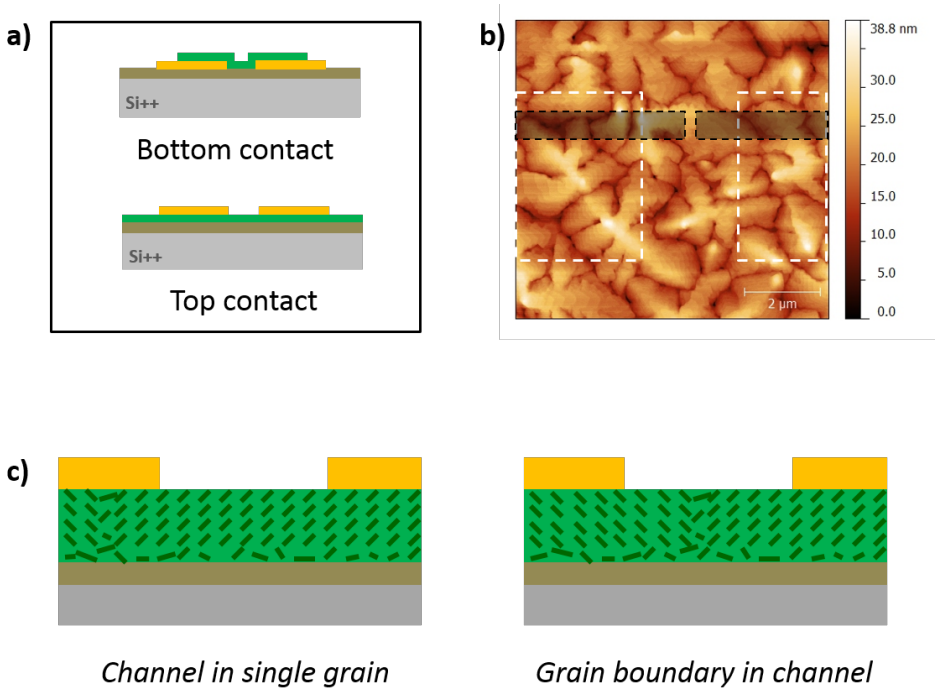

Figure 5.4: Schematic showing a) the difference between top- and bottom-contact OTFTs, b) an AFM of pentacene grains with outlines of the electrodes possible with photolithgraphy (white dashed) and e-beam patterning (black dashed). c) shows the proposed experiment enabled by e-beam patterning comparing OTFTs with and without a grain boundary between the electrodes.

and HFE 7200 were gratefully received from Orthogonal Inc. FC 770 was purchased from Fluoryx Inc and used as received. Pentacene, trifluorotoluene (TFT) and hexanes were purchased from Sigma Aldrich and used as received. Test grade and highly doped p-type silicon wafers were purchased from Wafer Reclaim Services Inc.

Table 5.1: GPC Results

Polymer	M_n	PDI
1C1F	15 000	2.3
1C3F	17 000	2.1
2C6F	20 000	2.5
1C8F	19 000	2.1
2C8F (batch 1)	19 000	2.2
2C8F (batch 2)	22 000	2.2
3C8F	21 000	2.3

5.3.2 Methods

Polymer Synthesis The poly(fluorinated methacrylate) (PFMA) polymers were synthesized via radical polymerization as described previously [101]. The procedure was adapted slightly to synthesize the copolymers of PFMA-1C1F and PFMA-2C8F by adding the weight fraction of the respective monomers in a Schlenck tube to attain the desired copolymer ratio. Table 5.1 shows the results of gel permeation chromatography (GPC) measurements of the PFMA polymers conducted at Asahi Glass Co. using a fluorinated solvent [127].

Dose Tests PFMA was filtered with a 0.2 μm Nylon filter and spincoated at 2000 rpm directly on to silicon substrates. The wafer was baked at 90 °C for 60 seconds to remove any residual solvent. The sample was then exposed on a JEOL 6300 E-beam system with a 500 pA beam current.

Device Fabrication A gate dielectric consisting of 50 nm of alumina was grown via atomic layer deposition on a Si++ wafer using a Flex ALD system. 30 nm of pentacene was then grown in a dedicated organic deposition chamber at a

rate of 1 Ås^{-1} in a vacuum of 6x10^{-8} Torr while the substrate was heated to 60 °C. PFMA resist was then filtered and spin coated at 2000 rpm on top and exposed and developed as detailed above. 25 nm of gold is then thermally evaporated on to the substrate at a vacuum of 2x10^{-6} Torr and lift off is performed in HFE 7600 for 15 minutes with gentle agitation by pipette.

5.4 Results and Discussion

5.4.1 Patterning PFMA-2C8F

First, a simple dose test is conducted in which PFMA-2C8F is spincoated from HFE 7600, a relatively good fluorinated solvent, and developed in FC 770, a poor fluorinated solvent, as shown in Figure 5.5. The polymer is found to be e-beam sensitive at doses ranging from 20 to 200 μC cm^{-2}, however the results are surprising in several ways. First, a switch from positive-tone to negative-tone behavior is observed at around 60 μC cm^{-2}. Secondly, PMMA generally requires a dose above 50 μC cm^{-2} in order to give a positive-tone pattern, yet PFMA-2C8F shows patterns at a significantly lower dose. In fact, at higher doses it appears that even the *backscattered* electrons provide a dose sufficient to cause positive-tone behavior (i.e. main chain scission) in the surrounding resist (making the negative-tone patterns visible). This indicates that PFMA-2C8F is very sensitive, more so than PMMA, despite the presence of the alkyl spacer separating the electron-withdrawing fluorines from the polymer backbone.

A switch from positive-tone to negative-tone behavior is also observed in PMMA, but usually occurs at a much higher dose, around 500 μC cm^{-3}, where

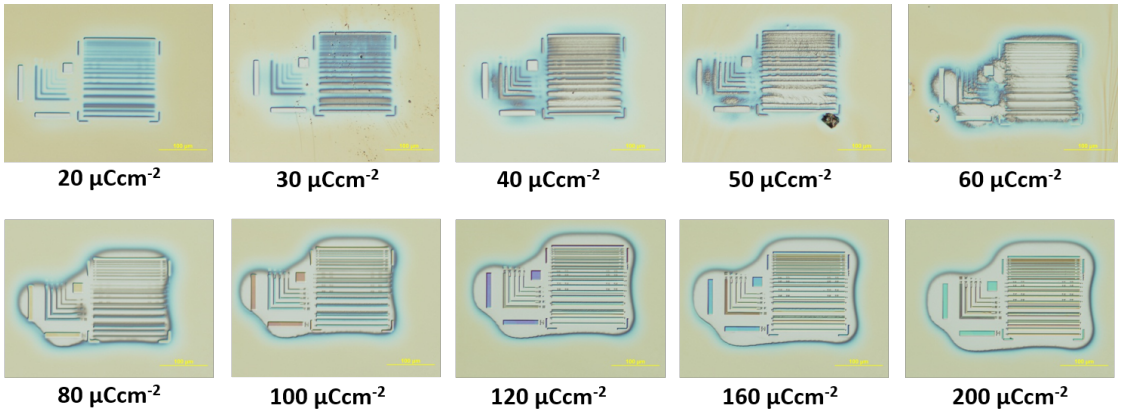

Figure 5.5: Dose test of PFMA-2C8F developed in FC 770.

enough energy is provided to begin cross-linking the PMMA hence increasing its molecular weight and reducing its solubility compared to unexposed PMMA. The fact that this switch occurs at a much lower dose in PFMA-2C8F suggests that it is a result of a different mechanism. The main difference between PMMA and PFMA-2C8F is the fluorinated side chain. This leads to the hypothesis that the switch to negative-tone behavior results from the scission of the side chain from the polymer main chain, thus removing its solubility in the fluorinated developing solvent. A comparison of the e-beam decomposition mechanisms of PMMA and PFMA-2C8F (proposed) is shown in Figure 5.6.

More light is shed on the switch from positive- to negative-tone by the result of altering the developing solvent. Figure 5.7 shows the results of exposing the same PFMA-2C8F film then developing it in HFE 7200 (a stronger fluorinated solvent than FC 770). No patterns were observed at doses below 60 μC cm^{-2} and only negative-tone behavior is observed at doses above that. This can be explained by understanding that HFE 7200 is strong enough to dissolve the un-

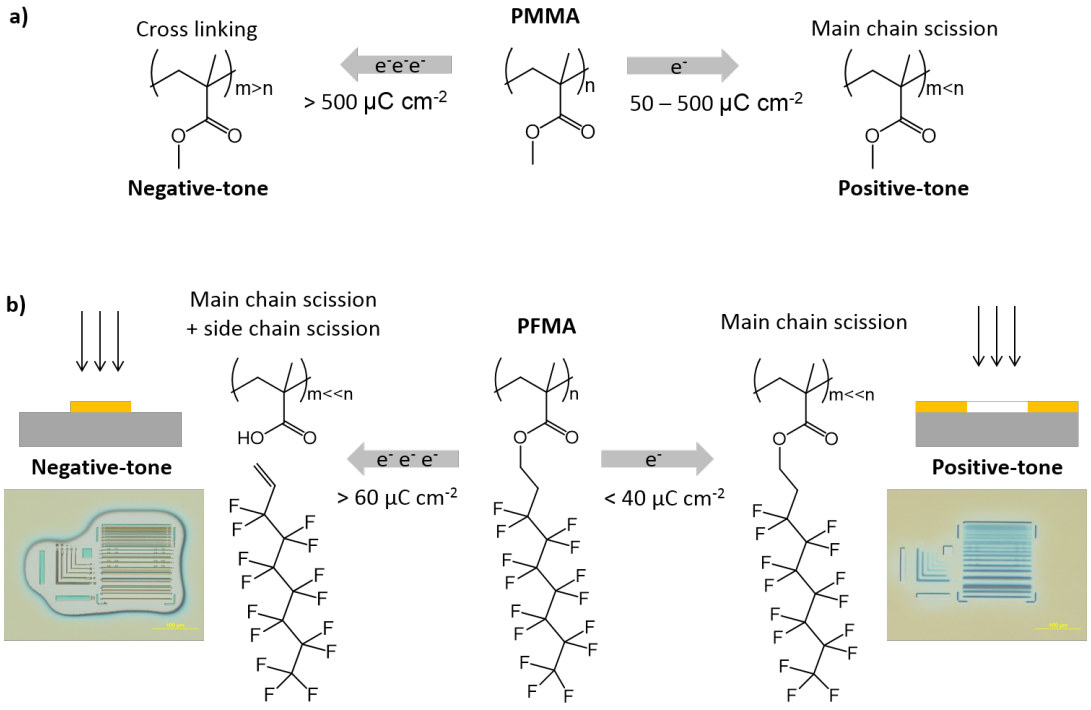

Figure 5.6: Diagram comparing the resist mechanisms of a) PMMA and b) PFMA-2C8F (proposed).

exposed PFMA-2C8F. It therefore presumably removes all of the PFMA-2C8F and the only polymer remaining on the sample is *insoluble* in the fluorinated solvent and must have had its fluorinated side chain partially or fully removed. This result indicates that side chain scission occurs at and above doses of 60 μC cm^{-2}. As this leads to undesirable negative-tone behavior and problems with stripping, if PFMA-2C8F is to make a successful positive-tone resist it must be exposed with a dose of less than this, regardless of the developing solvent.

When the features of the exposed patterns in Figure 5.5 were measured with a profilometer the positive-tone patterns were found to not be cleared down to the substrate. For this reason the developing time was increased as shown in

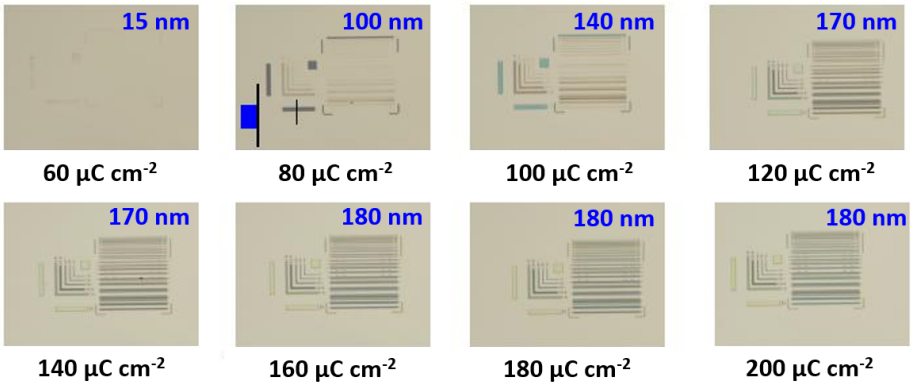

Figure 5.7: Dose test of PFMA-2C8F developed in HFE 7200. Numbers is blue indicate profilometer measurements of the patterned resist thickness. *Optical images taken by J. K. Lee.*

Figure 5.8. However, no matter how much the developing time was increased the patterns did not clear, while the thickness of the unexposed resist decreased linearly.

Another curious observation from the PFMA-2C8F dose test is that at higher doses the resulting negative-tone patterns were *thicker* than the unexposed film thickness, and that the thickness increased with developing time. This suggests that although the side-chain-scissioned PFMA-2C8F is not soluble in FC 770 there is enough favorable interaction between the polymer and solvent to cause it to swell.

5.4.2 Patterning PFMA-1C1F

Some interesting results were obtained from patterning experiments with poly(2,2,2-trifluoroethyl methacrylate) referred to here as PFMA-1C1F and

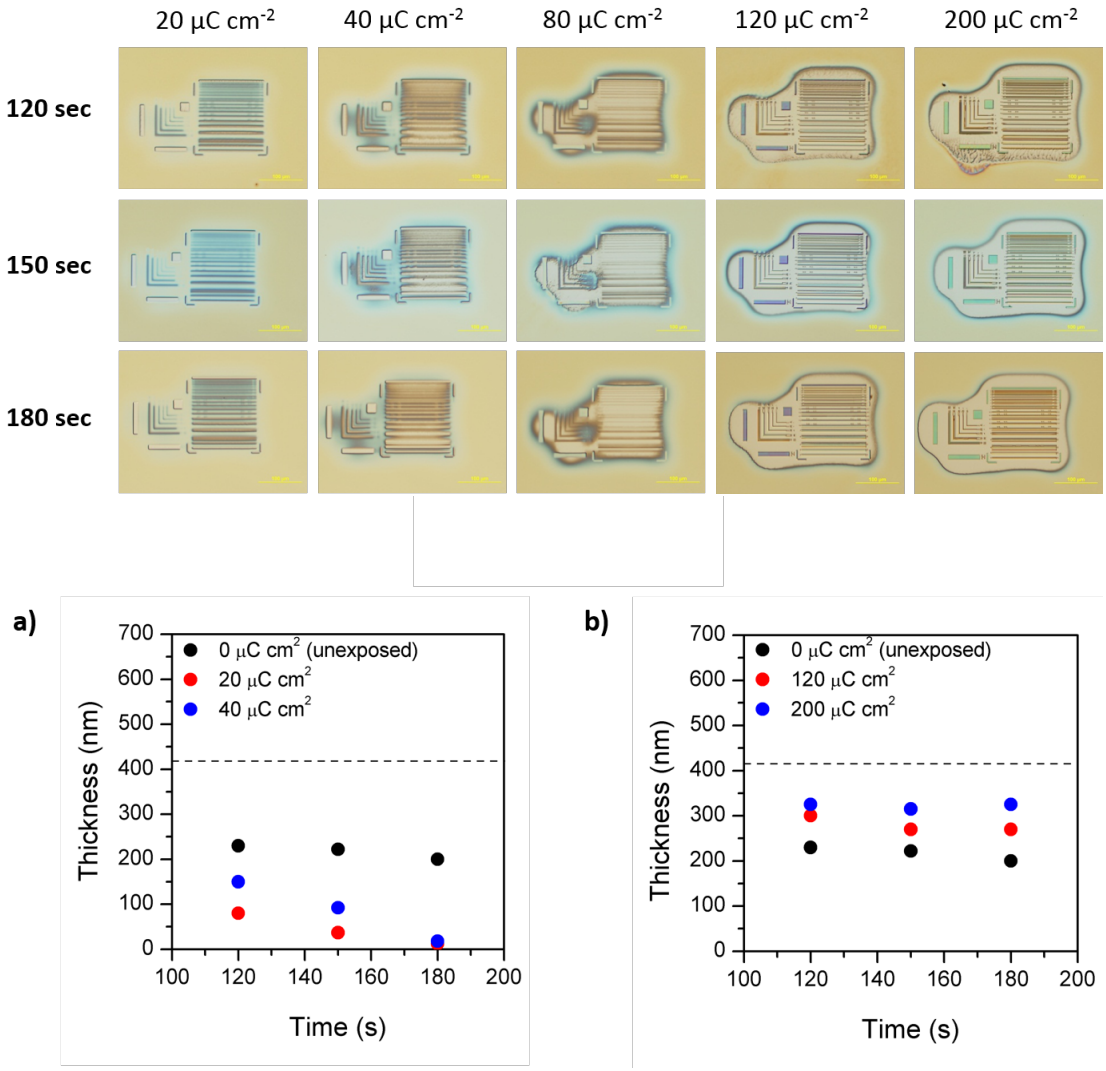

Figure 5.8: The effect of developing time on test patterns exposed in PFMA-2C8F and developed in FC 770. The plots show thickness variation with time for the a) positive-tone and b) negative-tone patterns. Those with mixed behavior could not be measured for lack of a reference point.

shown in Figure 5.2 as polymer D. The solubility of PFMA polymers in fluorinated solvents depends on several factors including their molecular weight, the strength of the solvent and the length of the fluorinated side chain. PFMA-1C1F was investigated as it exhibits the lowest possible limit of the latter of these - essentially a one unit long fluorinated side chain. As it has already been used as a high-sensitivity, high-resolution e-beam resist the key question is whether it can be processed in fluorinated solvents.

Its limited fluorination causes PFMA-1C1F to be insoluble in FC 770, HFE 7200, HFE 7300 and HFE 7500. It does dissolve in HFE 7600 after 10 minutes of heating the solution to 90°C however, even with additional heating, good films of PFMA-1C1F could not be spin coated from HFE 7600. A rippled pattern indicating non-uniform thickness typical of spin coating from a bad solvent is observed in all conditions tested - as visible in Figure 5.9. For this reason, trifluorotoluene (TFT) was used to spin coat good films of PFMA-1C1F. Although TFT is a partially fluorinated solvent it is not orthogonal to organic electronic materials as it has significant aryl character too.

The results of patterning PFMA-1C1F are shown in Figures 5.9 and 5.10. It is found that HFE 7600 dissolved the unexposed areas while HFE 7200 did not develop patterns, so a 1:1 mixture of HFE 7600:HFE 7200 is used. This is sufficient to dissolve the exposed areas faster than the unexposed regions. Only faint patterns are achieved in the films spin coated from HFE 7600 but nice patterns with significant contrast are attained with the films spin coated from TFT. At these low doses the back scattered dose was not enough to cause exposure.

Figure 5.11 plots the thicknesses of exposed patterns with time. The dissolution is seen to be linear until it reaches the last 20 nm or so. Hence even at

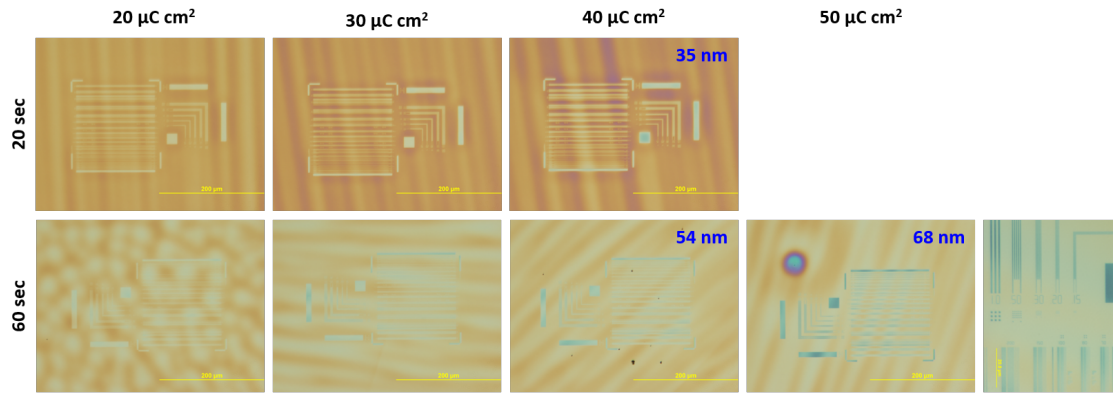

Figure 5.9: Optical images of test patterns spin coated form HFE 7600, exposed at 20, 30, 40 or 50 μC cm^{-2} then developed in a 1:1 mixture of HFE 7600:HFE 7200 for 20 or 60 seconds. Inset shows pattern at higher magnification. The unexposed film thickness is 250 nm after 20 sec and 200 nm after 60 sec. The depth of exposed features is noted in blue where profilometer measurements were successful. Ripples indicate thickness variations of approximately 15 nm.

developing times that should result in cleared patterns a thin 10 - 15 nm thick layer of polymer is still measured to exist in the exposed regions. It is unknown what caused this uncleared layer but there are several possibilities. There could be some kind of adhesion between the substrate and the PFMA preventing the dissolution of a very thin layer closest to the substrate. This could be investigated by testing exposures on different substrate materials. Alternatively, there could be a very small fraction of polymer in the exposed regions that loses its fluorination and collects at the base of the features. If this is the case it might be expected that the thickness of this layer varies with dose.

Although PFMA-1C1F cannot be used as an orthogonal e-beam resist, as it cannot be spin coated from a fluorinated solvent, these results suggest that HFEs

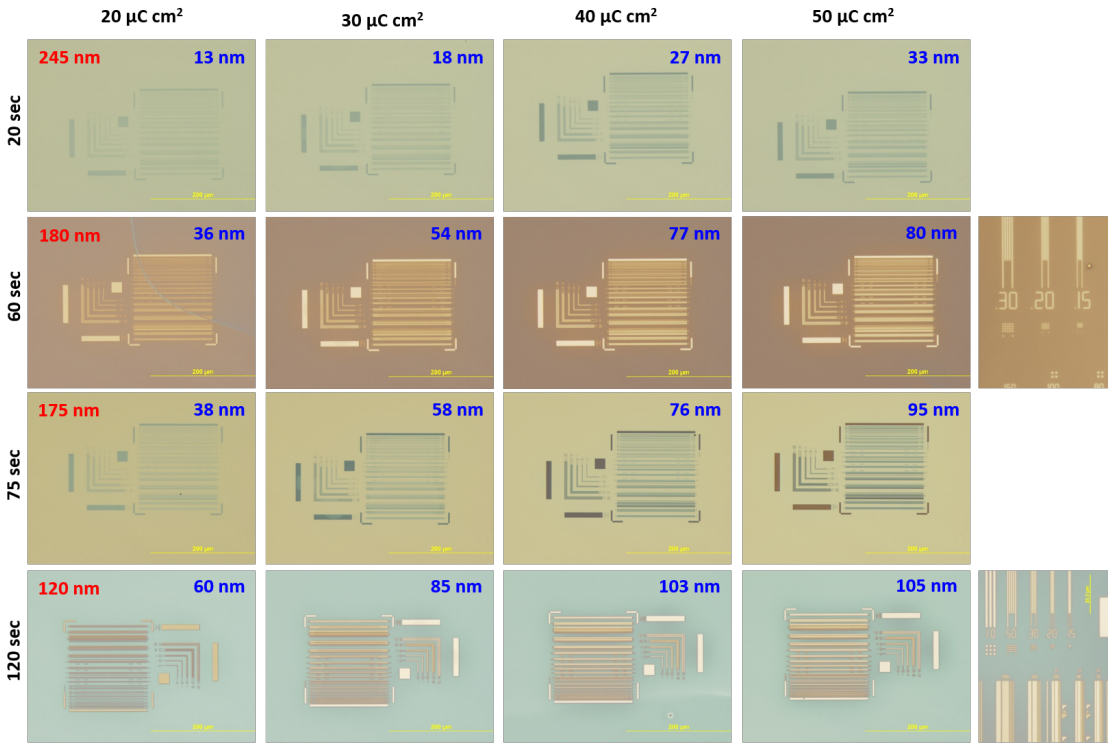

Figure 5.10: Optical images of test patterns spin coated form TFT, exposed at 20, 30, 40 or 50 μC cm^{-2} then developed in a 1:1 mixture of HFE 7600:HFE 7200 for 20, 60, 75 or 120 seconds. Insets show patterns at higher magnification. The depth of exposed features is noted in blue and the unexposed thickness is noted in red.

may well be a better developing solvent than the conventionally used mixtures of MIBK and IPA resulting in neater patterns. It might be possible to make a successful resist with PFMA-1C1F by reducing the molecular weight of the starting material.

Also the orthogonality of the PFMA-1C1F itself needs to be tested. Its low level of fluorination might mean it adheres too well to organic active materials and damages or alters them, or may not strip completely.

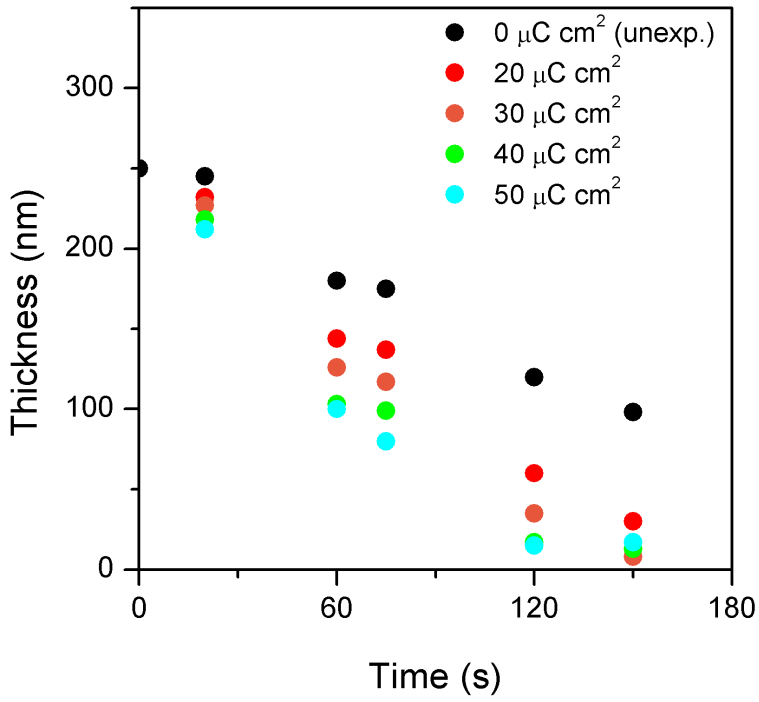

Figure 5.11: Plot showing the variation in thickness with time of developing patterns of PFMA-1C1F in a 1:1 mix of HFE 7200: HFE 7600 for different doses.

5.4.3 Patterning other PFMAs

Patterning tests were conducted on four other PFMA polymers. PFMA-1C8F and PFMA-2C6F are found to be unsuitable for further development because the *unexposed* films are soluble in FC 770. As this is the poorest fluorinated solvent available there is no way to form positive-tone patterns without removing all of the resist.

PFMA-3C8F was found to be insoluble in FC 770 but soluble (for spin coat-

ing) in HFE 7600 so a dose test was performed as shown in Figure 5.12. It shows very similar behavior to PFMA-2C8F - with a switch from positive- to negative-tone behavior and the negative-tone patterns swelling to an increasing extent with increasing dose.

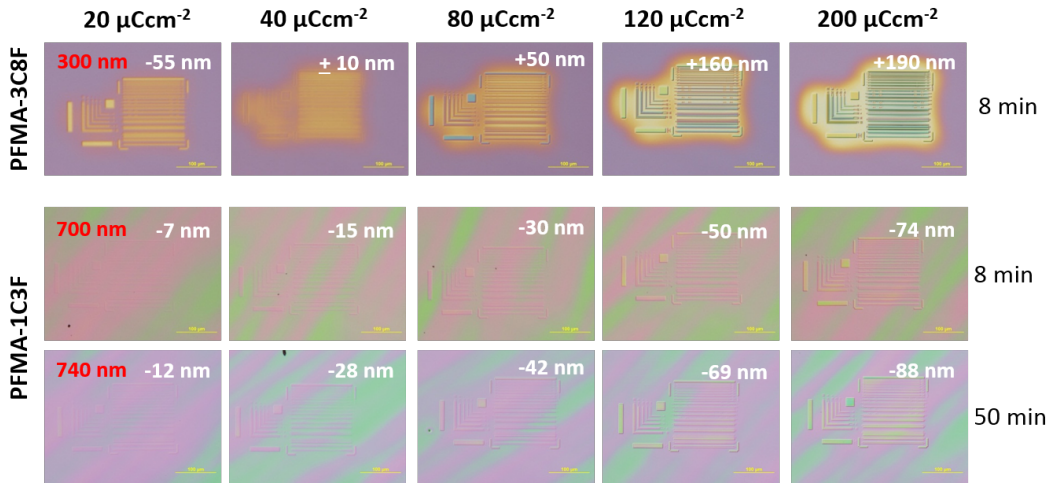

Figure 5.12: Dose tests of PFMA-3C8F and PFMA-1C3F spin coated form HFE 7600 and developed in FC 770 for varying times.

PFMA-1C3F was also found to be insoluble in FC 770 and only poorly soluble in HFE 7600. When spin coated from HFE 7600 a rippled film with non-uniform thickness is obtained. Positive-tone patterns are observed at all doses tested - there was no switch to negative-tone behavior at higher doses. But this resist is also relatively insensitive compared to PFMA-2C8F with patterns only showing thickness differences of tens of nanometers. Even the extremely long developing times tested did not improve pattern contrast with dissolution of the exposed regions apparently halting.

5.4.4 Patterning PFMA-2C8F / PFMA-1C1F copolymers

In an attempt to maintain the good patternability of PFMA-1C1F while making it processible in fluorinated solvents it was copolymerized with PFMA-2C8F thus increasing the overall extent of fluorination. Three new polymers were synthesized with PFMA-1C1F:PFMA-2C8F ratios of 9:1, 1:1 and 1:3. The 9:1 polymer behaves very similarly to PFMA-1C1F - it is soluble in HFE 7600 with heating, but does not spincoat well. The 1:1 polymer is soluble in HFE 7600 and the unexposed regions are insoluble in FC 770 so a pattering test was run. Only very faint patterns were observed, but slightly better patterns were attained using HFE 7500 as the developer as shown in Figure 5.13. Surprisingly the smaller amount of PFMA-1C1F in the 1:3 polymer was enough to reduce the solubility of the polymer in HFE 7600 to result in a rippled film from spin coating. Faint patters with a switch from positive to negative-tone behavior were also observed when developed in FC 770, even though the bulk 1:3 polymer is soluble in FC 770.

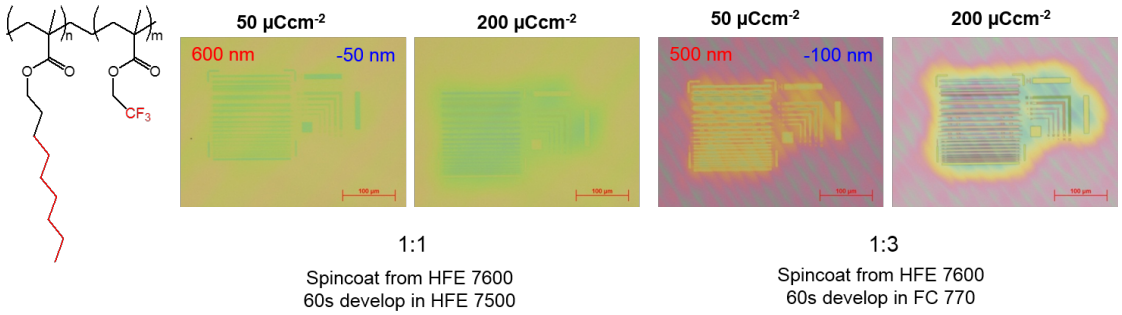

Figure 5.13: The structure of the copolymer followed by patterns in the 1:1 and 1:3 copolymers of PFMA-1C1F:PFMA-2C8F. The unexposed film thickness is noted in red and the pattern height relative to this is indicated in blue.

5.4.5 Towards Device Fabrication

In order for PFMA to be used a resist for device fabrication it must function well on top of organic active materials, rather than just on silicon. Figure 5.14 shows dose tests of PFMA-2C8F conducted on top of a pentacene film grown on silicon. The resist behaves similarly to when only a silicon substrate is used.

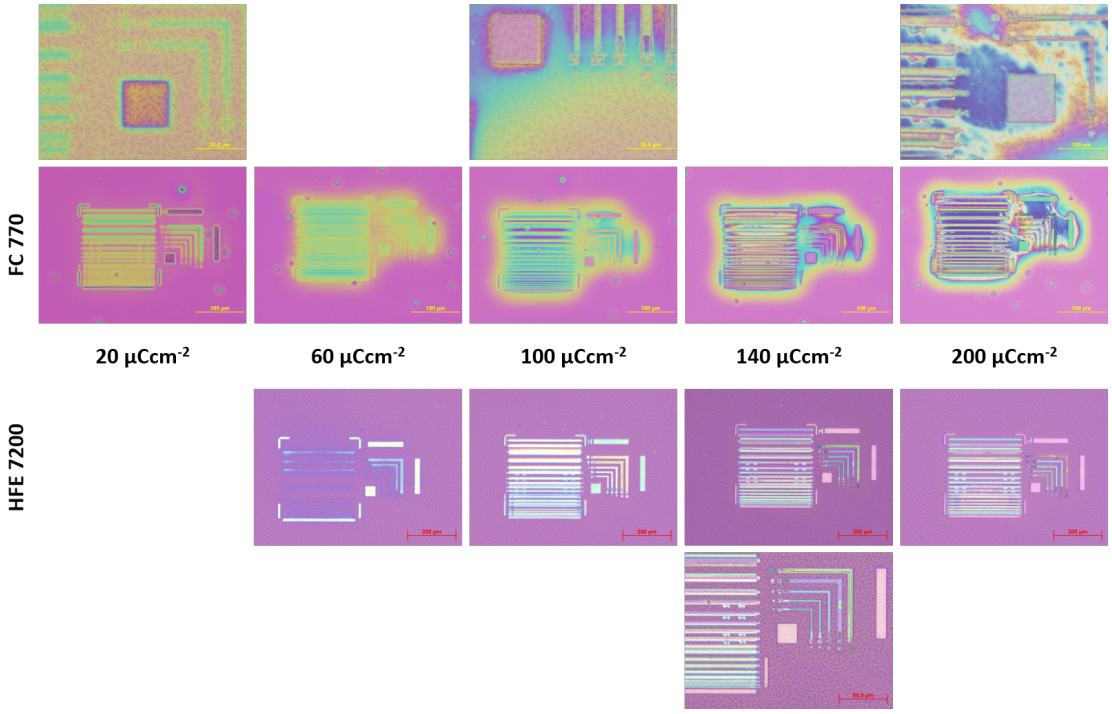

Figure 5.14: Dose tests of PFMA-2C8F patterned on top of pentacene and developed in FC 700 (positive-/negative-tone) and HFE 7200 (negative-tone). Some images at higher magnification are also shown.

As positive-tone patterns were not clearing down to the underlying layer rendering them useless, initial device fabrication tests were conducted using PFMA-2C8F as a negative-tone resist. This is not ideal for two reasons. First, it means that in the fabrication of a top-contact OTFT the channel area must be

exposed to the e-beam dose potentially damaging the organic active material to be studied. Second, the pattern must be designed such that the areas *surrounding* the electrodes must be exposed, rather than the electrodes themselves, which is usually a much larger area making the e-beam exposure slower and more costly.

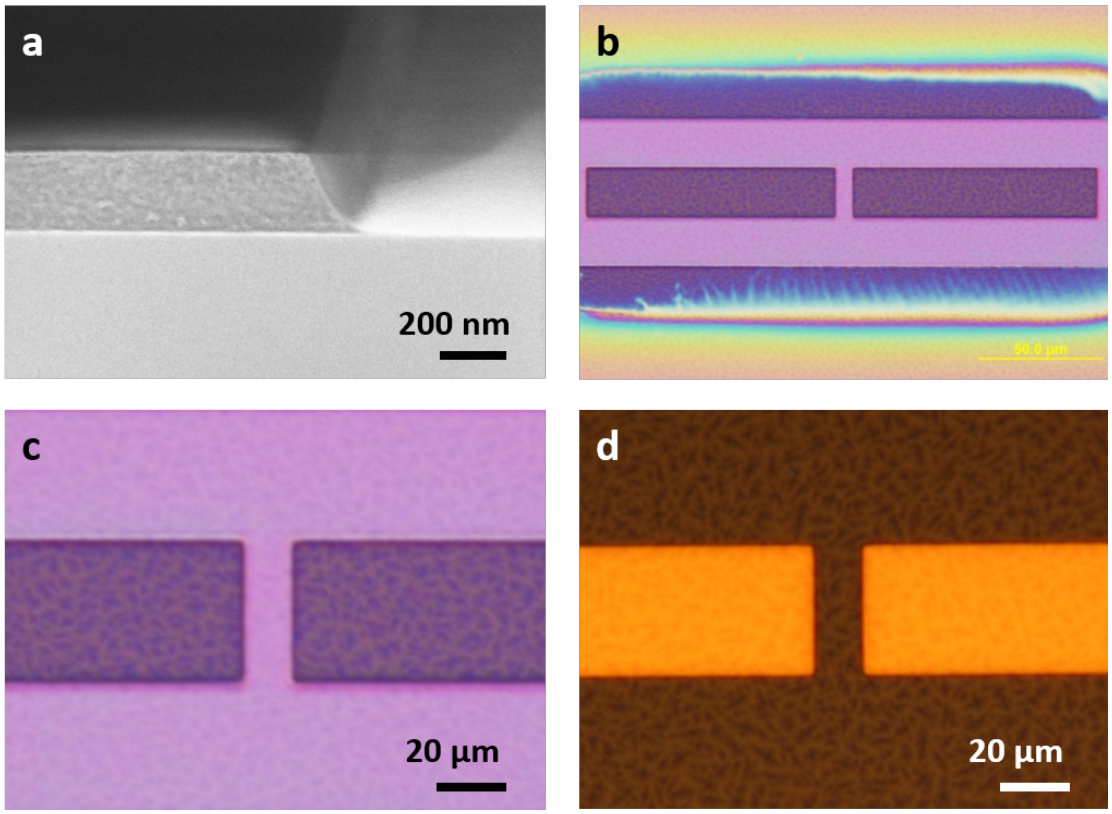

Figure 5.15: a) shows an SEM image of the side wall profile of PFMA-2C8F exposed at 200 μC cm^{-2} and developed in HFE 7200. The angle is 63°. b) shows the pattern exposed for device fabrication and c) again shows the exposed PFMA-2C8F resist on pentacene, and d) shows the finished device after 25 nm of gold is thermally deposited and lifted off to give electrodes on top of the pentacene separated by 7 μm.

5.5 Conclusions

This investigation explores the use of fluorinated polymethacrylates as orthogonal positive-tone resists sensitive to electron beam exposure. In PFMA-2C8F is was found that side chain scission causing a loss of solubility in the fluorinated developing solvent resulted in a switch from positive- to negative-tone behavior at a relatively low dose. This switch was observed in several other PFMA resists investigated. PFMA-1C1F showed very promising patterns but is not fully orthogonal as it cannot be spincoated from a fluorinated solvent. Initial results are ambiguous on whether this could be mediated by copolymerization with a more fluorinated monomer such as PFMA-2C8F.

The best positive patterns were made at the lowest dose and these might be improved further at even *lower* doses. The key problem being that, even with long developing times, the pattern would not clear down to the substrate leaving a 15 - 20 nm thick layer at the bottom of features. This issue appears to be the main one standing on the route to developing a good positive-tone orthogonal e-beam resist. Further investigation of the interaction with the substrate, and exposures at doses below 20 μC cm^{-2} may well solve this problem. The fact that the backscattered dose results in positive-tone behavior that does clear to the substrate offers hope.

PFMA-2C8F was used in negative-tone mode to begin developing a device fabrication process - the ultimate goal of this work. Gold electrodes were successfully deposited on top of pentacene separated by a 7 μm channel region.

CHAPTER 6

CONCLUSIONS AND OUTLOOK

The core concept of chemical orthogonality has proven to be extremely powerful, and might even be *necessary* to enable the future manufacture of organic-containing structures. Although other classes of materials might exhibit some chemical orthogonality to organic materials, fluorinated materials are the logical choice because fluorine is the *most* electronegative element in the periodic table leading to the lowest possible intermolecular forces, which are the basis of their orthogonality to organics. There are, of course, many potential directions that further investigations could take - each project described could be extended - but three in particular stand out: first a better understanding of the **fundamental science** that results in chemical orthogonality, second, the adaption of these patterning techniques to **biological applications** and third, high resolution orthgonal patterning **combined with block copolymer lithography** could have significant potential *outside* of organic electronics. However, this area of research is always going to be limited by the success of organic electronics itself (an other related areas) which some have expressed skepticism over. Organic-containing structures are unlikely to ever be manufactured on a scale comparable to silicon electronics, but at the same time, it appears that they will be the enabling factor in several areas of niche applications.

6.1 General

Predicting solubility If solution processing is to become a controllable, reliable manufacturing process a lot more needs to be know about the effect of solvent selection. This is currently done by time-consuming, inexact 'trial and

error' methods, there is no systematic way to determine what solvent will dissolve what material, what microstructure it will result in, or how much interaction there will be. There appears to be a great need to better understand the fundamental science relevant to the solubility of active polymeric materials. Some work exists on the Hildebrand solubility parameter [128], but has not been extended to the multitude of new tailored polymers developed for organic electronics. The Hildebrand solubility parameter essentially sums all the intermolecular forces between two molecules to determine whether they would be soluble or miscible. This is notoriously difficult for large complex molecules such as these, so perhaps there is space for a computational study that could handle large amounts of data to begin to establish general trends in the solubility of these new materials.

Damage to organics Another issue related to the orthgonality is the extent of any damage or alteration of the organics being processed. Zakhidov textitet al. demonstrated that organic transistor performance was not altered by exposure to hydrofluoroether (HFE) solvents. But for orthogonal processing to be taken up more widely there is a need to demonstrate that it is truly non-damaging. Other combinations of materials need to be tested. The effect of depositing and stripping fluoropolymers (such as the fluorinated methacrylates used in Chapters 3, 4 and 5) on top of organics needs to be tested. Figure 6.1 shows a sample of pentacene with apparent fluoropolymer residue. Avoiding damage relies on the lack of interaction between the organics and the fluorinated processing materials - but 'fluorinated' materials can be fully fluorinated, or partially fluorinated. Is there a threshold above which damage will not occur?

Etch residue It was also observed that the fluorinated methacrylates used

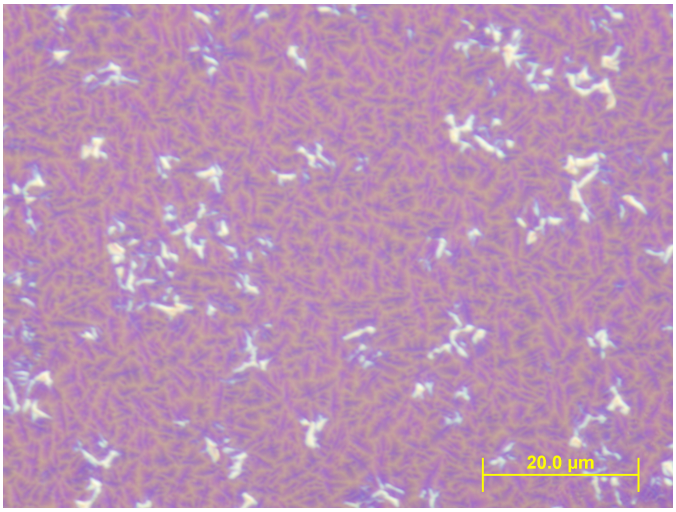

Figure 6.1: Optical image of an example of pentacene (grains are visible) that had a fluoropolymer (PFMA) spincoated on then stripped in fluorinated (HFE) solvent. The white features appear to be PFMA residue. This was not always observed, but it is not know what caused it to appear in this instance.

would leave some kind of residue if they had been exposed to an oxygen plasma etch step. Bare silicon that had had fluorinated methacrylate spincoated on and etched away, as shown in Figure 6.2, remained more hydrophobic than bare silicon would be expected to be. An XPS measurement indicated some fluorinated remained on the surface, but this could not be removed by washing in fluorinated solvents. This residue was never fully characterized. The length of fluorinated side chain may affect the formation of residue, but a solid solution was never found.

Artificial orthogonality Whether a deposited organic is affected by a solvent is largely determined by their interaction at the surface of the organic. This leads to the question of whether the surface of an organic could be made to 'appear' fluorinated, and hence orthogonal, when the bulk of the materials is not. Sur-

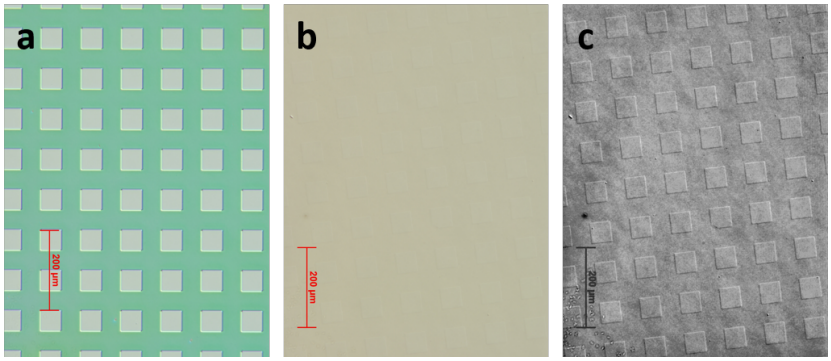

Figure 6.2: Optical images of a) patterned fluoropolymer (PFMA) on silicon, and b) the same sample after washing in fluorinated solvent (HFE) which is expected to be bare silicon. Part c) shows the same image as in b) but with enhanced contrast and in greyscale, so that residue can clearly be seen.

factants such as FOTS can bind to inorganic surfaces and expose a fluorinated chain, significantly altering the wettabliity of that surface. Could attachment of surfactants to organic surfaces perhaps be enough to protect them during processing with conventional organic solvents? It would be essential that the surfactant not damage the organic material, which could be tricky if its active role relies on its surface. To go a step further, could surfactant attachment be made reversible (using a photochemical reaction?) so that a material's orthogonality could be conveniently turned on and off as desired?

6.2 Biomaterials Applications

Biocompatibility In addition to patterning materials for organic electronics orthogonal processing can be used to pattern bioactive molecules such as proteins, as demonstrated by Midthun *et al.* [101]. As interfacing with or incorporating

biological materials could be a key application of organic electronics patterning of biological materials may have wider scope, even outside of organic electronics. However, Midthun's study only briefly examined how truly 'biocompatible' orthogonal processing is. Biological materials are even more delicate than organic semiconductors hence the processing requirements are even stricter. If they are to retain thier biological function biomolecules cannot be heated much above room temperature and must not dry out. In addition to Midthun's results, unpublished work on photolithographic patterning suggest that proteins are not damaged by exposure to fluorinated solvents, but *are* altered by having fluoropolymer deposited on top and stripped, as described in Figure 6.3. It is likely that deposition of fluoropolymer on top of biomolecules causes them to dry out and be denatured. This problem could possibly be resolved by inserting a hydrogel layer between the biomolecule and fluoropolymer in order to maintain the presence of essential water.

Combined organic and biomolecule patterning All patterning methods described in this work could be used to pattern combinations of biological and organic electronic materials side by side, or on top of each other. This could be significant if the main application of future organic electronic becomes interfacing *in situ* with biological systems.

6.3 Monolayers

Intermediate thicknesses This project allowed the formation of 1-2 nm thick layers of light emitting polymer, and spincoating can form 10 nm thick layers. It may be possible to attain intermediate thickness with a combination of orthog-

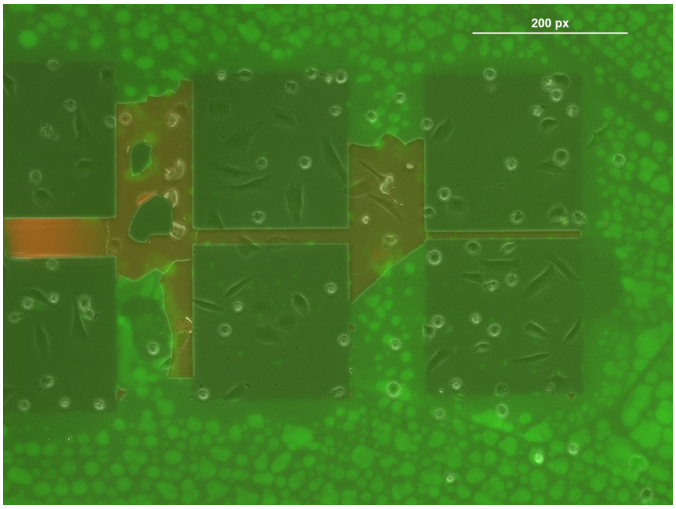

Figure 6.3: Fluorescence image of a sample that has two proteins that aid cell adhesion (both labeled with green fluorophore) patterned next to each other that was then seeded with cells. The square areas contain the second protein deposited and were exposed to fluorosolvent (HFE). All other areas have the first protein deposited on them and this was covered by fluoropolymer (PFMA) and exposed to fluorosolvent. Cells have only attached to the second protein, indicating that the biological function of the second protein has been maintained while that of the first protein has been damaged by the processing conditions. The red patches are fluoropolymer that has not stripped properly.

onal processing and the crosslinking method described by Png *et al.* [38]. The thickness of active polymer crosslinked could be controlled if the crosslinker was carried in from the underlying layer via diffusion in an annealing step. This would allow studies of the effect of thickness on recombination in polymer light emitting diodes that wouldn't require interpolation. However beyond such a study it is hard to imagine further uses of this approach.

6.4 Fluoropolymer Barrier Layer Patterning

Edge effect Having produced patterns of unprecedented complexity the obvious way to improve on this technique would be to address the edge effect problem which saw an significant accumulations of organic remain at the edge of features even after the lift off step. There are various factors that might reduce this effect, such as, varying the concentration or solvent of the solution deposited organic, the surface treatment of the barrier layer and solvent or thermal annealing. However it is anticipated that it would be difficult to remove this effect completely - it has been observed with other proposed patterning mechanisms. Reduction of the edge effect is also expected to reduce restrictions on the layout of patterns as a smaller cross-section of organic material would be exposed to organic solvent during the deposition of subsequent organics.

6.5 Inkjet Printing of Fluoropolymers

Chemical patterning Due to their orthogonality, fluorinated inks could be used to direct the deposition of subsequent orthogonal organic inks. A fluorinated surfactant has already been used in a similar way to enhance the resolution of inkjet printing [129]. Wells could be formed in fluoro-ink to confine subsequent drops of organic ink. This could be used to reduce resolution, improve alignment or even influence the microstructure of the organic. By acting as barrier layers, patterning layers or surface modification treatments, orthogonal inks have the capacity to significantly enhance what is possible in functional printing.

Combining with photolithography If roll-to-roll processing is to dominate in this area an new way of depositing photoresist must be used, as spincoating will not be applicable. Inkjet printing is one option, hence it would be interesting to investigate the issues associated with conducting photolithography using photoresist that has been deposited by inkjet. How would drop thickness variations affect feature resolution? Could process steps be combined so that inkjet printed resist is used first as an etch mask then photolithographically patterned and used for a lift off step? How would the imprecision of inkjet printing affect yield over a large area?

6.6 Orthogonal E-Beam Resist

Block Copolymer (BCP) lithography is being explored as a technique to pattern on the tens of nanometers scale with high throughput capacity (which e-beam cannot match). BCPs are also organic so could themselves be patterned using an orthogonal resist. The combination of these two patterning layers, which could be stacked on top of each other thanks to the fluoropolymer's orthogonality, has significant potential. BCPs can be used to reproduce the same feature over a large area quickly and cheaply, but are essentially limited to arrays of lines or dots. They lack the ability to form arbitrary shapes as desired, such as a break or connection in an array of lines. These could be filled in using a fluorpolymer resist in combination with e-beam lithography as it is a direct-write method. As long as these were small in area they would not significantly reduce throughput. This would allow the formation of many more useful patterns at the dimensions desired for device and circuit fabrication. Such an orthogonal patternable layer could be the key to enabling real-world use of BCP lithography.

REFERENCES

[1] P. Liu, Y. Wu, H. Pan, B. S. Ong, and S. Zhu, "High-Performance Polythiophene Thin-Film Transistors Processed with Environmentally Benign Solvent," *Macromolecules*, vol. 43, pp. 6368–6373, Aug. 2010.

[2] G. Klärner, J.-I. Lee, V. Y. Lee, E. Chan, J.-P. Chen, A. Nelson, D. Markiewicz, R. Siemens, J. C. Scott, and R. D. Miller, "Cross-linkable Polymers Based on Dialkylfluorenes," *Chemistry of Materials*, vol. 11, pp. 1800–1805, July 1999.

[3] C. D. Müller, A. Falcou, N. Reckefuss, M. Rojahn, V. Wiederhirn, P. Rudati, H. Frohne, O. Nuyken, H. Becker, and K. Meerholz, "Multi-colour organic light-emitting displays by solution processing.," *Nature*, vol. 421, pp. 829–33, Feb. 2003.

[4] A. Charas, H. Alves, J. M. Martinho, L. Alcácer, O. Fenwick, F. Cacialli, and J. Morgado, "Photoacid cross-linkable polyfluorenes for optoelectronics applications," *Synthetic Metals*, vol. 158, pp. 643–653, Sept. 2008.

[5] F. C. Krebs and M. Jø rgensen, "High Carrier Mobility in a Series of New Semiconducting PPV-Type Polymers," *Macromolecules*, vol. 36, pp. 4374–4384, June 2003.

[6] M. Vasilopoulou, D. Georgiadou, G. Pistolis, and P. Argitis, "Tuning the Emitting Color of Organic Light-Emitting Diodes Through Photochemically Induced Transformations: Towards Single-Layer, Patterned, Full-Color Displays and White-Lighting Applications," *Advanced Functional Materials*, vol. 17, pp. 3477–3485, Nov. 2007.

[7] C. Newby, J.-K. Lee, and C. K. Ober, "The solvent problem: Redissolution of macromolecules in solution-processed organic electronics," *Macromolecular Research*, vol. 21, pp. 248–256, Apr. 2013.

[8] M. Zhu and C. Yang, "Blue fluorescent emitters: design tactics and applications in organic light-emitting diodes.," *Chemical Society reviews*, vol. 42, pp. 4963–76, June 2013.

[9] Z. Li, Z. R. Li, and H. Meng, eds., *Organic Light-Emitting Materials and Devices*. CRC Press, 2010.

[10] A. Nathan, A. Ahnood, M. T. Cole, Y. Suzuki, P. Hiralal, F. Bonaccorso, T. Hasan, L. Garcia-Gancedo, A. Dyadyusha, S. Haque, P. Andrew, S. Hofmann, J. Moultrie, A. J. Flewitt, A. C. Ferrari, M. J. Kelly, J. Robertson, G. A. J. Amaratunga, and W. I. Milne, "Flexible Electronics: The Next Ubiquitous Platform," *Proceedings of the IEEE*, vol. 100, pp. 1486–1517, May 2012.

[11] J. B.-H. Tok and Z. Bao, "Recent advances in flexible and stretchable electronics, sensors and power sources," *Science China Chemistry*, vol. 55, pp. 718–725, Feb. 2012.

[12] W. S. Wong and A. Salleo, *Flexible Electronics: Materials and Applications*. Springer, 2009.

[13] V. Subramanian, J. Frechet, P. Chang, D. Huang, J. Lee, S. Molesa, A. Murphy, D. Redinger, and S. Volkman, "Progress Toward Development of All-Printed RFID Tags: Materials, Processes, and Devices," *Proceedings of the IEEE*, vol. 93, pp. 1330–1338, July 2005.

[14] D. Mitzi, ed., *Solution Processing of Inorganic Materials*. Wiley, 2009.

[15] R. Owens, P. Kjäll, A. Richter-Dahlfors, F. Cicoira, and G. G. Malliaras, "Organic bioelectronics: A new era for organic electronics," *Biochimica et Biophysica Acta*, vol. 1830, no. 9, pp. 4286–4287, 2013.

[16] R. M. Owens and G. G. Malliaras, "Organic Electronics at the Interface with Biology," *MRS Bulletin*, vol. 35, pp. 449–456, Jan. 2011.

[17] P. Lin and F. Yan, "Organic thin-film transistors for chemical and biological sensing.," *Advanced materials*, vol. 24, pp. 34–51, Jan. 2012.

[18] E. Menard, M. A. Meitl, Y. Sun, J.-U. Park, D. J.-L. Shir, Y.-S. Nam, S. Jeon, and J. A. Rogers, "Micro- and nanopatterning techniques for organic electronic and optoelectronic systems.," *Chemical reviews*, vol. 107, pp. 1117–60, Apr. 2007.

[19] Y. Xu, F. Zhang, and X. Feng, "Patterning of Conjugated Polymers for Organic Optoelectronic Devices," *Small*, vol. 7, pp. 1338–1360, May 2011.

[20] K. T. Kamtekar, A. P. Monkman, and M. R. Bryce, "Recent advances in white organic light-emitting materials and devices (WOLEDs).," *Advanced materials (Deerfield Beach, Fla.)*, vol. 22, pp. 572–82, Feb. 2010.

[21] A. Facchetti, "π-Conjugated Polymers for Organic Electronics and Photovoltaic Cell Applications ," *Chemistry of Materials*, vol. 23, pp. 733–758, Feb. 2011.

[22] A. C. Grimsdale, K. L. Chan, R. E. Martin, P. G. Jokisz, and A. B. Holmes, "Synthesis of light-emitting conjugated polymers for applications in electroluminescent devices.," *Chemical reviews*, vol. 109, pp. 897–1091, Mar. 2009.

[23] A. a. Zakhidov, J.-K. Lee, H. H. Fong, J. a. DeFranco, M. Chatzichristidi, P. G. Taylor, C. K. Ober, and G. G. Malliaras, "Hydrofluoroethers as Orthogonal Solvents for the Chemical Processing of Organic Electronic Materials," *Advanced Materials*, vol. 20, pp. 3481–3484, July 2008.

[24] P. G. Taylor, J.-K. Lee, A. a. Zakhidov, M. Chatzichristidi, H. H. Fong, J. a. DeFranco, G. G. Malliaras, and C. K. Ober, "Orthogonal Patterning of PEDOT:PSS for Organic Electronics using Hydrofluoroether Solvents," *Advanced Materials*, vol. 21, pp. 2314–2317, June 2009.

[25] J.-K. Lee, M. Chatzichristidi, A. A. Zakhidov, H. S. Hwang, E. L. Schwartz, J. Sha, P. G. Taylor, H. H. Fong, J. A. DeFranco, E. Murotani, W. W. H. Wong, G. G. Malliaras, and C. K. Ober, "Acid-diffusion behaviour in organic thin films and its effect on patterning," *Journal of Materials Chemistry*, vol. 19, no. 19, p. 2986, 2009.

[26] J.-K. Lee, M. Chatzichristidi, A. A. Zakhidov, P. G. Taylor, J. A. DeFranco, H. S. Hwang, H. H. Fong, A. B. Holmes, G. G. Malliaras, and C. K. Ober, "Acid-sensitive semiperfluoroalkyl resorcinarene: an imaging material for organic electronics.," *Journal of the American Chemical Society*, vol. 130, pp. 11564–5, Sept. 2008.

[27] H. H. Fong, J.-K. Lee, Y.-F. Lim, A. a. Zakhidov, W. W. H. Wong, A. B. Holmes, C. K. Ober, and G. G. Malliaras, "Orthogonal processing and patterning enabled by highly fluorinated light-emitting polymers.," *Advanced materials (Deerfield Beach, Fla.)*, vol. 23, pp. 735–9, Feb. 2011.

[28] A. a. Zakhidov, H. H. Fong, J. a. DeFranco, J.-K. Lee, P. G. Taylor, C. K. Ober, G. G. Malliaras, M. He, and M. G. Kane, "Fabrication of polymer-

based electronic circuits using photolithography," *Applied Physics Letters*, vol. 99, no. 18, p. 183308, 2011.

[29] X. Gong, S. Wang, D. Moses, G. C. Bazan, and A. J. Heeger, "Multilayer Polymer Light-Emitting Diodes: White-Light Emission with High Efficiency," *Advanced Materials*, vol. 17, pp. 2053–2058, Sept. 2005.

[30] H. S. Hwang, A. A. Zakhidov, J.-K. Lee, X. André, J. A. DeFranco, H. H. Fong, A. B. Holmes, G. G. Malliaras, and C. K. Ober, "Dry photolithographic patterning process for organic electronic devices using supercritical carbon dioxide as a solvent," *Journal of Materials Chemistry*, vol. 18, p. 3087, June 2008.

[31] J. Huang, R. Xia, Y. Kim, X. Wang, J. Dane, O. Hofmann, A. Mosley, A. J. de Mello, J. C. de Mello, and D. D. C. Bradley, "Patterning of organic devices by interlayer lithography," *Journal of Materials Chemistry*, vol. 17, no. 11, p. 1043, 2007.

[32] D.-S. Leem, P. H. Wöbkenberg, J. Huang, T. D. Anthopoulos, D. D. Bradley, and J. C. DeMello, "Micron-scale patterning of high conductivity poly(3,4-ethylendioxythiophene):poly(styrenesulfonate) for organic field-effect transistors," *Organic Electronics*, vol. 11, pp. 1307–1312, July 2010.

[33] J. A. DeFranco, B. S. Schmidt, M. Lipson, and G. G. Malliaras, "Photolithographic patterning of organic electronic materials," *Organic Electronics*, vol. 7, pp. 22–28, Feb. 2006.

[34] B. M. Dhar, G. S. Kini, G. Xia, B. J. Jung, N. Markovic, and H. E. Katz, "Field-effect-tuned lateral organic diodes.," *Proceedings of the National*

Academy of Sciences of the United States of America, vol. 107, pp. 3972–6, Mar. 2010.

[35] J.-F. Chang, M. C. Gwinner, M. Caironi, T. Sakanoue, and H. Sirringhaus, "Conjugated-Polymer-Based Lateral Heterostructures Defined by High-Resolution Photolithography," *Advanced Functional Materials*, vol. 20, pp. 2825–2832, Sept. 2010.

[36] C.-Y. Chang, F.-Y. Tsai, S.-J. Jhuo, and M.-J. Chen, "Enhanced OLED performance upon photolithographic patterning by using an atomic-layer-deposited buffer layer," *Organic Electronics*, vol. 9, pp. 667–672, Oct. 2008.

[37] C.-C. Kuo and T. N. Jackson, "Direct lithographic top contacts for pentacene organic thin-film transistors," *Applied Physics Letters*, vol. 94, p. 053304, Feb. 2009.

[38] R.-Q. Png, P.-J. Chia, J.-C. Tang, B. Liu, S. Sivaramakrishnan, M. Zhou, S.-H. Khong, H. S. O. Chan, J. H. Burroughes, L.-L. Chua, R. H. Friend, and P. K. H. Ho, "High-performance polymer semiconducting heterostructure devices by nitrene-mediated photocrosslinking of alkyl side chains.," *Nature materials*, vol. 9, pp. 152–8, Feb. 2010.

[39] C. J. Drury, C. M. J. Mutsaers, C. M. Hart, M. Matters, and D. M. de Leeuw, "Low-cost all-polymer integrated circuits," *Applied Physics Letters*, vol. 73, p. 108, July 1998.

[40] F. C. Krebs and H. Spanggaard, "Direct emissive pattern formation in PPV-type polymer with built-in photoresist properties and the application to light emitting devices," *Synthetic Metals*, vol. 148, pp. 53–59, Jan. 2005.

[41] Y.-L. Loo, R. L. Willett, K. W. Baldwin, and J. A. Rogers, "Additive, nanoscale patterning of metal films with a stamp and a surface chemistry mediated transfer process: Applications in plastic electronics," *Applied Physics Letters*, vol. 81, p. 562, July 2002.

[42] S. K. Park, Y. H. Kim, J. I. Han, D. G. Moon, and W. K. Kim, "High-performance polymer tfts printed on a plastic substrate," *IEEE Transactions on Electron Devices*, vol. 49, pp. 2008–2015, Nov. 2002.

[43] T. Granlund, T. Nyberg, L. Stolz Roman, M. Svensson, and O. Inganäs, "Patterning of Polymer Light-Emitting Diodes with Soft Lithography," *Advanced Materials*, vol. 12, pp. 269–273, Feb. 2000.

[44] D. Li and L. J. Guo, "Micron-scale organic thin film transistors with conducting polymer electrodes patterned by polymer inking and stamping," *Applied Physics Letters*, vol. 88, p. 063513, Feb. 2006.

[45] M. M. Deshmukh, D. C. Ralph, M. Thomas, and J. Silcox, "Nanofabrication using a stencil mask," *Applied Physics Letters*, vol. 75, p. 1631, Sept. 1999.

[46] O. Vazquez-Mena, T. Sannomiya, M. Tosun, L. G. Villanueva, V. Savu, J. Voros, and J. Brugger, "High-resolution resistless nanopatterning on polymer and flexible substrates for plasmonic biosensing using stencil masks.," *ACS nano*, vol. 6, pp. 5474–81, June 2012.

[47] I. Yagi, K. Shigeto, K. Tsukagoshi, and Y. Aoyagi, "Alignment-Free Top-Contact Formation for Organic Thin Film Transistors with Submicron-Length Channel," *Japanese Journal of Applied Physics*, vol. 44, pp. L479–L481, Apr. 2005.

[48] F. Ante, D. Kälblein, U. Zschieschang, T. W. Canzler, A. Werner, K. Takimiya, M. Ikeda, T. Sekitani, T. Someya, and H. Klauk, "Contact doping and ultrathin gate dielectrics for nanoscale organic thin-film transistors.," *Small (Weinheim an der Bergstrasse, Germany)*, vol. 7, pp. 1186–91, May 2011.

[49] H. Ogihara, M. Fukasawa, and T. Saji, "Method for patterning various nanomaterials: electrochemical deposition of patterned Ni thin films and their utilization as a strippable mask.," *ACS applied materials & interfaces*, vol. 3, pp. 2108–11, June 2011.

[50] J.-K. Lee, H. H. Fong, A. a. Zakhidov, G. E. McCluskey, P. G. Taylor, M. Santiago-Berrios, H. D. Abruna, A. B. Holmes, G. G. Malliaras, and C. K. Ober, "Semiperfluoroalkyl Polyfluorenes for Orthogonal Processing in Fluorous Solvents," *Macromolecules*, vol. 43, pp. 1195–1198, Feb. 2010.

[51] A. Pogantsch, S. Rentenberger, G. Langer, J. Keplinger, W. Kern, and E. Zojer, "Tuning the Electroluminescence Color in Polymer Light-Emitting Devices Using the Thiol-Ene Photoreaction," *Advanced Functional Materials*, vol. 15, pp. 403–409, Mar. 2005.

[52] S.-M. Park, M. Stoykovich, R. Ruiz, Y. Zhang, C. Black, and P. Nealey, "Directed Assembly of Lamellae- Forming Block Copolymers by Using Chemically and Topographically Patterned Substrates," *Advanced Materials*, vol. 19, pp. 607–611, Feb. 2007.

[53] D. O'Hagan, "Understanding organofluorine chemistry. An introduction to the C-F bond.," *Chemical Society reviews*, vol. 37, pp. 308–19, Mar. 2008.

[54] P. Kirsch, *Modern fluoroorganic chemistry synthesis, reactivity, applications*. Weinheim :: Wiley-VCH,, 2013.

[55] J. N. Israelachvili, *Intermolecular and Surface Forces, Third Edition: Revised Third Edition*. Academic Press, 2011.

[56] G. Siegmund, W. Schwertfeger, A. Feiring, B. Smart, F. Behr, H. Vogel, and B. McKusick, *Ullmann's Encyclopedia of Industrial Chemistry - Fluorine Compounds, Organic*. Weinheim, Germany: Wiley-VCH Verlag GmbH & Co. KGaA, June 2000.

[57] G. G. Hougham, P. E. Cassidy, K. Johns, and T. Davidson, eds., *Fluoropolymers 2: Properties*. Springer, 1999.

[58] S. Biswas and K. Vijayan, "Friction and wear of PTFE a review," *Wear*, vol. 158, pp. 193–211, Oct. 1992.

[59] W. Eisenmenger and M. Haardt, "Observation of charge compensated polarization zones in polyvinylindenfluoride (PVDF) films by piezoelectric acoustic step-wave response," *Solid State Communications*, vol. 41, no. 12, pp. 917–920, 1982.

[60] C. J. Brabec, M. Heeney, I. McCulloch, and J. Nelson, "Conducting polymers for carbon electronics themed issue," *Chemical Society reviews*, vol. 40, no. 7, pp. 1185 – 1199, 2010.

[61] V. Cirkva, B. Ameduri, B. Boutevin, and O. Palet, "Chimistry of [(perfluoroalkyl)methyl] oxiranes. Regioselectivity of ring opening with O-nucleophiles and preparation of amphiphilic monomers," *Journal of Fluorine Chemistry*, vol. 84, pp. 53–61, 1997.

[62] A. Rastogi, M. Y. Paik, and C. K. Ober, "Development of a directly patterned low-surface-energy polymer brush in supercritical carbon dioxide.," *ACS applied materials & interfaces*, vol. 1, pp. 2013–20, Sept. 2009.

[63] N. Sundararajan, S. Yang, K. Ogino, S. Valiyaveettil, X. Zhou, C. K. Ober, S. K. Obendorf, and R. D. Allen, "Supercritical CO 2 Processing for Submicron Imaging of Fluoropolymers," *Chemistry of Materials*, vol. 12, pp. 41–48, Jan. 2000.

[64] J. Tsibouklis, P. Graham, P. J. Eaton, J. R. Smith, T. G. Nevell, J. D. Smart, and R. J. Ewen, "Poly (perfluoroalkyl methacrylate) Film Structures : Surface Organization Phenomena , Surface Energy Determinations , and Force of Adhesion Measurements," *Macromolecules*, vol. 33, pp. 8460–8465, 2000.

[65] R. R. Thomas, D. R. Anton, W. F. Graham, M. J. Darmon, B. B. Sauer, K. M. Stika, and D. G. Swartzfager, "Preparation and Surface Properties of Acrylic Polymers Containing Fluorinated Monomers," *Macromolecules*, vol. 30, pp. 2883–2890, May 1997.

[66] A. Sekiya and S. Misaki, "The potential of hydrofluoroethers to replace CFCs, HCFCs and PFCs," *Journal of Fluorine Chemistry*, vol. 101, pp. 215–221, Feb. 2000.

[67] P. Clark and L. Zazzera, "The Use of Segregated Hydrofluoroethers in Semiconductor Wafer Processing," in *The 17th Annual SEMI/IEEE ASMC 2006 Conference*, pp. 296–300, IEEE, 2006.

[68] W.-T. Tsai, "Environmental risk assessment of hydrofluoroethers (HFEs).," *Journal of hazardous materials*, vol. 119, pp. 69–78, Mar. 2005.

[69] T. G. Stange, M. Roy, D. F. Evans, and W. A. Hendrickson, "Scanning tunneling microscopy and atomic force microscopy characterization of polystyrene spin-coated onto silicon surfaces," *Langmuir*, vol. 8, pp. 920–926, 1992.

[70] S. R. Forrest, "Ultrathin Organic Films Grown by Organic Molecular Beam Deposition and Related Techniques.," *Chemical reviews*, vol. 97, pp. 1793–1896, Oct. 1997.

[71] Z. Yu, H. Yan, K. Lu, Y. Zhang, and Z. Wei, "Self-assembly of two-dimensional nanostructures of linear regioregular poly(3-hexylthiophene)," *RSC Advances*, vol. 2, p. 338, Dec. 2012.

[72] M. Onoda and K. Yoshino, "Fabrication of self-assembled multilayer heterostructure of poly(p-phenylene vinylene) and its use for an electroluminescent diode," *Journal of Applied Physics*, vol. 78, p. 4456, Oct. 1995.

[73] A. C. Fou, O. Onitsuka, M. Ferreira, M. F. Rubner, and B. R. Hsieh, "Fabrication and properties of light-emitting diodes based on self-assembled multilayers of poly(phenylene vinylene)," *Journal of Applied Physics*, vol. 79, p. 7501, May 1996.

[74] J. H. Burroughes, D. D. C. Bradley, A. R. Brown, R. N. Marks, K. Mackay, R. H. Friend, P. L. Burns, and A. B. Holmes, "Light-emitting diodes based on conjugated polymers," *Nature*, vol. 347, pp. 539–541, Oct. 1990.

[75] G. Grem, G. Leditzky, B. Ullrich, and G. Leising, "Realization of a blue-light-emitting device using poly(p-phenylene)," *Advanced Materials*, vol. 4, pp. 36–37, Jan. 1992.

[76] P. L. Burn, A. B. Holmes, A. Kraft, D. D. C. Bradley, A. R. Brown, and R. H. Friend, "Synthesis of a segmented conjugated polymer chain giving a blue-shifted electroluminescence and improved efficiency," *Journal of the Chemical Society, Chemical Communications*, p. 32, Jan. 1992.

[77] H. Vestweber, A. Greiner, U. Lemmer, R. F. Mahrt, R. Richert, W. Heitz, and H. Bssler, "Progress towards processible materials for light-emitting devices using poly(p-phenylphenylenevinylene)," *Advanced Materials*, vol. 4, pp. 661–662, Oct. 1992.

[78] Y. Ohmori, M. Uchida, K. Muro, and K. Yoshino, "Blue Electroluminescent Diodes Utilizing Poly(alkylfluorene)," *Japanese Journal of Applied Physics*, vol. 30, pp. L1941–L1943, Nov. 1991.

[79] H. Jiang, J. Feng, G. Wen, W. Wei, X. Xu, and H. Wei, "Progress in Fluorene-Based Electroluminescent Materials," *Progress in Chemistry*, vol. 17, no. 5, pp. 818–825, 2005.

[80] L.-P. Lu, D. Kabra, K. Johnson, and R. H. Friend, "Charge-Carrier Balance and Color Purity in Polyfluorene Polymer Blends for Blue Light-Emitting Diodes," *Advanced Functional Materials*, vol. 22, pp. 144–150, Jan. 2012.

[81] G. E. McCluskey, S. E. Watkins, A. B. Holmes, C. K. Ober, J.-K. Lee, and W. W. H. Wong, "Semi-perfluoroalkyl polyfluorene with varying fluorine content: synthesis and photophysical properties," *Polymer Chemistry*, Mar. 2013.

[82] T. Granlund, L. A. A. Pettersson, and O. Inganas, "Determination of the emission zone in a single-layer polymer light-emitting diode through optical measurements," *Journal of Applied Physics*, vol. 89, p. 5897, June 2001.

[83] N. C. Erickson and R. J. Holmes, "Investigating the Role of Emissive Layer Architecture on the Exciton Recombination Zone in Organic Light-Emitting Devices," *Advanced Functional Materials*, pp. n/a–n/a, Apr. 2013.

[84] P. J. Cumpson, "Angle-resolved XPS and AES: Depth-resolution limits and a general comparison of properties of depth-profile reconstruction methods," *Journal of Electron Spectroscopy and Related Phenomena*, vol. 73, pp. 25–52, May 1995.

[85] J. Stöhr, *NEXAFS Spectroscopy (Springer Series in Surface Sciences)*. Springer, 2003.

[86] D. A. Outka and J. Stohr, "Curve fitting analysis of near-edge core excitation spectra of free, adsorbed, and polymeric molecules," *The Journal of Chemical Physics*, vol. 88, p. 3539, Mar. 1988.

[87] B. Watts, S. Swaraj, D. Nordlund, J. Lüning, and H. Ade, "Calibrated NEXAFS spectra of common conjugated polymers.," *The Journal of chemical physics*, vol. 134, p. 024702, Jan. 2011.

[88] Y. Ma, H. Yang, J. Guo, C. Sathe, A. Agui, and J. Nordgren, "Structural and electronic properties of low dielectric constant fluorinated amorphous carbon films," *Applied Physics Letters*, vol. 72, p. 3353, June 1998.

[89] J. Genzer, E. Sivaniah, E. J. Kramer, J. Wang, H. Körner, M. Xiang, K. Char, C. K. Ober, B. M. DeKoven, R. A. Bubeck, M. K. Chaudhury, S. Sambasivan, and D. A. Fischer, "The Orientation of Semifluorinated Alkanes Attached to Polymers at the Surface of Polymer Films," *Macromolecules*, vol. 33, pp. 1882–1887, Mar. 2000.

[90] A. Fujimori, Y. Sugita, H. Nakahara, E. Ito, M. Hara, N. Matsuie, K. Kanai, Y. Ouchi, and K. Seki, "Change of molecular packing and orientation from monolayer to multilayers of hydrogenated and fluorinated carboxylates studied by in-plane X-ray diffraction together with NEXAFS spectroscopy at C K-edge," *Chemical Physics Letters*, vol. 387, pp. 345–351, Apr. 2004.

[91] L. Andruzzi, A. Hexemer, X. Li, C. K. Ober, E. J. Kramer, G. Galli, E. Chiellini, and D. A. Fischer, "Control of surface properties using fluorinated polymer brushes produced by surface-initiated controlled radical polymerization.," *Langmuir : the ACS journal of surfaces and colloids*, vol. 20, pp. 10498–506, Nov. 2004.

[92] Y. Jung, T.-Y. Cho, D. Y. Yoon, C. W. Frank, and J. Lüning, "Surface Characteristics of Polyfluorene Films Studied by Polarization-Dependent NEXAFS Spectroscopy," *Macromolecules*, vol. 38, pp. 867–872, Feb. 2005.

[93] B. Watts, T. Schuettfort, and C. R. McNeill, "Mapping of Domain Orientation and Molecular Order in Polycrystalline Semiconducting Polymer Films with Soft X-Ray Microscopy," *Advanced Functional Materials*, vol. 21, pp. 1122–1131, Mar. 2011.

[94] A. W. Vermeer, M. G. Bremer, and W. Norde, "Structural changes of IgG induced by heat treatment and by adsorption onto a hydrophobic Teflon surface studied by circular dichroism spectroscopy," *Biochimica et Biophysica Acta (BBA) - General Subjects*, vol. 1425, pp. 1–12, Sept. 1998.

[95] B. Coupe and W. Chen, "A New Approach to Surface Functionalization of Fluoropolymers," *Macromolecules*, vol. 34, no. 6, pp. 1533–1535, 2001.

[96] A. Teichler, J. Perelaer, and U. S. Schubert, "Inkjet printing of organic elec-

tronics comparison of deposition techniques and state-of-the-art developments," *Journal of Materials Chemistry C*, vol. 1, no. 10, p. 1910, 2013.

[97] H. S. Hwang, A. a. Zakhidov, J.-K. Lee, X. André, J. a. DeFranco, H. H. Fong, A. B. Holmes, G. G. Malliaras, and C. K. Ober, "Dry photolithographic patterning process for organic electronic devices using supercritical carbon dioxide as a solvent," *Journal of Materials Chemistry*, vol. 18, no. 26, p. 3087, 2008.

[98] C.-C. Kuo and T. N. Jackson, "Direct lithographic top contacts for pentacene organic thin-film transistors," *Applied Physics Letters*, vol. 94, no. 5, p. 053304, 2009.

[99] L. M. Siperko and R. R. Thomas, "Chemical and physical modification of fluoropolymer surfaces for adhesion enhancement: a review," *Journal of Adhesion Science and Technology*, vol. 3, pp. 157–173, Jan. 1989.

[100] D. Brewis and R. Dahm, *Adhesion to Fluoropolymers, Volume 16*. iSmithers Rapra Publishing, 2006.

[101] K. M. Midthun, P. G. Taylor, C. Newby, M. Chatzichristidi, P. S. Petrou, J.-K. Lee, S. E. Kakabakos, B. A. Baird, and C. K. Ober, "Orthogonal Patterning of Multiple Biomolecules Using an Organic Fluorinated Resist and Imprint Lithography.," *Biomacromolecules*, Feb. 2013.

[102] S. Pira, "The future of inkjet printing to 2017: Global market forecasts," tech. rep., Smithers Pira, 2012.

[103] B. Derby, "Inkjet Printing of Functional and Structural Materials: Fluid Property Requirements, Feature Stability, and Resolution," *Annual Review of Materials Research*, vol. 40, pp. 395–414, June 2010.

[104] H. Sirringhaus and T. Shimoda, "Inkjet Printing of Functional Materials," *MRS Bulletin*, vol. 28, no. 11, pp. 802–806.

[105] L. Setti, A. Fraleoni-Morgera, B. Ballarin, A. Filippini, D. Frascaro, and C. Piana, "An amperometric glucose biosensor prototype fabricated by thermal inkjet printing.," *Biosensors & bioelectronics*, vol. 20, pp. 2019–26, Apr. 2005.

[106] M. Nakamura, A. Kobayashi, F. Takagi, A. Watanabe, Y. Hiruma, K. Ohuchi, Y. Iwasaki, M. Horie, I. Morita, and S. Takatani, "Biocompatible inkjet printing technique for designed seeding of individual living cells.," *Tissue engineering*, vol. 11, pp. 1658–66, Jan. 2006.

[107] D. Dimitrov, K. Schreve, and N. de Beer, "Advances in three dimensional printing state of the art and future perspectives," *Rapid Prototyping Journal*, vol. 12, pp. 136–147, Jan. 2006.

[108] C. B. Hunt, R. A. Askeland, L. Slevin, and K. A. Prasad, "High-Quality Inkjet Color Graphics Performance on Plain Paper," *Hewlett-Packard Journal*, vol. 45, no. 1, 1994.

[109] B.-J. de Gans, E. Kazancioglu, W. Meyer, and U. S. Schubert, "Ink-jet Printing Polymers and Polymer Libraries Using Micropipettes," *Macromolecular Rapid Communications*, vol. 25, pp. 292–296, Jan. 2004.

[110] P. Calvert, "Inkjet Printing for Materials and Devices," *Chemistry of Materials*, vol. 13, pp. 3299–3305, Oct. 2001.

[111] Alexander Kamyshny,Joachim Steinke,Shlomo Magdassi, "Metal-based Inkjet Inks for Printed Electronics," *The Open Applied Physics Journal*, vol. 411, no. 19, pp. 19 – 36, 2011.

[112] B. Derby, "Inkjet printing ceramics: From drops to solid," *Journal of the European Ceramic Society*, vol. 31, pp. 2543–2550, Nov. 2011.

[113] J. T. Delaney, P. J. Smith, and U. S. Schubert, "Inkjet printing of proteins," *Soft Matter*, vol. 5, no. 24, p. 4866, 2009.

[114] S. Lee, J.-S. Park, and T. R. Lee, "The wettability of fluoropolymer surfaces: influence of surface dipoles.," *Langmuir : the ACS journal of surfaces and colloids*, vol. 24, pp. 4817–26, May 2008.

[115] Y. Ko, B. Ratner, and A. Hoffman, "Characterization of hydrophilichydrophobic polymeric surfaces by contact angle measurements," *Journal of Colloid and Interface Science*, vol. 82, pp. 25–37, July 1981.

[116] S. Wu, "Calculation of interfacial tension in polymer systems," *Journal of Polymer Science Part C: Polymer Symposia*, vol. 34, pp. 19–30, Mar. 2007.

[117] B.-J. deGans, P. Duineveld, and U. Schubert, "Inkjet Printing of Polymers: State of the Art and Future Developments," *Advanced Materials*, vol. 16, pp. 203–213, Feb. 2004.

[118] S.-J. Kim, H. Beveridge, J. T. Koberstein, and I. Kymissis, "Isolation of organic field-effect transistors by surface patterning with an UV/ozone process," *Journal of Vacuum Science & Technology B: Microelectronics and Nanometer Structures*, vol. 27, p. 1057, Apr. 2009.

[119] Z. Cui, ed., *Nanofabrication: Principles, Capabilities and Limits*. Springer, 2009.

[120] D. R. Medeiros, a. Aviram, C. R. Guarnieri, W.-S. Huang, R. Kwong, C. K. Magg, a. P. Mahorowala, W. M. Moreau, K. E. Petrillo, and M. An-

gelopoulos, "Recent progress in electron-beam resists for advanced mask-making," *IBM Journal of Research and Development*, vol. 45, no. 5, pp. 639–650, 2001.

[121] M. Kakuchi, S. Sugawara, K. Murase, and K. Matsuyama, "Poly (Fluoro Methacrylate) as Highly Sensitive, High Contrast Positive Resist," no. October, pp. 1648–1651, 1977.

[122] J. R. Strahan, J. R. Adams, W.-L. Jen, A. Vanleenhove, C. C. Neikirk, T. Rochelle, R. Gronheid, and C. G. Willson, "Fluorinated Polymethacrylates as Highly Sensitive Non-chemically Amplified e-beam Resists," vol. 7273, pp. 72733G–72733G–10, Mar. 2009.

[123] R. Ruiz, D. Choudhary, B. Nickel, T. Toccoli, K.-C. Chang, A. C. Mayer, P. Clancy, J. M. Blakely, R. L. Headrick, S. Iannotta, and G. G. Malliaras, "Pentacene Thin Film Growth," *Chemistry of Materials*, vol. 16, pp. 4497–4508, Nov. 2004.

[124] H. Sirringhaus, "Device Physics of Solution-Processed Organic Field-Effect Transistors," *Advanced Materials*, vol. 17, pp. 2411–2425, Oct. 2005.

[125] Y. Zhang, J. Petta, S. Ambily, Y. Shen, D. Ralph, and G. Malliaras, "30 nm Channel Length Pentacene Transistors," *Advanced Materials*, vol. 15, pp. 1632–1635, Oct. 2003.

[126] I. Kymissis, C. D. Dimitrakopoulos, and S. Purushothaman, "Patterning pentacene organic thin film transistors," *Journal of Vacuum Science & Technology B: Microelectronics and Nanometer Structures*, vol. 20, p. 956, May 2002.

[127] T. Isemura, R. Kakita, and K. Kawahara, "Dichloropentafluoropropanes as solvents for size exclusion chromatography," *Journal of Chromatography A*, vol. 1026, pp. 109–116, Feb. 2004.

[128] D. T. Duong, B. Walker, J. Lin, C. Kim, J. Love, B. Purushothaman, J. E. Anthony, and T.-Q. Nguyen, "Molecular solubility and hansen solubility parameters for the analysis of phase separation in bulk heterojunctions," *Journal of Polymer Science Part B: Polymer Physics*, vol. 50, pp. 1405–1413, Oct. 2012.

[129] C. W. Sele, T. von Werne, R. H. Friend, and H. Sirringhaus, "Lithography-Free, Self-Aligned Inkjet Printing with Sub-Hundred-Nanometer Resolution," *Advanced Materials*, vol. 17, pp. 997–1001, Apr. 2005.

[130] K. E. Sohn, M. D. Dimitriou, J. Genzer, D. A. Fischer, C. J. Hawker, and E. J. Kramer, "Determination of the electron escape depth for NEXAFS spectroscopy.," *Langmuir*, vol. 25, pp. 6341–8, June 2009.

[131] J. Genzer, E. J. Kramer, and D. A. Fischer, "Accounting for Auger yield energy loss for improved determination of molecular orientation using soft x-ray absorption spectroscopy," *Journal of Applied Physics*, vol. 92, p. 7070, Dec. 2002.

APPENDIX A

NEXAFS DATA

A.1 Experimental Data

During the course of this investigation 822 scans of 137 different samples were taken during four visits to the synchrotron. A small amount of these data are not fit for use due to mistakes in the equipment setup that went unnoticed at the time, or unexpected results that could not have been anticipated. However, the majority of the data collected are included in this appendix. Inclusion in an appendix rather than the main chapter is considered more appropriate due to numerous null results. Only the few most pivotal results indispensable to the story of monolayer formation are included in the discussion in the main chapter. Much of the detail included here might be useful to a student that continues this project or works on a similar one, and would not otherwise be published.

The NEXAFS scans in the following sections are all labeled with their exact structure in the bottom right hand corner of the plot. A letter is included at the beginning to indicate during which run they were taken where **[A]** = April 2012, **[B]** = July 2012, **[C]** = November 2012, and **[D]** = April 2013. The parameters being compared are highlighted in red, for clarity, and the order parameter of a peak, if calculated, is noted above it in blue.

Early in the project it was imagined that device performance could be improved by increasing the extent of the order of the π-system in the monolayer so this aim motivated many of the experiments attempted. Due to a huge range of variable parameters (underlayer material, underlayer thickness monolayer

material, solvent for spincoating, solvent for rinsing, annealing time, annealing temperature, process order and timing...) experiments could not always be completely systematic so the samples were selected to give as much information as possible.

The majority of these experiments were an attempt to increase polymer chain mobility to allow the molecules to adopt a more ordered configuration. However, the order parameter, S, associated with C=C π^* peak remained noticeably unchanged by all these different conditions, generally falling in the range $0.1 \leq S \leq 0.2$.This attest to the monolayer's stability and indicates the bonding holding it in place is firm and forms as soon as the two materials come into contact.

A.1.1 Materials

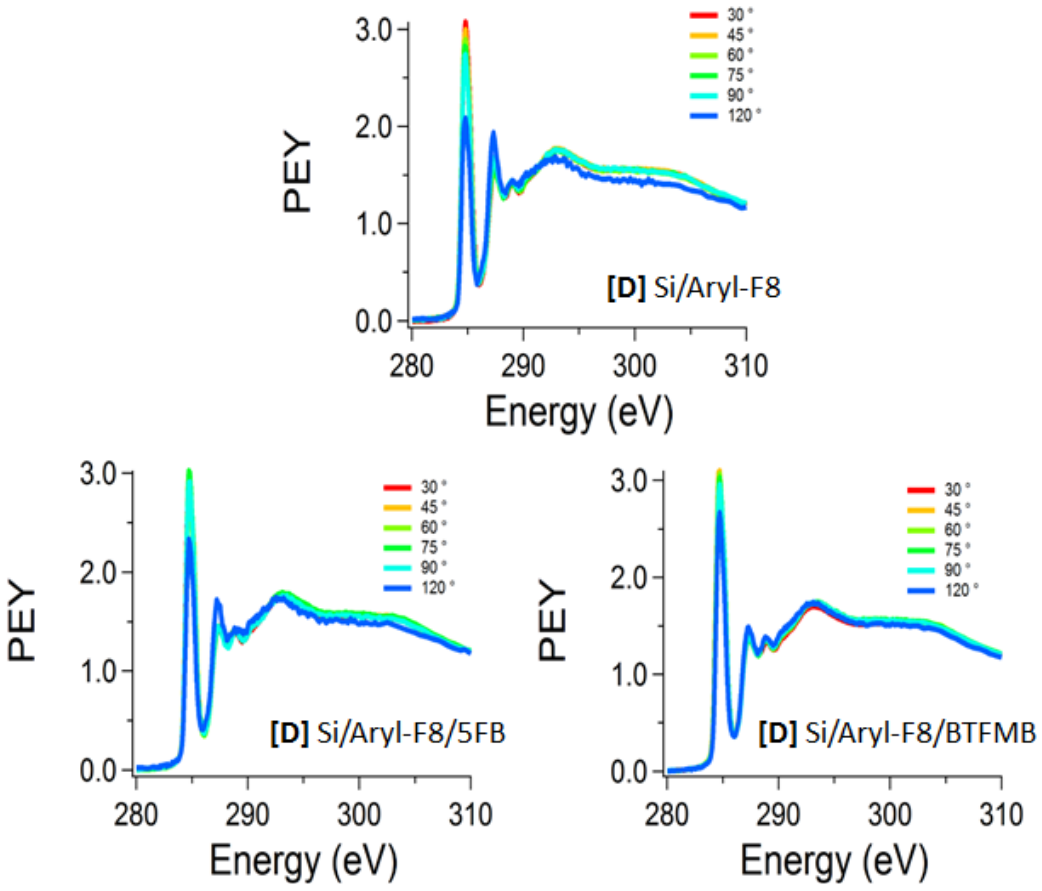

Figure A.1: **Aryl-F8 surface and the effect of fluorinated solvents.** Scans of the a single 20 nm thick layer of aryl-F8 show five peaks with the a particularly prominent C=C π^* peak at 285 eV and none of the peaks attributed to C-F present. The surface is seen to be unaffected by rinsing with the fluorinated solvents, 5FB and BTFMB.

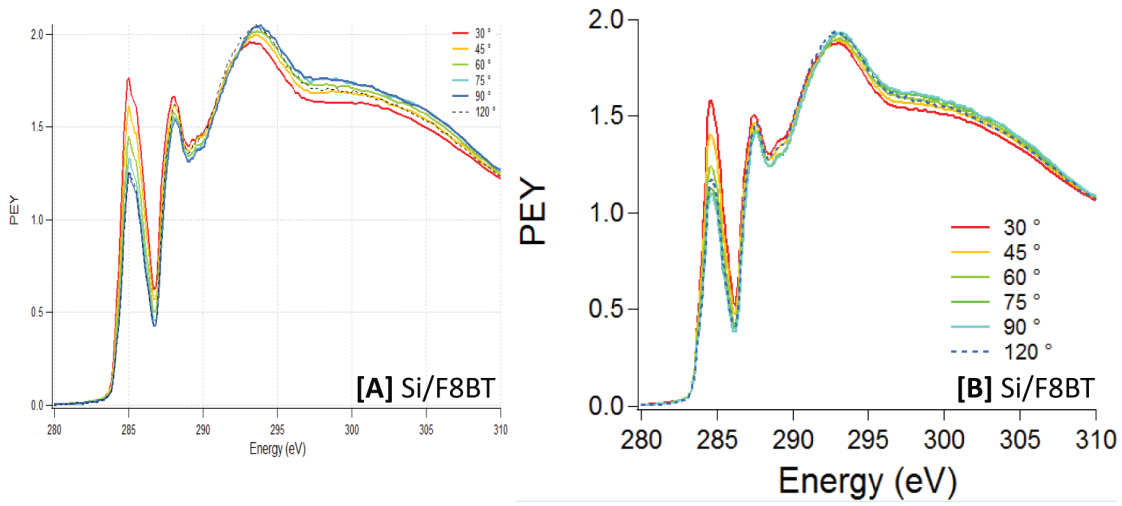

Figure A.2: **F8BT surface.** Scans of a single 20 nm thick layer of F8BT show the same five peaks as aryl-F8. The two scans, taken months apart, illustrate how reproducible this technique is.

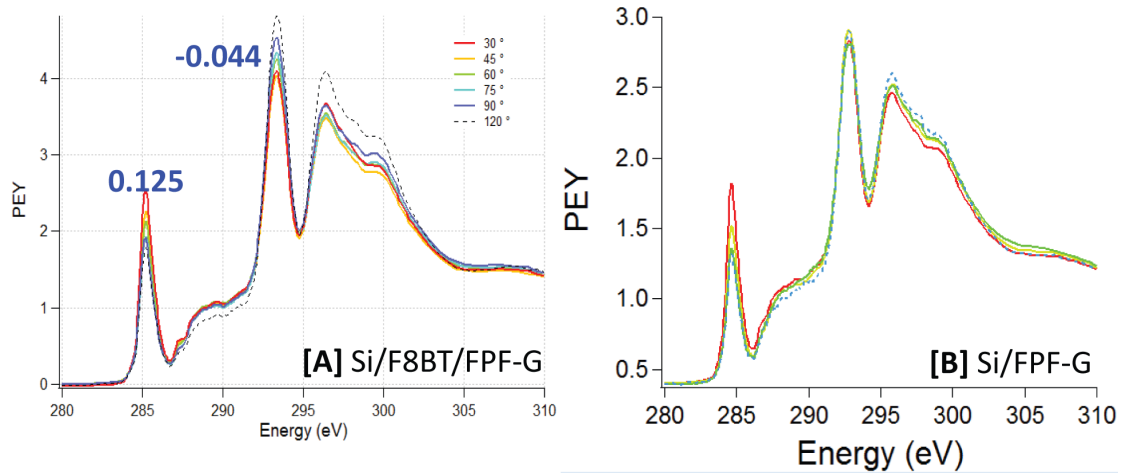

Figure A.3: **FPF-G surface.** Scans of 20 nm thick FPF-G layers show additional peaks attributed to the C-F bonding. The intensity of these C-F peaks varies slightly with angle but the order parameter calculated is insignificant. This indicates that the C-F sidechains are not induced to align out of plane, presumably because they are not that densely packed. again, the two scans taken months apart illustrates the reproducibility.

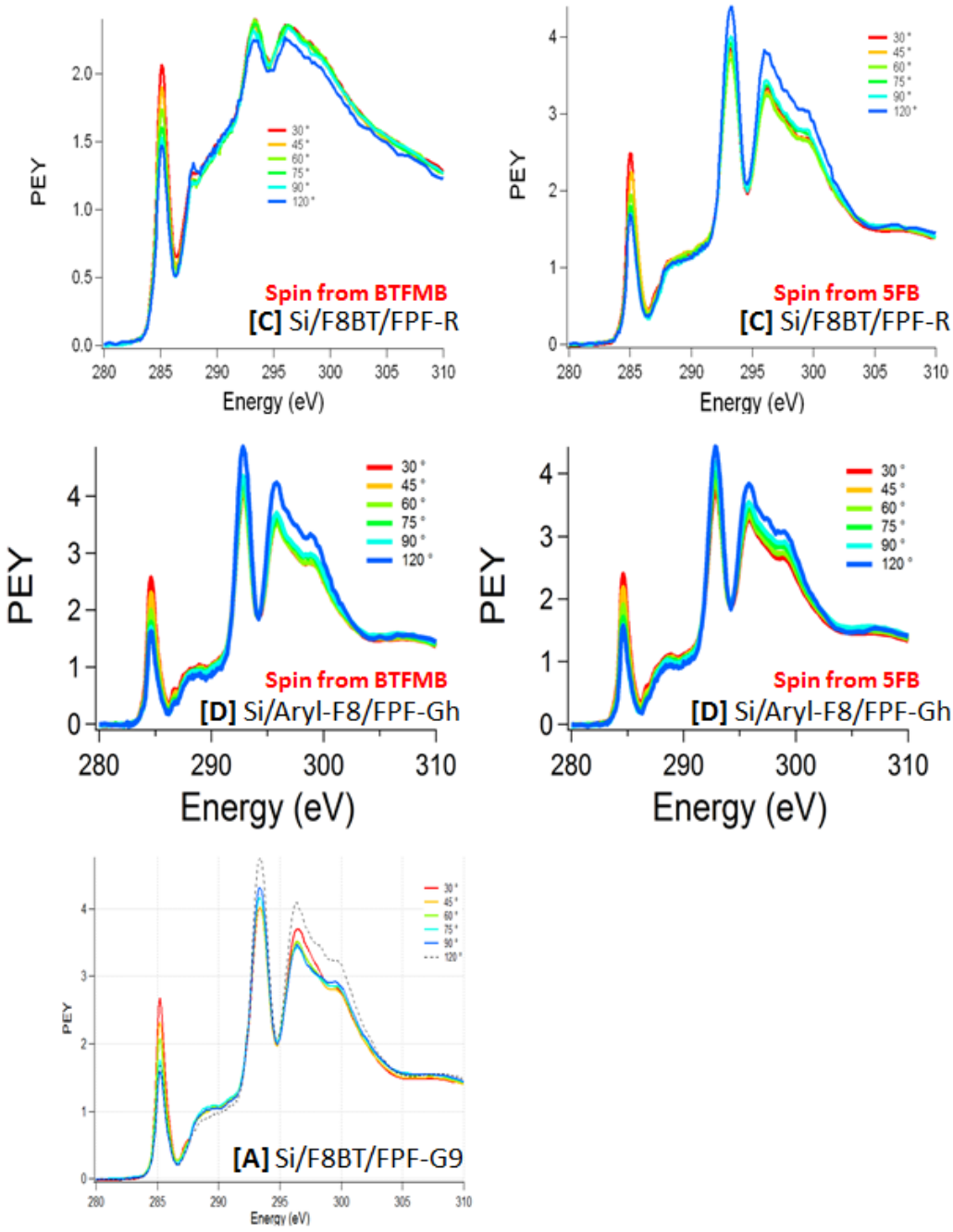

Figure A.4: **Other fluorinated polyfluorene surfaces.** Scans of other 20 nm thick fluorinated polyfluorenes all exhibit the peaks attributed to C-F. FPF-Gh is a polymer with the same chemical structure at FPF-G but synthesized to have higher molecular weight [Mn(FPF-G) = 52k, Mn(FPF-Gh) = 95k]. FPF-G9 is composed of the same monomers as FPF-G but with a different ratio [fluorinated polyfluorene:benzothiadiazole is 3:1 in FPF-G and 9:1 in FPF-G9].

A.1.2 Basic Monolayers

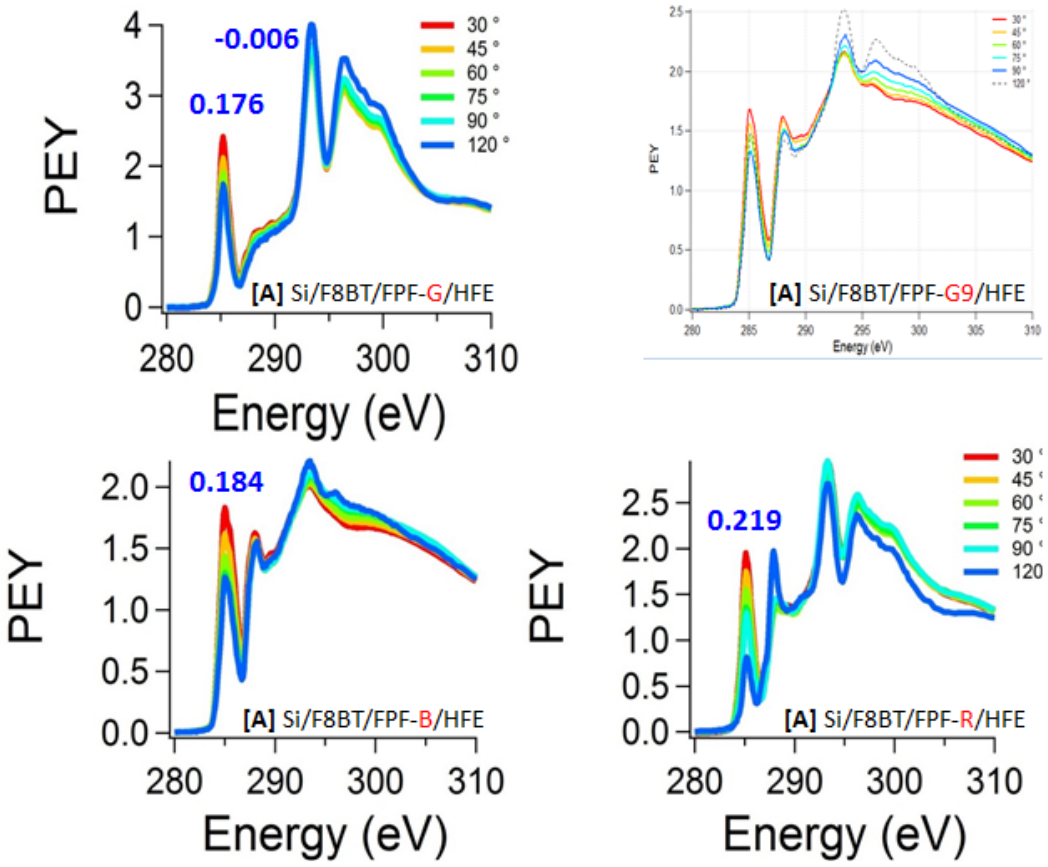

Figure A.5: **Fluorinated polyfluorene monolayers.** Scans of four different fluorinated polyfluorene monolayers formed on F8BT after rinsing in HFE show similar peaks. The C-F peaks of FPF-G and FPF-R monolayers have similar intensities to their thick films while those of the FPF-G9 and FPF-B are significantly reduced. The FPF-R sample shows the greatest variation in peak intensity observed, but (repeated) calculations showed the order parameter was still only 0.219.

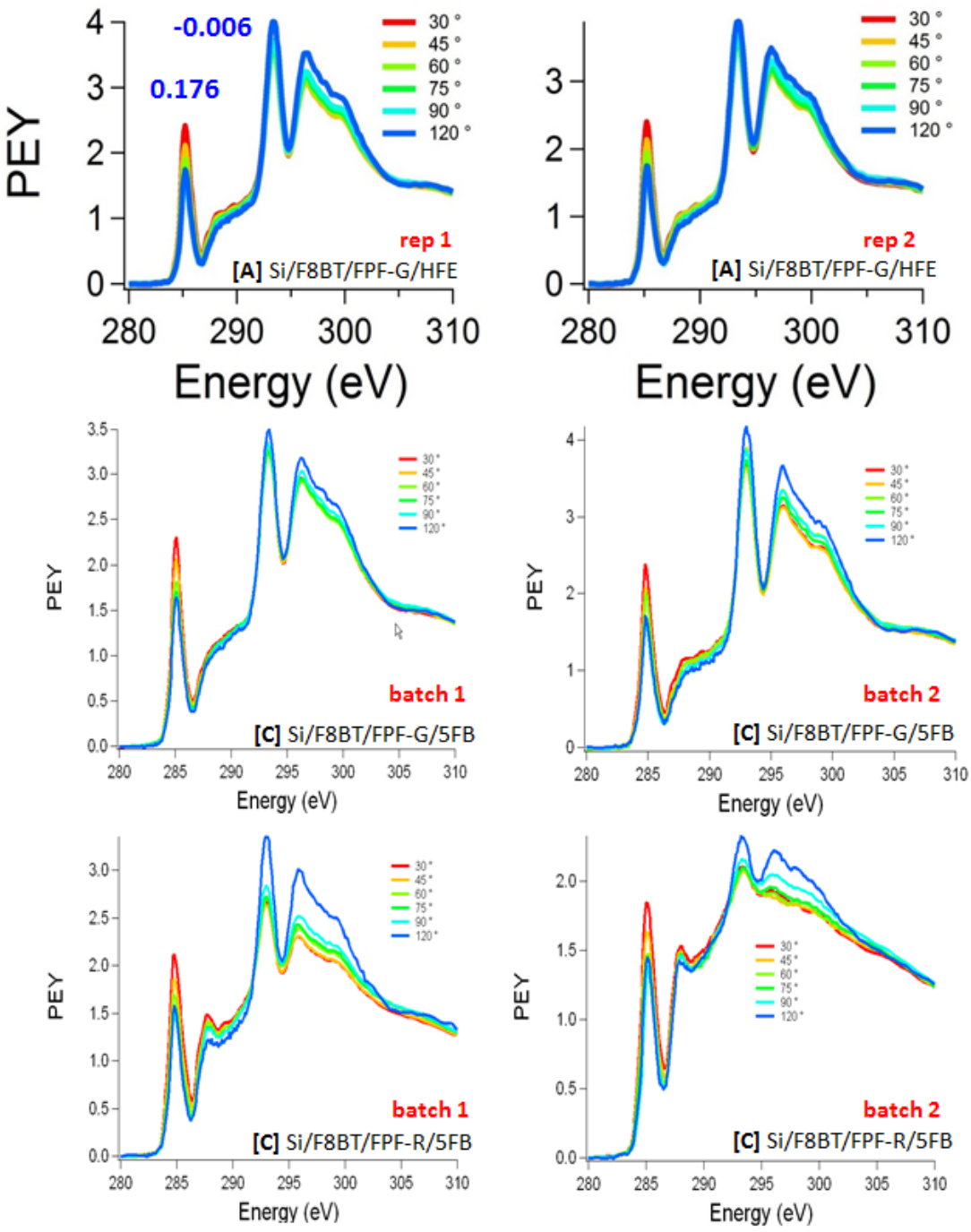

Figure A.6: **Reproducibility.** Repeat readings of the same FPF-G monolayer show very good reproducibility. As do scans of FPF-G monolayers made with batches of the FPF-G polymer that were synthesized at different times (and in different labs). The scans of FPF-R monolayers made with different batches do show a difference in intensity of the C-F peaks.

A.1.3 Solvents

Three solvents are used, at various times, in the formation of monolayers. The hydrofluoroethers (HFEs) used in much of the other orthogonal processing work are not good solvents for the fluorinated polyfluorenes, however HFEs can be used in the rinsing step to form monolayers - presumably because these polymers are more easily dissolved in thin film form due to a much greater surface area. Bis(trifluoromethyl)benzene (BTFMB) is a fluorinated solvent which also has significant aryl character making it much more similar to the fluorinated polyfluorene chemical structure. It therefore solvated them well enough for the spin coating and rinsing steps. Part way through the NEXAFS experiments the solubility of the fluorinated polyfluorenes was tested in a variety of solvents similar to BTFMB. This brought to light pentfluorobenzene (5FB) which was found to be an even better solvent for the fluorinated polyfluorenes than BTFMB.

In forming the monolayers two solvents are required - one for spin coating the fluorinated polyfluorene, one for rinsing the majority of the fluorinated polyfluorene away - and these need not be the same. It is found that monolayers are most likely to form if the fluorinated polyfluorene is spin coated from 5FB, the stronger solvent, and rinsed with BTFMB, the slightly weaker solvent. This is therefore the default used throughout these scans unless otherwise noted.

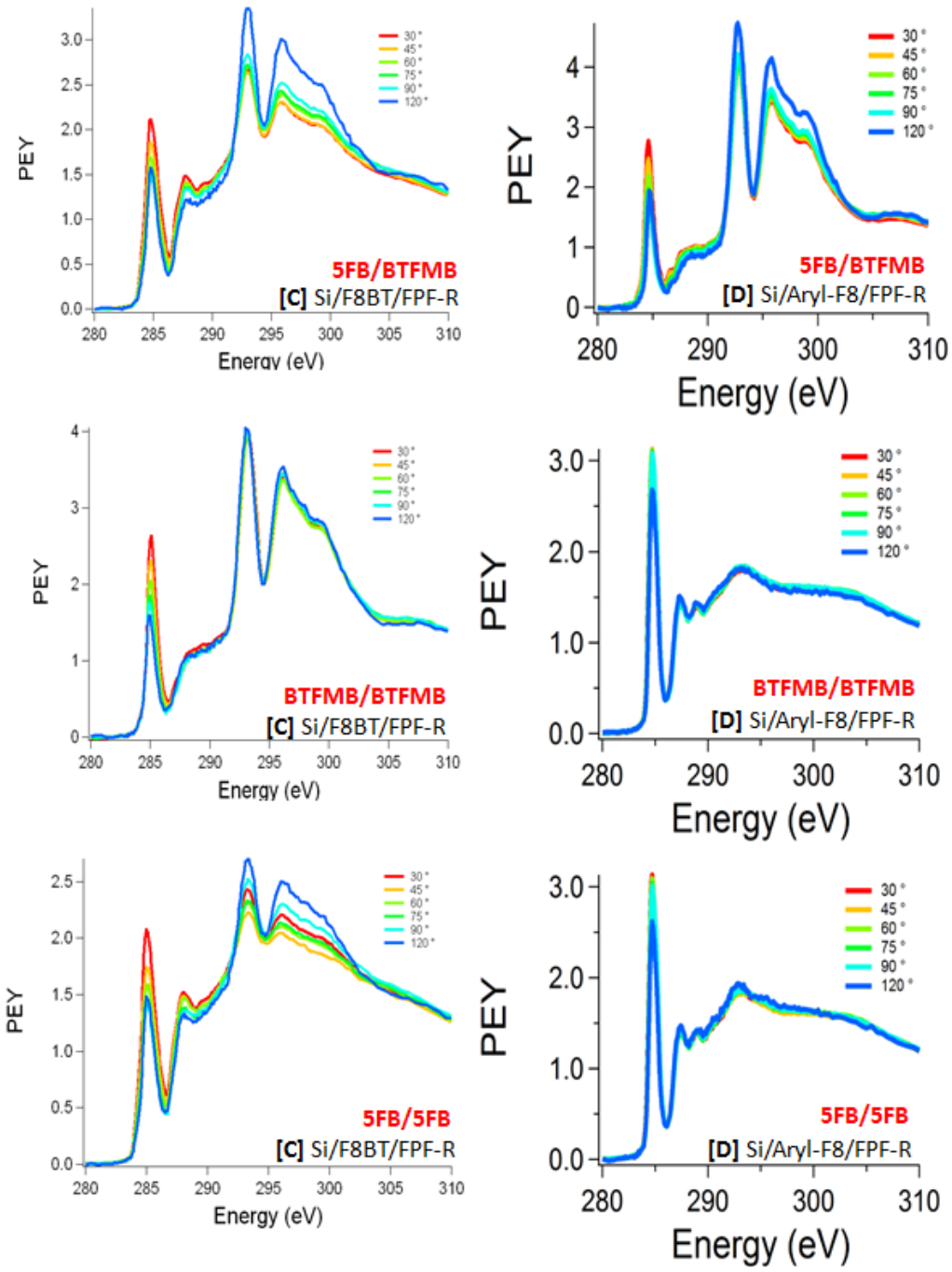

Figure A.7: **Effect of solvent variation on FPF-R monolayer formation.** Monolayers of FPF-R form on F8BT and Aryl-F8 when spin-coated from 5FB and rinsed in BTFMB. However, when the same solvent is used for both steps monolayers only form on F8BT and not on Aryl-F8 (the scans are the same as bare Aryl-F8 with no C-F peaks implying no monolayer formed). The reasons behind this are discussed subsequently.

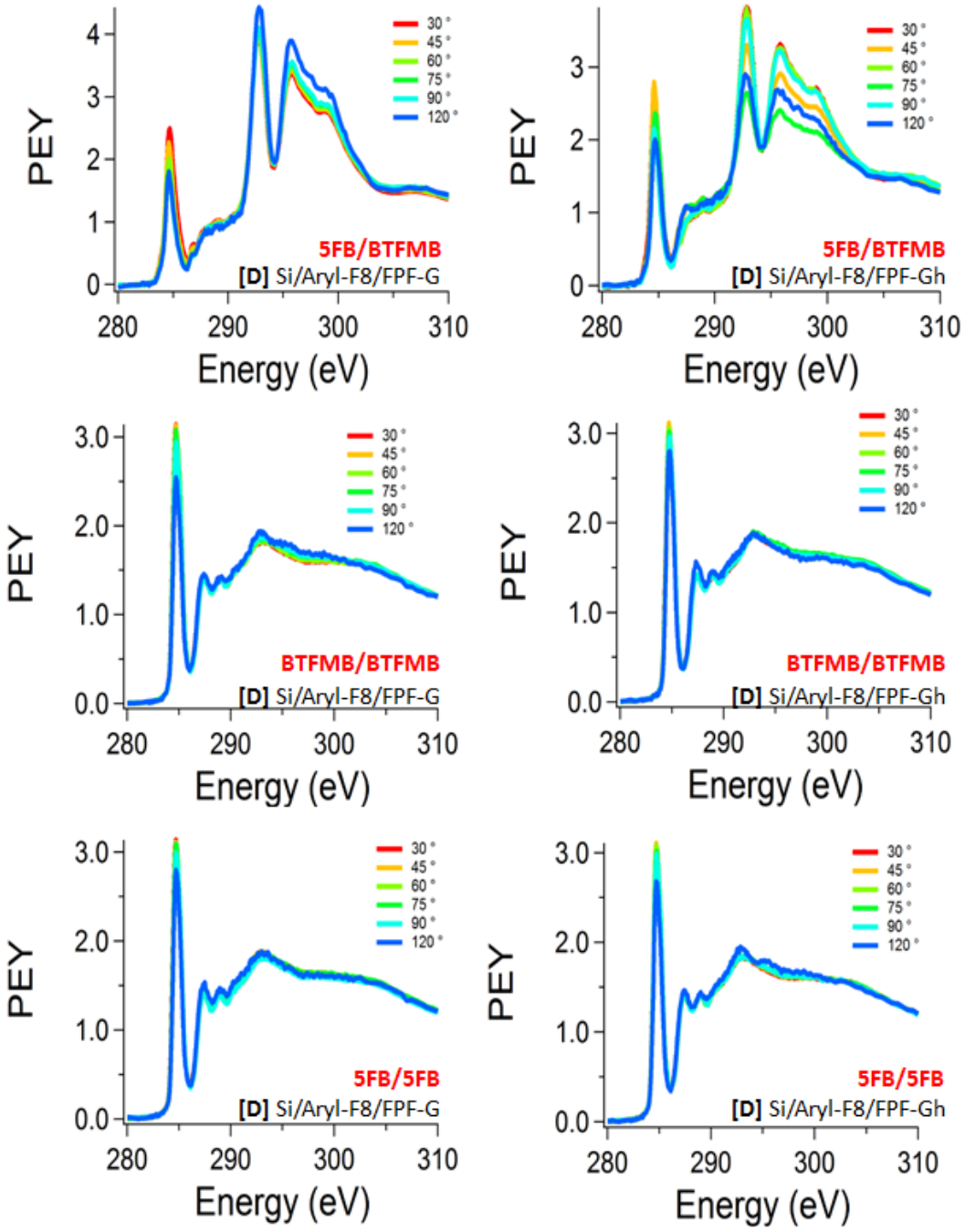

Figure A.8: **Effect of solvent variation on FPF-G monolayer formation.** Just as with FPF-R, monolayers of FPF-G and FPF-Gh form on Aryl-F8 when spincoated from 5FB and rinsed with BTFMB but do not form if the same solvent is used for both steps. The monolayers formed from the high molecular weight FPF-Gh do not differ greatly compared to those formed with FPF-G.

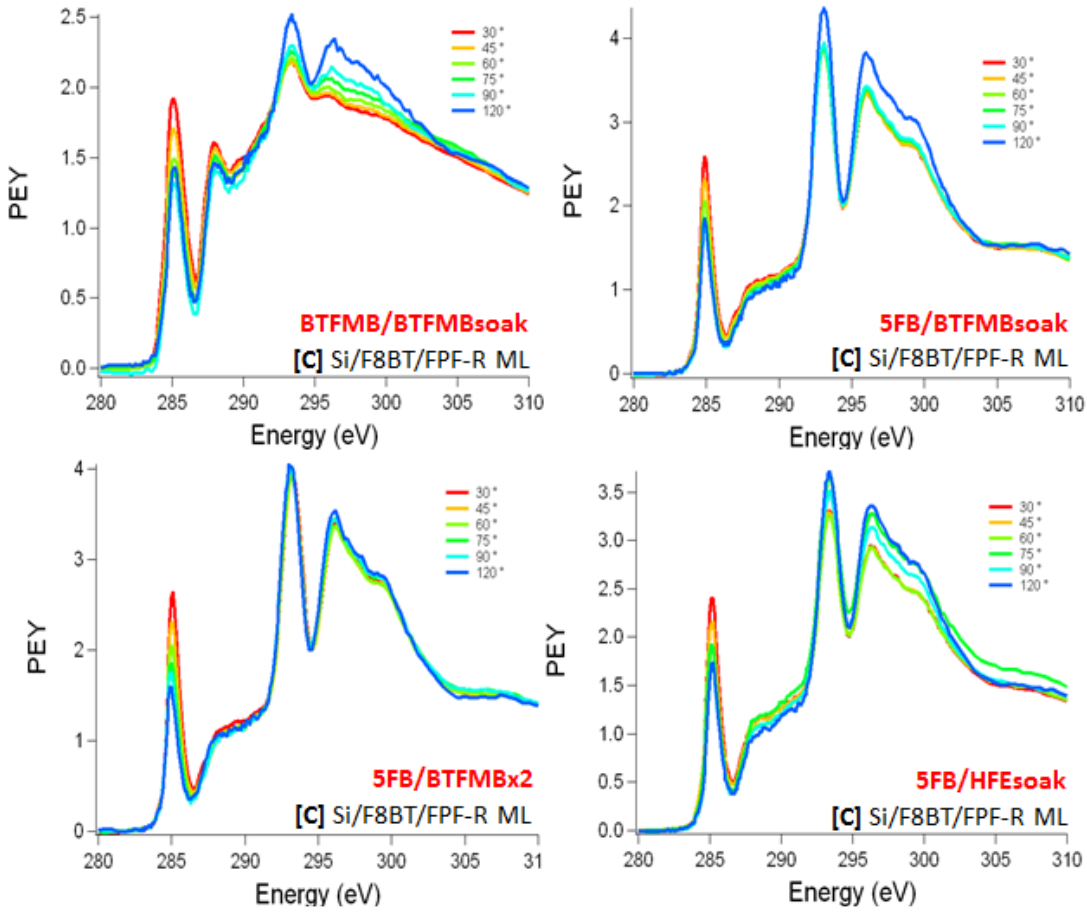

Figure A.9: **Effect of varying the rinse step on formation of FPF-R monolayers.** The standard rinse step was performed by pipetting solvent onto the substrate then immediately spinning it off, and repeating this once. This figure shows that soaking the monolayer in fluorosolvent for 60 seconds forms very similar monolayers, and importantly, that they are stable over time and resistant to the solvent.

A.1.4 Substrates

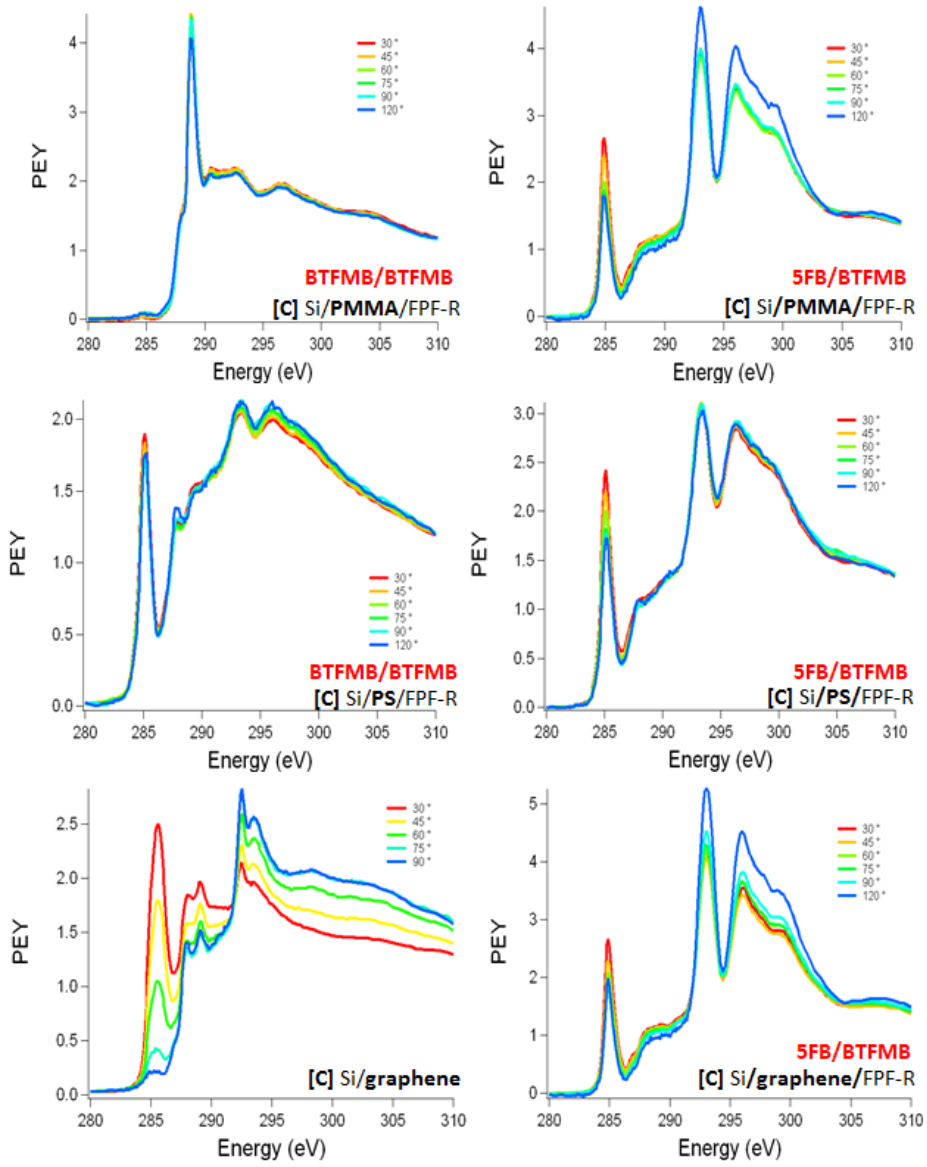

Figure A.10: **Effect of substrate on monolayer formation.** Monolayer formation is attempted on a variety of underlayers. FPF-R monolayers spincoated from 5FB and rinsed in BTFMB form on PMMA, PS and graphene. When only BTFMB is used monolayers form on PS but not PMMA. The scan of bare graphene shows an extremely ordered C=C π^* peak, as expected, but this does not increase the ordering in the FPF-R monolayer.

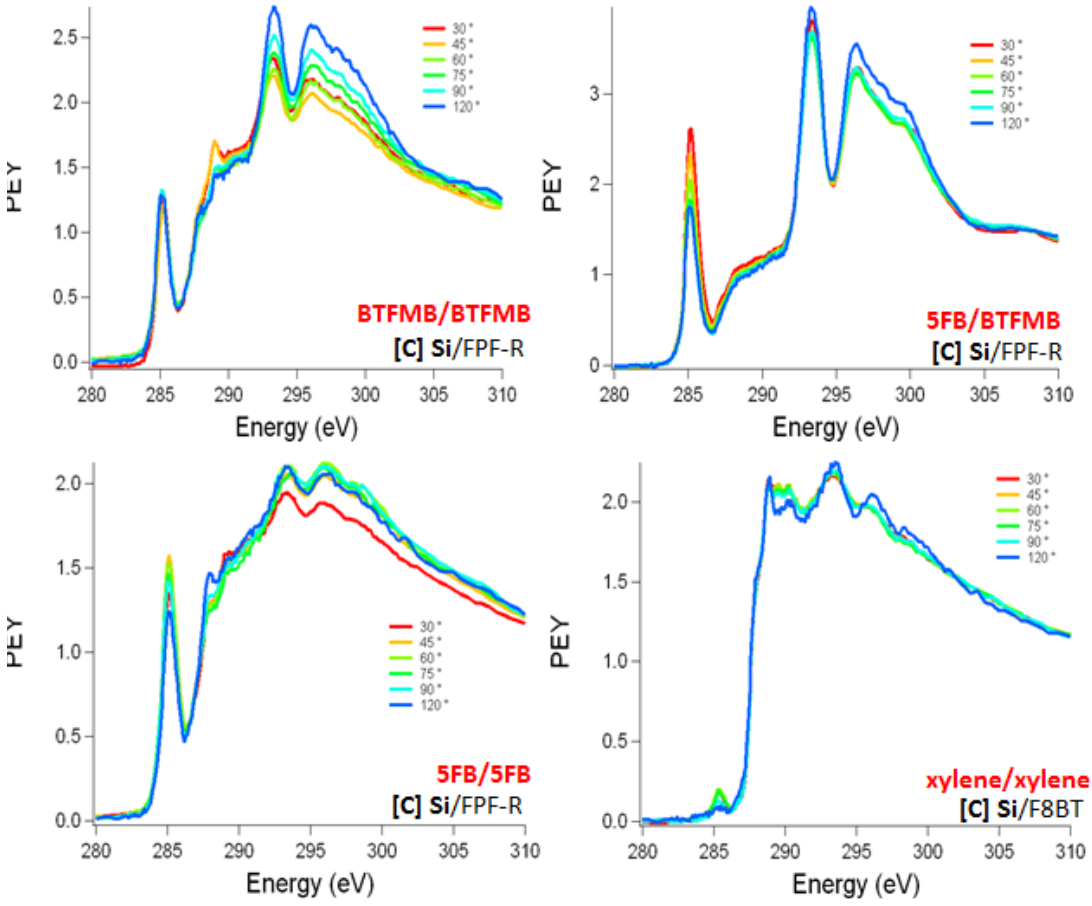

Figure A.11: **Monolayer formation on silicon.** Monolayers of FPF-R spin-coated from any combination of solvents formed on bare (untreated) silicon. Meanwhile a monolayer of F8BT does not form on silicon.

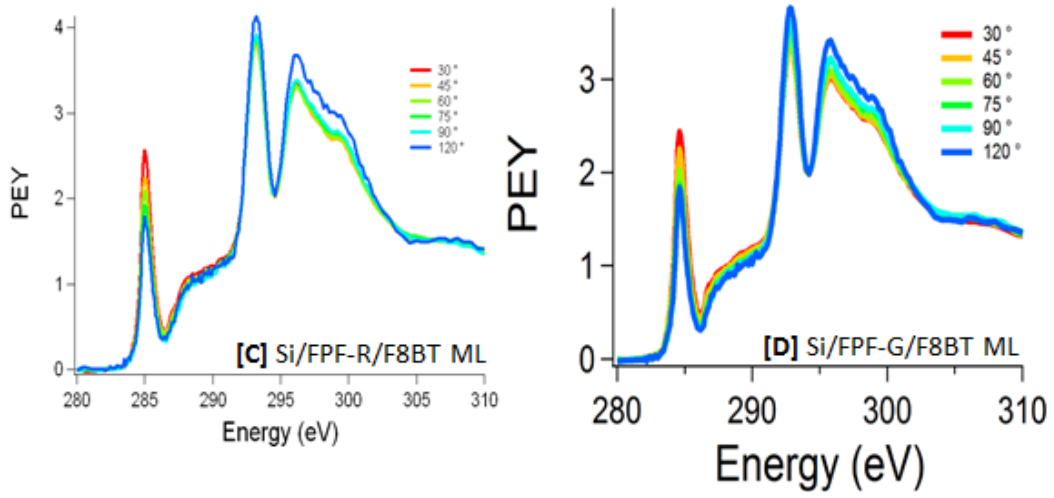

Figure A.12: **Monolayers of F8BT.** Monolayers of F8BT do not form on FPF-R or FPF-G. (No reduction in the intensity of the fluorine peaks is observed which would be expected if the fluorinate polyfluorene polymer were covered by a non-fluorinated polyfluorene monolayer.)

A.1.5 Annealing

In another attempt to increase the degree of ordering of the fluorinate polyflurene π-system samples were annealed in a variety of ways. It was hoped that this would increase chain mobility and hence increase order. However the following observations show that no annealing step alters the order parameter.

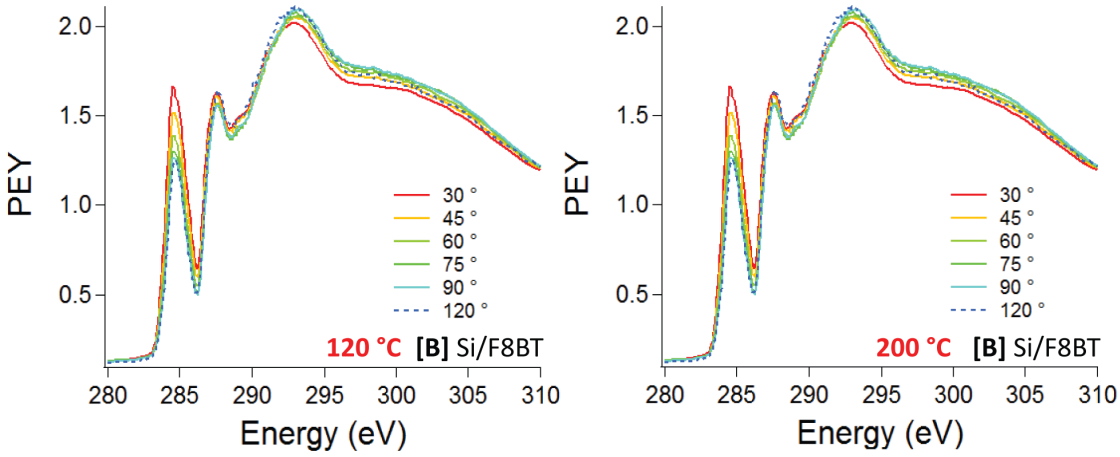

Figure A.13: **Effect of annealing on the F8BT surface.** The molecular ordering of the F8BT is unaffect by annealing at 120 °C or 200 °C for 1 hour. (It was thought that increasing the molecular order at the surface of the underlayer may induce more order in the monolayer.)

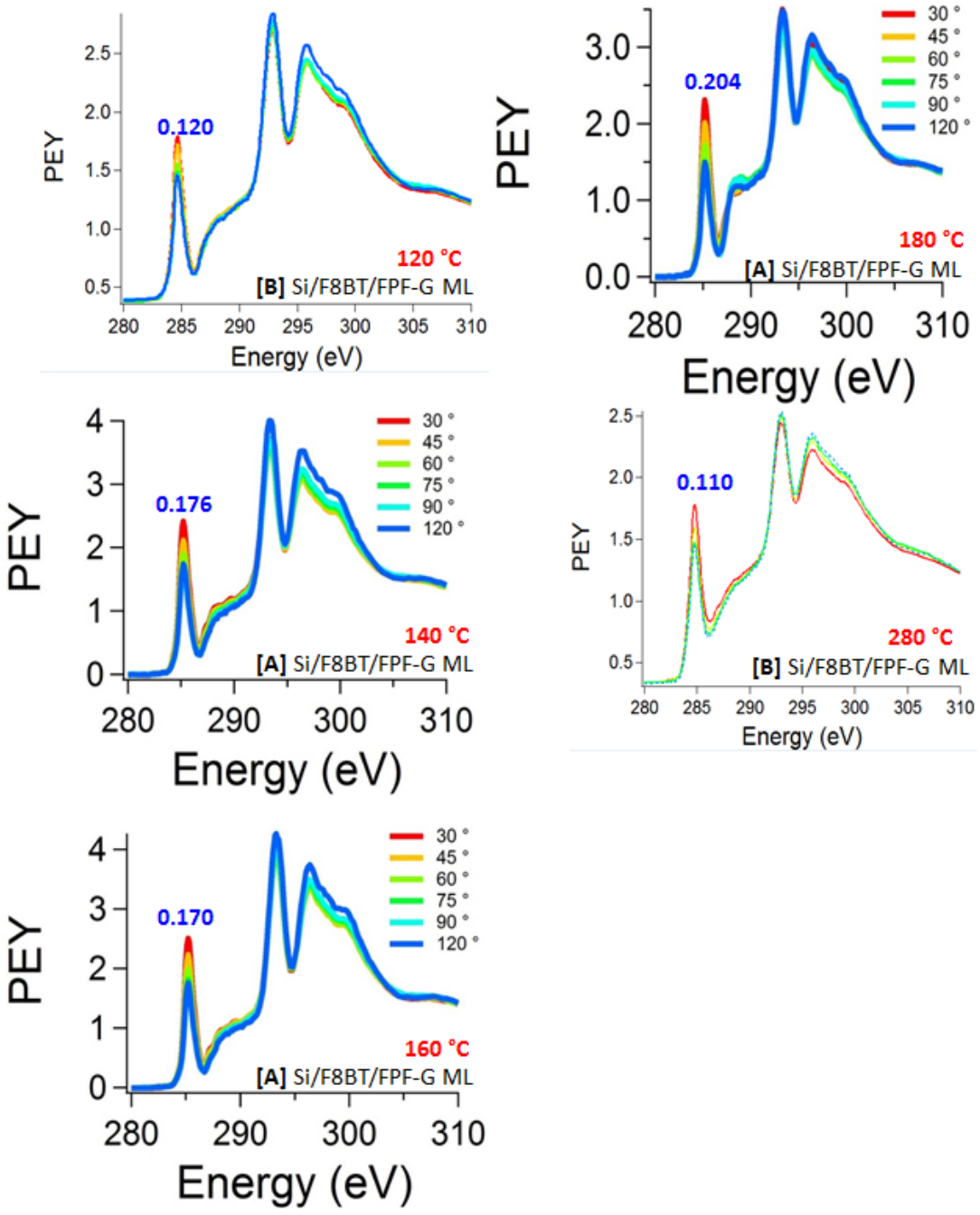

Figure A.14: **Effect of varying annealing temperature on FPF-G monolayers.** FPF-G monolayers are annealed for 1 hour before the rinse step, at the temperatures indicated. There is no obvious trend in the extent of ordering with increasing annealing temperature.

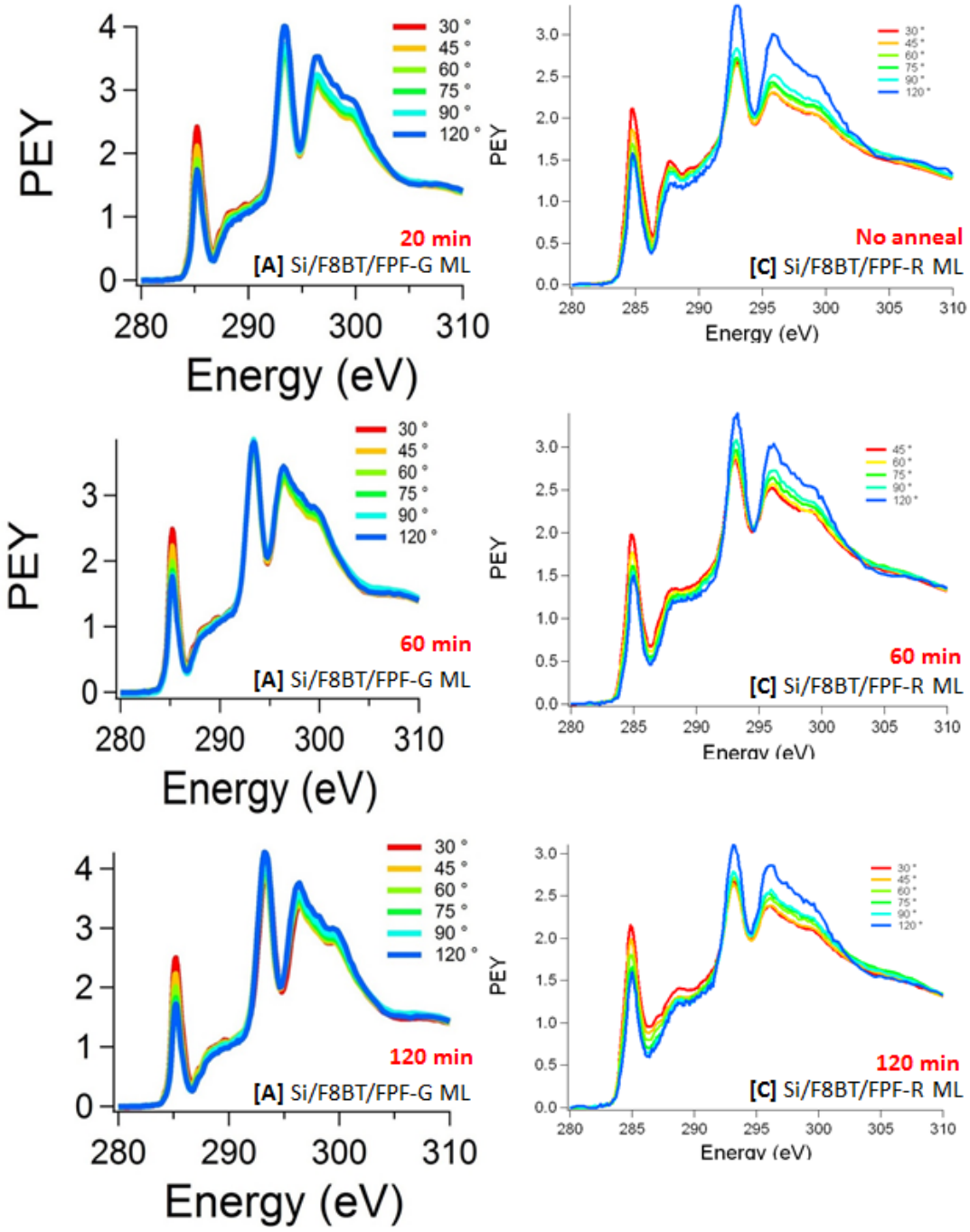

Figure A.15: **Effect of varying annealing time.** FPF-G and FPF-R monolayers are annealed before the rinse step at 180 °C for varying times. No variation in the extent of ordering is apparent.

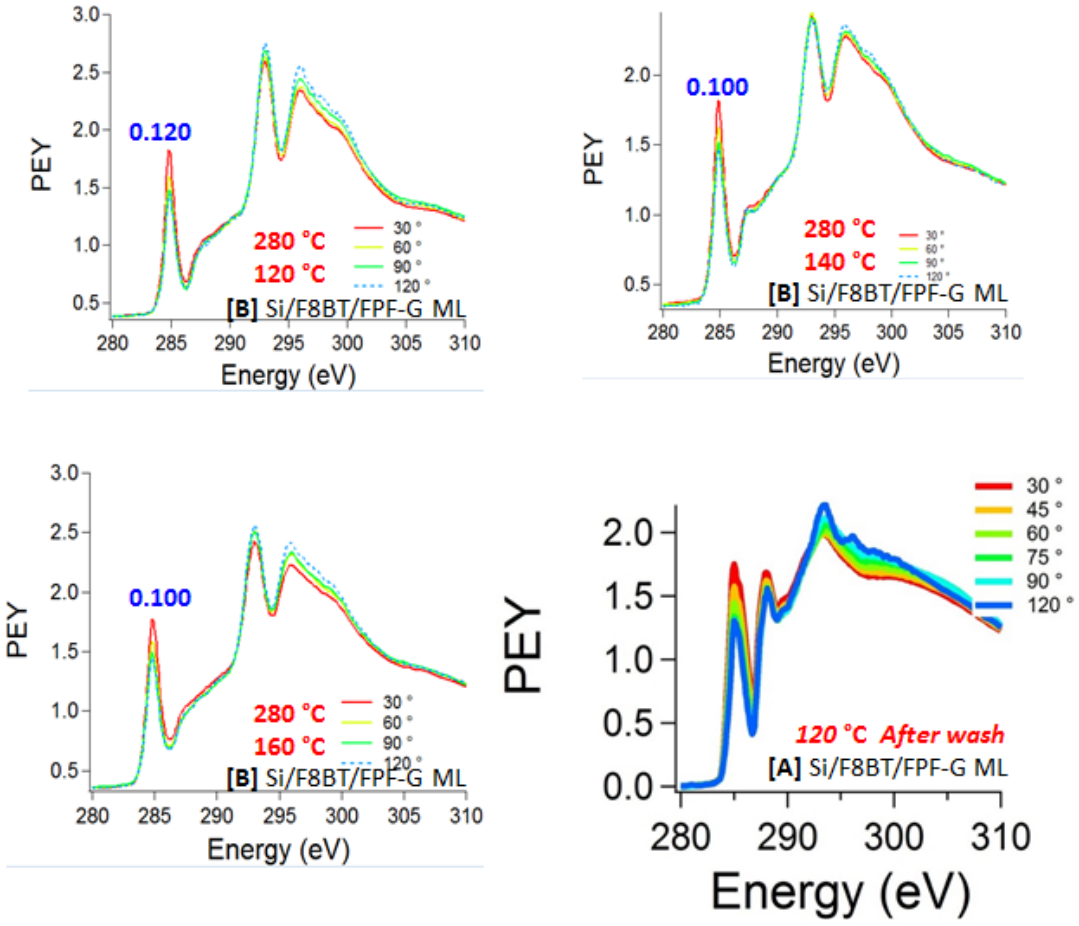

Figure A.16: **Effect of annealing both the underlayer and monolayer.** The F8BT underlayer is first annealed for 1 hour at 280 °C then the FPF-G layer is annealed before the rinse step. This does not result in an increase in order. Annealing the monolayer *after* the rinse step was also tried but did not affect the ordering of the C=C π^* peak.

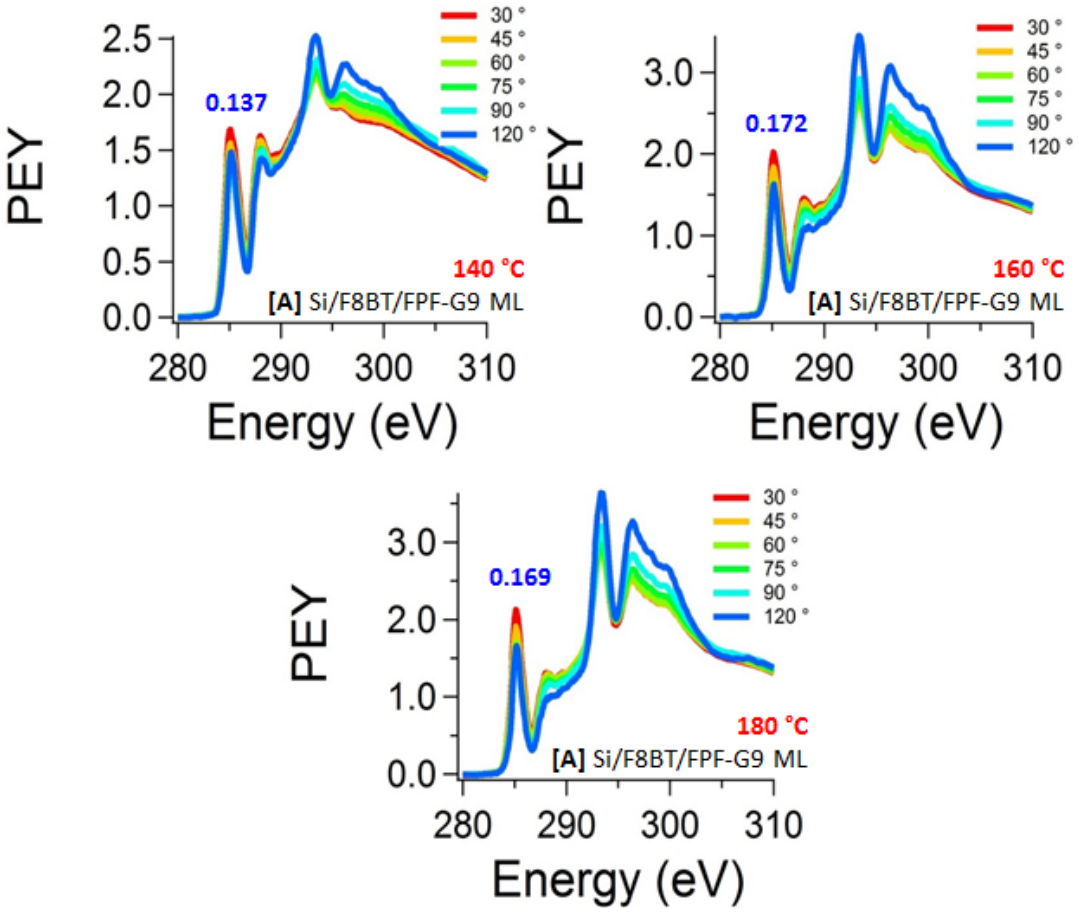

Figure A.17: **Effect of annealing on FPF-G9 monolayers.** Annealing for 1 hour before the rinse step also had no effect on the ordering of the C=C π^* peak in FPF-G9 monolayers.

A.1.6 Other Methods Intended to Increase Order

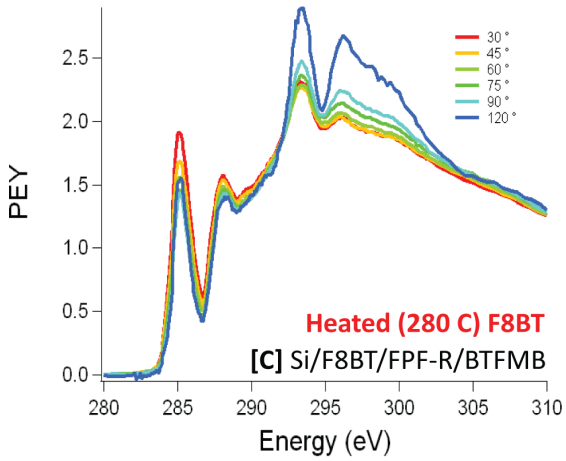

Figure A.18: **Effect of heated substrate on monolayer formation.** The F8BT was heated to 280 °C before immediately spincoating the FPF-R layer. This does not result in an increase in order.

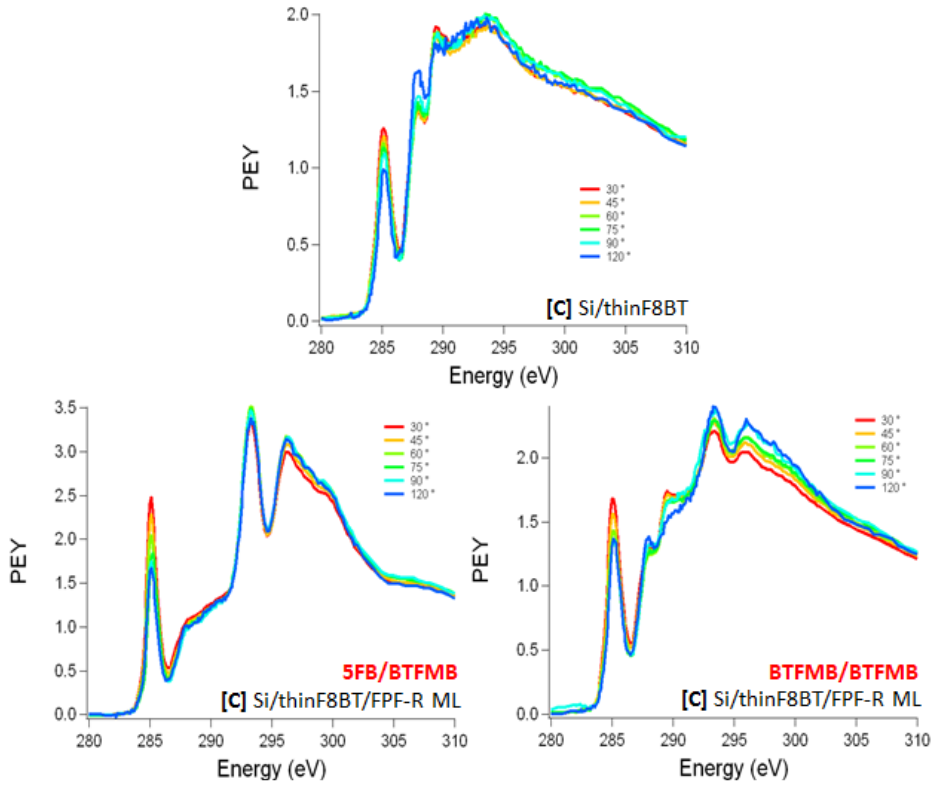

Figure A.19: **Effect of reducing underlayer thickness on monolayer formation.** There is evidence in the literature that F8BT is more ordered at the interface with silicon. By spincoating F8BT from a more dilute 1 mg/ml solution in xylenes, 2-3 nm thick layers can be formed. As this corresponds to only a few molecules thick it was hoped that the order might be maintained up to the top surface, and there, induce order in the monolayer. However, increased order is not observed in the thin F8BT nor the monolayers formed on it from 5FB or BTFMB.

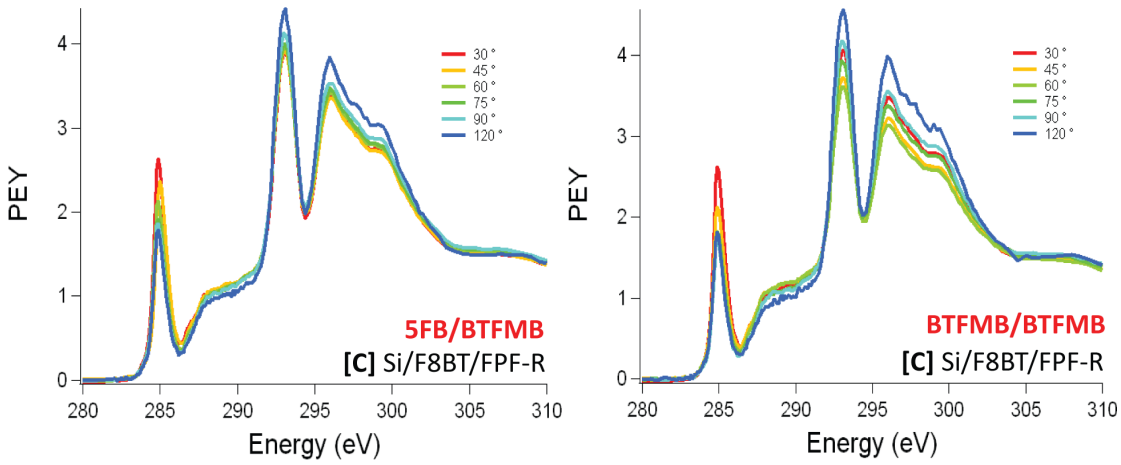

Figure A.20: **Effect of waiting before rinse step.** Monolayers were formed which, during the spincoating of the FPF-R layer, the solution was pooled on the surface for 1 min. before spinning was started. This meant the monolayer-forming molecules on top of the F8BT were held in solution (a state in which they have increased mobility) for longer than usual before being solidified. No increase in order is observed.

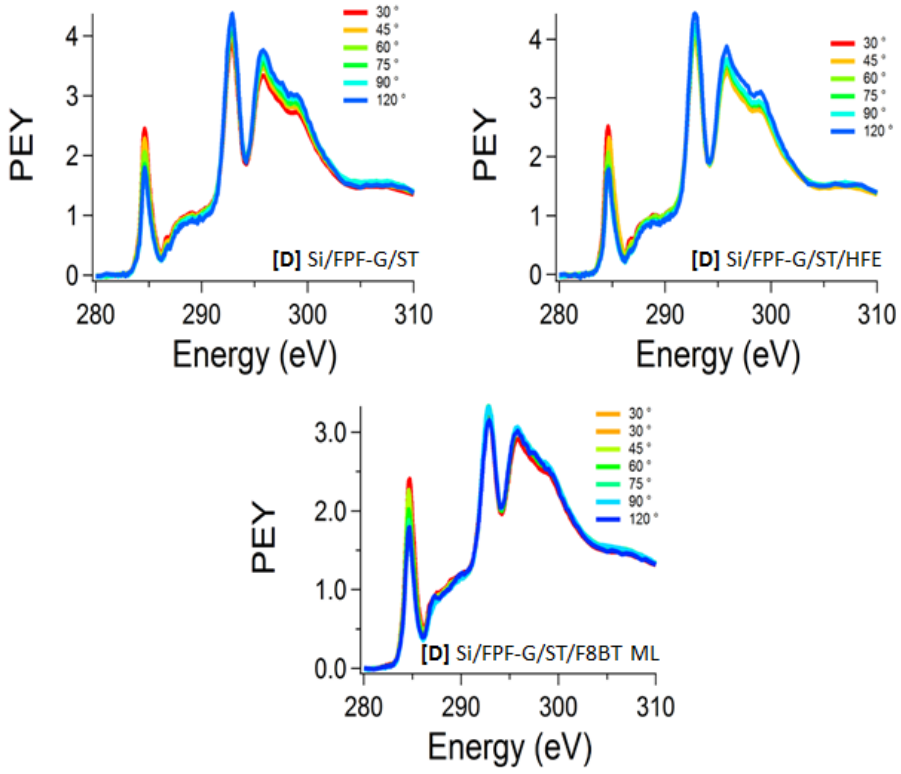

Figure A.21: **Effect of treating the underlayer with a surfactant.** Adhesion of other polymers on top of the fluorinated polyfluorenes is difficult due to the fluorinated surface. Samples of FPF-G were treated with a commercially available surfactant, Fluorad®430, to see whether the fluorinated surface could be modified to allow adhesion of F8BT on the surface, and therefore formation of F8BT monolayers. The surfactant appears not to alter the FPF-G surface and F8BT monolayer formation is unsuccessful.

A.1.7 Depth Profiling

The sampling depth of the partial electron yield (PEY) in NEXAFS is typically 2.4 nm (with a retarding voltage of -150 V applied to the detector) [130] but can be varied from 1.5 nm (-250 V) to 3.4 nm (-50 V) as described by Genzer *et al.* [131]. Some preliminary scans were made using this depth profiling technique.

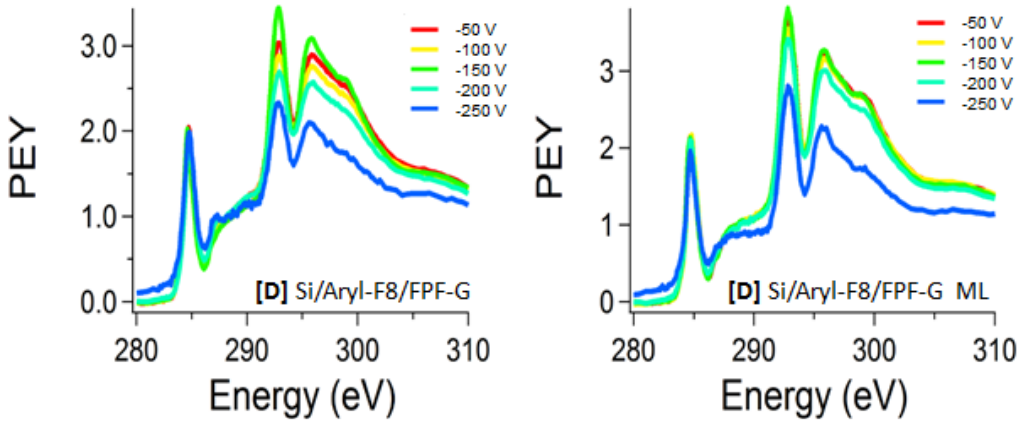

Figure A.22: **Summary of depth profiling on a FPF-G surface and monolayer.** The same sample is scanned with varying retarding voltages of -50 V, -100 V, -150 V, -200V and -250 V applied to the detector to vary the sampling depth. The intensity of the C=C π^* peak in both the FPF-G and FPF-G monolayer does not appear to vary with depth. However the intensity of the C-F peaks is reduced in the shallower scan, contrary to expectations and the indications of the angular dependence of these peaks. (Scans at 120° are particularly surface sensitive and often show a greater intensity of the C-F peaks).

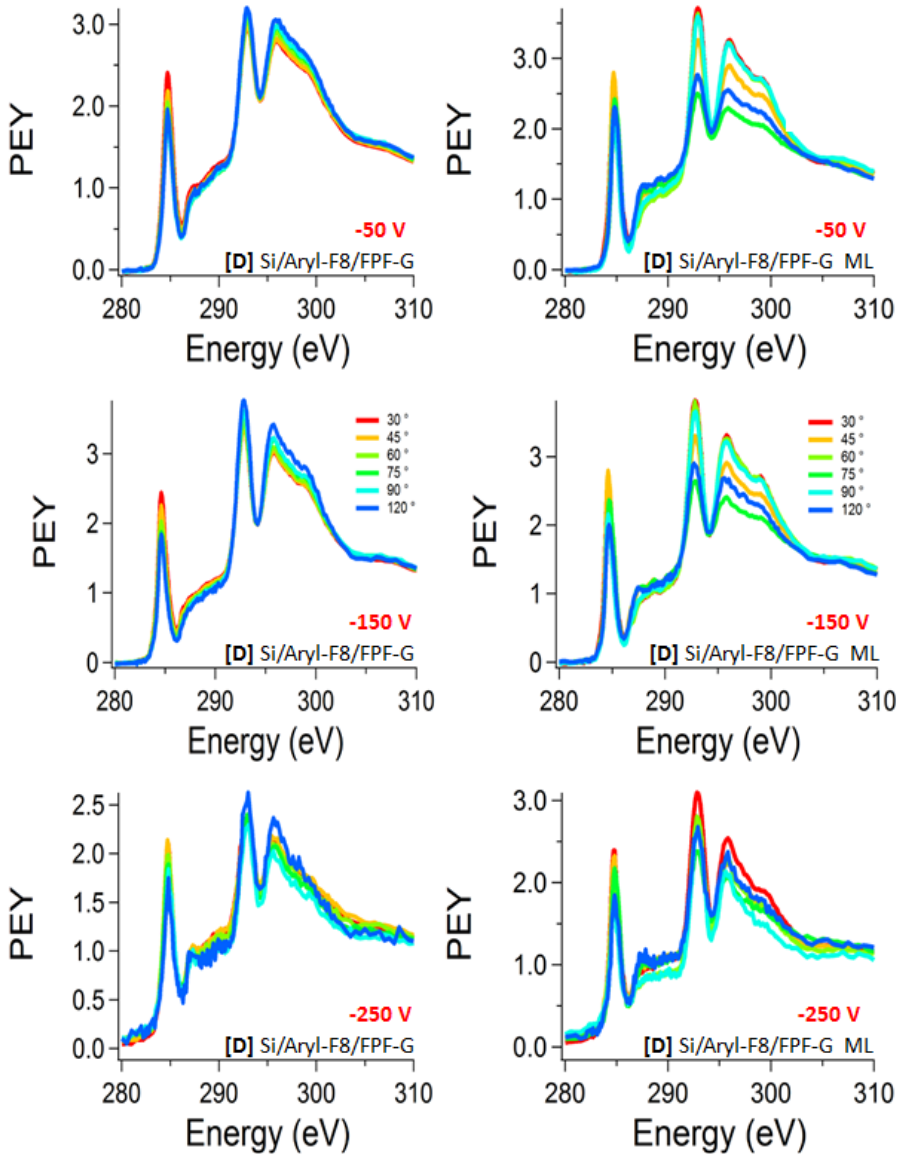

Figure A.23: **Scans at different depths.** The angular dependence of peak intensity can be measured at various depths. However, these scans show the extent of ordering does not vary greatly with the change in depth.